NASA CR-174621

ION EXTRACTION CAPABILITIES OF TWO-GRID ACCELERATOR SYSTEMS

(NASA-CR-174621) ION EXTRACTION CAPABILITIES OF TWO-GRID ACCELERATOR SYSTEMS M.S. Thesis (Colorado State Univ.) 111 p HC A06/MF A01 CSCL 21C
N84-19468
Unclas
G3/20 11913

PREPARED FOR

LEWIS RESEARCH CENTER

NATIONAL AERONAUTICS AND SPACE ADMINISTRATION

Grant NGR-06-002-112

by

Dean C. Rovang

Approved by

Paul J. Wilbur

Feb. 1984

Department of Mechanical Engineering
Colorado State University
Fort Collins, Colorado

1. Report No. NASA CR 174621	2. Government Accession No.	3. Recipient's Catalog No.
4. Title and Subtitle ION EXTRACTION CAPABILITIES OF TWO-GRID ACCELERATOR SYSTEMS		5. Report Date Feb. 1984
		6. Performing Organization Code
7. Author(s) Dean C. Rovang and Paul J. Wilbur		8. Performing Organization Report No.
9. Performing Organization Name and Address Department of Mechanical Engineering Colorado State University Fort Collins, Colorado 80523		10. Work Unit No.
		11. Contract or Grant No. NGR-06-002-112
12. Sponsoring Agency Name and Address National Aeronautics and Space Administration Washington, D.C. 20546		13. Type of Report and Period Covered
		14. Sponsoring Agency Code

15. Supplementary Notes Grant Monitor - William Kerslake, NASA Lewis Research Center, Cleveland, Ohio 44135. This report is a reproduction of the M.S. Thesis of Dean C. Rovang. It is submitted to the sponsor and to the distribution list in this form both as a presentation of the technical material, and as an indication of the academic program supported by the grant.

16. Abstract

An experimental investigation into the ion extraction capabilities of two-grid accelerator systems common to electrostatic ion thrusters is described. This work resulted in a large body of experimental data which facilitates the selection of the accelerator system geometries and operating parameters necessary to maximize the extracted ion current. Results suggest that the impingement-limited perveance is not dramatically affected by reductions in screen hole diameter to 0.5 mm. Impingement-limited performance is shown to depend most strongly on grid separation distance, accelerator hole diameter ratio, the discharge-to-total accelerating voltage ratio, and the net-to-total accelerating voltage ratio. Results obtained at small grid separation ratios suggest a new grid operating condition where high beam current per hole levels are achieved at a specified net accelerating voltage. It is shown that this operating condition is realized at an optimum ratio of net-to-total accelerating voltage ratio which is typically quite high. The apparatus developed for this study is also shown to be well suited for measuring the electron backstreaming and electrical breakdown characteristics of two-grid accelerator systems.

17. Key Words (Suggested by Author(s)) Electrostatic Thruster Ion Acceleration	18. Distribution Statement Unclassified - Unlimited

19. Security Classif. (of this report) Unclassified	20. Security Classif. (of this page) Unclassified	21. No. of Pages 109	22. Price*

* For sale by the National Technical Information Service, Springfield, Virginia 22161

TABLE OF CONTENTS

LIST OF FIGURES

I. INTRODUCTION

To reduce the number of electrostatic ion thrusters required for a space propulsion mission and hence the cost and mass of the thruster subsystem, it is generally desirable to increase the thrust densities of these devices above those attainable with currently available ion thrusters. To keep the thrusters operating at their optimum specific impulse this should be accomplished by increasing the ion beam current density extracted through the ion optics system without increasing the exiting ion velocity. To this end in recent years many experimental and theoretical investigations have been conducted to determine the ion beam extraction characteristics of accelerator systems used on electrostatic thrusters.[1-10] Because of the complexity of the theoretical considerations involved, the theoretical models used to date are generally considered to be useful for predicting general trends only. The experimental investigations on the other hand although considered more quantitative, have focused primarily on the ion beam divergence characteristics of these accelerator systems rather than the phenomena which limit extractable ion current density. The present investigation was therefore undertaken in an attempt to provide a more complete understanding of the phenomena which limit the ion extraction capabilities of two-grid accelerator systems. This investigation deals with the effects of variations in the accelerator system geometry and operating conditions of the ion thruster on these ion extraction limiting phenomena. It is believed that a more complete picture of the ion extraction capabilities of two-grid accelerator systems is provided because of the extended range of geometries and operating conditions over which these limiting phenomena are investigated.

Most of the data presented here were collected using screen holes having a 2 mm diameter which is typical for present day accelerator systems. A substantial amount of data is presented, however, that suggests that the basic relationships defining the ion extraction capabilities of ion optics systems are valid for screen hole diameters as small as 0.5 mm. This differs from previous experimental results[8,11-13] which have suggested that there might be a reduction in the ion extraction capabilities of accelerator systems utilizing grids with small screen hole diameters (<2.0 mm).

II. ION BEAM FORMATION

Accelerator System Operation

The essential components of a two-grid accelerator system are shown in Fig. 1a. Although the side view of a single circular aperture pair is depicted it should be noted that a multi-aperture system is implied. The accelerator system, consisting of a screen grid and an accelerator grid, is positioned so the screen grid is adjacent to a discharge chamber containing a low density plasma at a potential a few tens of volts above that of the screen grid. A plasma is generated in the discharge chamber by electron-bombardment of neutral propellant atoms.

Around each screen hole a plasma sheath forms which defines the boundary between the discharge plasma and the ion acceleration region. Potentials applied to the grids produce an electric field that accelerates the ions and repels the electrons coming into the sheath from the discharge plasma. Figure 1b illustrates the variation of electric potentials associated with the grid geometry of Fig. 1a. The solid line shows the potential variation through the grids themselves. This potential variation approximates but is not the same as that actually encountered by the ions. Under normal operating conditions, the dotted line shows the potential variation which the ions experience as they are accelerated through the extraction system. The ions are first accelerated from a high positive plasma potential to a negative potential near the potential applied to the accelerator grid. They are then

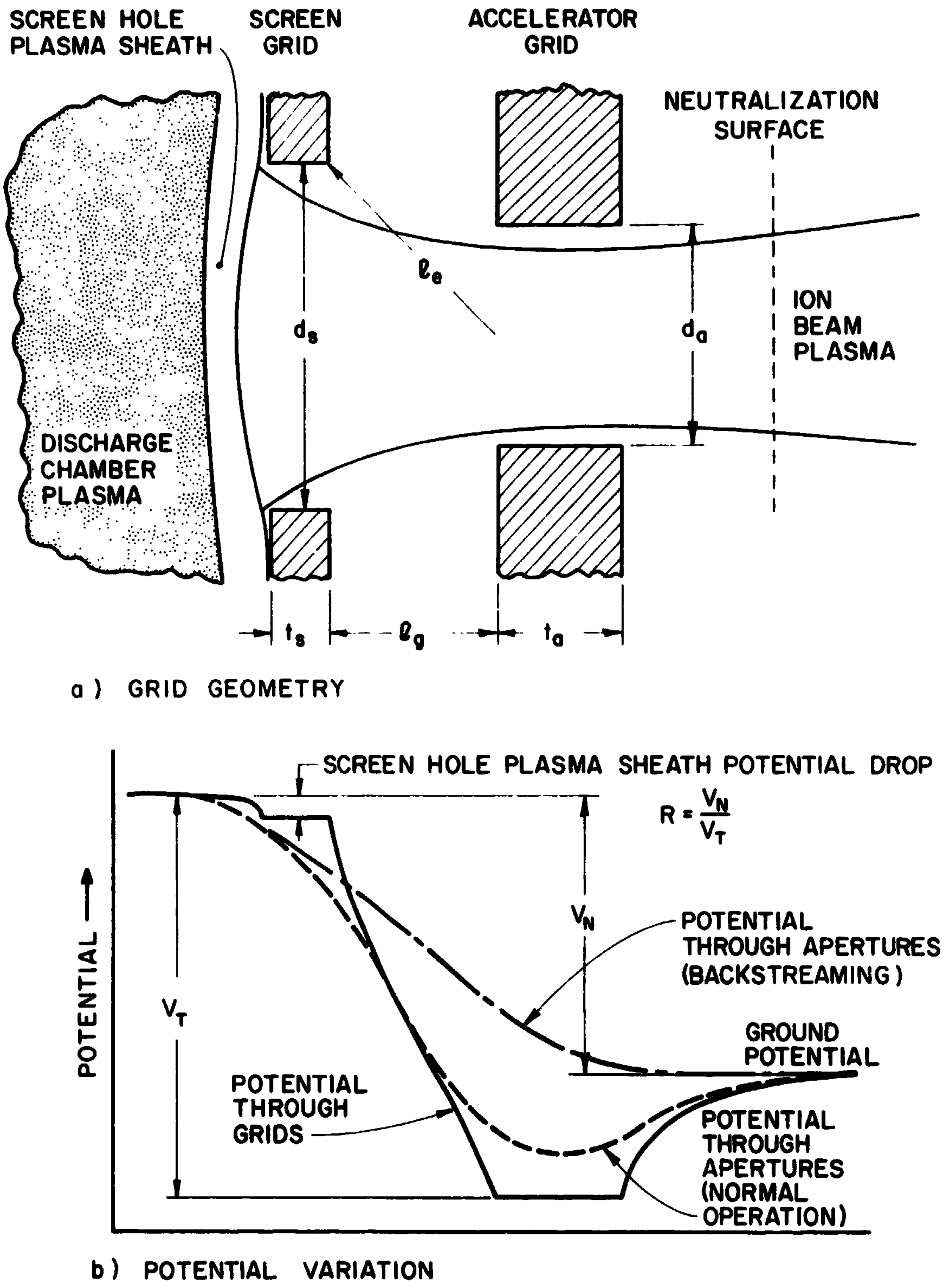

Figure 1. Two-Grid Acceleration System

decelerated as they pass from the plane of the accelerator grid to the region downstream that is held near ground potential. In this latter region electrons are supplied to maintain charge neutrality in the plasma associated with the ion beam. The potential difference between the plasma potential and ground potential is referred to as the net accelerating voltage (V_N) and it determines the exiting ion velocity. Because the discharge chamber plasma potential is near anode potential, the potential drop across the screen hole plasma sheath is approximately equal to the discharge voltage (V_D). The net accelerating voltage used herein is therefore defined as the sum of the discharge voltage and the screen voltage

$$V_N = V_D + V_S \; . \tag{1}$$

The total accelerating voltage applied to the accelerator system is defined as the sum of this net accelerating voltage and the absolute value of the potential applied to accelerator grid,

$$V_T = V_N + |V_A| \tag{2a}$$

or

$$V_T = V_D + V_S + |V_A| \; . \tag{2b}$$

The ratio of the net accelerating voltage to the total accelerating voltage (R) is defined as

$$R = \frac{V_N}{V_T} \; . \tag{3}$$

Phenomena Limiting Proper Grid Operation

In normal operation the concave shape of the sheath similar to that shown in Fig. 1a is observed. Experimental evidence obtained by Aston[18] showed that as the plasma density and consequently the ion flux to the sheath increases, the sheath moves closer to the hole and begins to flatten out. Eventually, an operating point is reached where the sheath is sufficiently flat or even slightly convex so that ions passing through the accelerator grid are no longer focused properly and they begin to impinge directly upon the accelerator grid. The direct impingement by these high velocity ions causes sputter erosion of the accelerator grid and this process can result in rapid destruction of this grid. The onset of this direct ion impingement thus limits the extractable ion current for a particular grid geometry and set of operating voltages.

Another phenomenon which can limit the operating range of the ion acceleration system is electron backstreaming. Electron backstreaming occurs when electrons in the downstream ion beam plasma find a path along which they can be accelerated through grid apertures directly into the discharge chamber. This condition occurs when the potential variation through the apertures is similar to that shown by the centerline in Fig. 1b. When this type of potential profile exists, the electrons in the beam plasma are no longer repelled by the negative potential on the accelerator grid and they are therefore able to backstream into the discharge chamber. This backstreaming electron current is undesirable primarily because it represents a power loss for the accelerator system and thus decreases the electrical efficiency of the thruster subsystem.

A final phenomenon which is generally considered to limit the operating range of the accelerator system is electrical breakdown through the region between the grids. Electrical breakdown occurs when the electric field strength that exists in the region between the grids exceeds the local electrical breakdown limit. When this happens large electron currents, typically sufficient in magnitude to be destructive, flow between the grids.

The remainder of this thesis deals with the specifics of how these three phenomena

1) direct ion impingement onto the accelerator grid
2) electron backstreaming
3) electrical breakdown

directly or indirectly limit ion extraction capabilities of a two-grid accelerator system.

Theoretical Considerations

Ion Extraction

Because the ion flow is space charge limited, there exists a limit to the amount of ion current that can be extracted from an accelerator system of this kind. The general relationship which describes these space charge effects is given by Poisson's equation

$$\nabla^2 V = -\rho/\varepsilon_o \tag{4}$$

where V is the electrostatic potential, ρ is the charge density and ε_o is the permittivity of free space. Solving this equation numerically in two or three dimensions is beyond the nature and scope of this study.*

---

*Probably the most concentrated effort in solving this problem numerically has been conducted by those people interested in neutral beam heating of fusion plasmas. Further details on investigations of this kind can be found in the literature.[14-16]

Considerable physical insight into the ion current density extraction capabilities of these accelerator systems, however, can be gained by considering the equation which results from a one-dimensional solution to the ion acceleration problem

$$j = \frac{4}{9} \varepsilon_o \left(\frac{2q}{m_i}\right)^{\frac{1}{2}} \frac{V_T^{3/2}}{\ell^2} \quad . \tag{5}$$

This equation, commonly referred to as Child's law,[17] describes the one-dimensional space charge limited current density, j, which can be drawn between two flat, parallel surfaces. Here q is the ion charge, m_i is its mass and ℓ represents the length through which the ions are accelerated by the potential difference applied between the surfaces (V_T). Applying Child's law to the three-dimensional geometry of the accelerator system requires an assumption concerning the acceleration length ℓ. In past theoretical and experimental investigations[5,8] the physical acceleration length used to correlate the performance of various grid geometries that are not truly one-dimensional is the effective acceleration length ℓ_e shown in Fig. 1a. For the geometry of this figure

$$\ell_e = [\ell_g^2 + \frac{d_s^2}{4}]^{\frac{1}{2}} \tag{6}$$

where ℓ_g represents the grid separation distance and d_s is the screen hole diameter. Substituting this effective acceleration length into the one-dimensional Child's law, and setting the beam current density (j) equal to the beamlet current (J) divided by the area of a screen grid hole, Eq. 5 can be written

$$\frac{J}{V_T^{3/2}} \left(\frac{\ell_e}{d_s}\right)^2 = \frac{\pi\varepsilon_o}{9} \left(\frac{2q}{m_i}\right)^{\frac{1}{2}} . \tag{7}$$

The collection of parameters on the left side of this expression is known as the normalized perveance per hole and it will be used in this thesis to correlate the performance of accelerator grid systems as a function of the various grid geometries and the operating conditions investigated. Of particular interest will be the impingement-limited normalized perveance per hole defined as the perveance per hole at the onset of excessive accelerator grid ion impingement. It should be noted that the right-hand side of Eq. 7 has a fixed value for a particular propellant. In the case of argon, the propellant used in this study, this value is 6.8×10^{-9} $A/V^{3/2}$. This value represents a theoretical limit to the maximum obtainable normalized perveance per hole and is indicative of the perveance expected at the impingement limit.

Electron Backstreaming

The dotted line of Fig. 1b shows the potential variation along the centerlines of grid aperture pairs that are operating normally. As the negative potential on the accelerator grid is reduced, however, the potentials through the accelerator grid become less and less negative until eventually a condition is reached where the potentials at all points along the centerline become positive (shown by the centerline in Fig. 1b). When this occurs electrons downstream of the accelerator grid in the beam plasma are free to backstream through the grid holes and into the discharge chamber. For a fixed net accelerating voltage the reduction in the magnitude of the accelerator grid potential that causes this transition from the dotted line to the centerline in Fig. 1b corresponds to an increase in the ratio of net-to-total accelerating voltage (R). The ratio of net-to-total accelerating voltage at which electron backstreaming is initiated is referred to as R_{max}. Using an analytical expression for the potential variation through an idealized accelerator system geometry,[19] Kaufman[20] first proposed the following relationship between the maximum allowable ratio of the net-to-total accelerating voltage ratio and the effective acceleration length normalized to the accelerator hole diameter,

$$(1-R_{max})\,\frac{\ell_e}{d_a} = \frac{1}{2\pi} \quad . \tag{8}$$

Based on the numerical results obtained by Latham,[4] Kaufman[20] then modified the above expression to include the effect of accelerator grid thickness,

$$(1-R_{max})\,\frac{\ell_e}{d_a} = \frac{1}{2\pi}\,\exp\left[-\frac{t_a}{d_a}\right] \quad . \tag{9}$$

More recently in order to include the data from his own more extensive numerical analysis,[5] Kaufman altered Eq. 9 slightly by changing the constant on the right hand side of the expression from $(1/2\,\pi)$ to 0.2, and obtained

$$(1-R_{max})\,\frac{\ell_e}{d_a} = 0.2\,\exp\left[-\frac{t_a}{d_a}\right] \tag{10a}$$

or

$$R_{max} = 1 - \frac{0.2}{\frac{\ell_e}{d_a}\cdot\exp\left[\frac{t_a}{d_a}\right]} \tag{10b}$$

Using this expression for R_{max}, unfortunately, did not provide a satisfactory correlation of the experimental results obtained in this study. It was found, however, that a fairly good correlation of the experimental results was obtained when the maximum allowed ratio of net-to-total accelerating voltage (R_{max}) was plotted simply as a function of an effective normalized length represented by the quantity

$$R_{max} = R_{max}\left(\frac{\ell_e}{d_a} \cdot \exp\left[\frac{t_a}{d_a}\right]\right) . \qquad (11)$$

Other correlations using different normalized effective lengths were attempted and even though these more complex empirical models appeared to facilitate improved correlations, the effective normalized length ($\ell_e/d_a \cdot \exp[t_a/d_a]$) was ultimately chosen as the correlating parameter because of its simplicity and also because of its historical and theoretical basis.

Electrical Breakdown

The electrical breakdown or "sparking" characteristics of ion thruster accelerator systems are generally considered not to be governed by Paschen's rule[21] relating electrical breakdown to the gap and pressure between two surfaces across which a potential difference is applied. The reason for this is that the large gaseous mean free paths associated with the typical low operating pressures of these accelerator systems are several orders of magnitude larger than the grid separation or "gap". Rather, the processes considered critical to determining the electrical breakdown characteristics of these systems are field emission of electrons and secondary electron emission resulting from ion bombardment of the negatively charged surface. Based on these considerations and utilizing the experimental and theoretical results of several other investigators, Kilpatrick developed the following criterion for electrical breakdown between two electrodes in a vacuum,[22]

$$W \cdot E^2 \cdot \exp[-170/E] = 1.8 \times 10^6 \ . \qquad (12)$$

In this expression W is the upper limit on the energies of the ions that are present (eV) and E is the maximum permissible electric field strength (kV/mm). More recently, two empirical relationships have been published by people working with neutral beam injection systems for fusion.[23,24] These are

$$E = 19/\ell_g^{\frac{1}{2}} \qquad (13)$$

and

$$E = 10 \qquad (14)$$

where E has the units of kV/mm and ℓ_g represents the electrode gap expressed in terms of millimeters. The above expressions predict higher maximum field strengths than those typically associated with ion thruster accelerator system operation (~2-6 kV/mm).[25-29] The reason for this disparity is unknown, but it is noteworthy that these above expressions were developed for accelerator systems with geometries and operating conditions that differ from those of typical ion thrusters for space applications and these differences may account for a part of this discrepancy in maximum permissible electric field strengths.

From a practical standpoint achieving higher electric fields is of interest to ion thruster operation because, for a given set of accelerator system operating voltages, a higher maximum permissible field strength permits operation at a closer grid separation which, in turn, generally facilitates operation at a higher current density.

III. APPARATUS AND PROCEDURE

Apparatus

All testing has been conducted on an 8 cm diameter by 10 cm long ion source with a mildly divergent magnetic field. The magnetic field was derived from a long solenoidal winding wrapped around the outside of the thruster body. A cylindrical copper anode was used and apart from this, nonmagnetic stainless steel construction was employed throughout the source. Refractory tungsten filaments were used for both the neutralizer and cathode emitters. The emission levels for both of these was controlled by adjusting the current flowing through the filaments from their ac power supplies. This source design was selected because it provided the high current density capability needed to assure a proper test of the grids, and it provided a stable discharge. Figure 2 shows a schematic of the basic ion source design with associated power supplies and instrumentation.

The grids were made from thin sheets of amorphous graphite. The grid aperture pattern used was a nineteen hole hexagonal array with a center-to-center hole spacing of 2.5 mm. The extraction region of the grids was masked down to a small area (~1 cm^2) near the axis of the source. This was done to help ensure ion extraction at each hole from a uniform plasma. The geometries of the grids were varied by selecting different diameter drills with which to machine the hole patterns in various thicknesses of graphite sheets. Each of the grid geometries

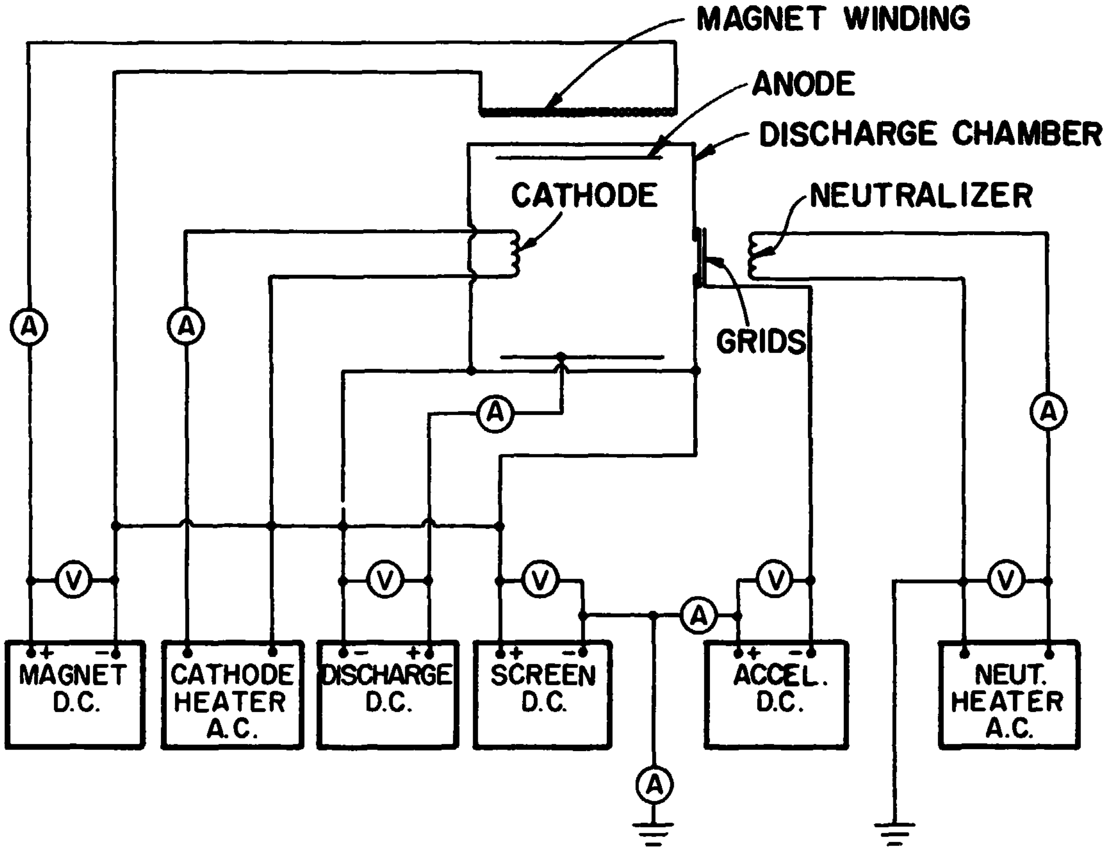

Figure 2. Ion Source Instrumentation Schematic

investigated in this study was operated over a wide range of grid separations using the variable grid spacing apparatus described next.

Because the grid separation distance was a very important parameter in this study, the test apparatus was designed so the grid separation could be varied while the ion source was being operated. This was accomplished, using the apparatus shown schematically in Fig. 3, by moving the fork-shaped wedge in the manner suggested by the large arrow. As this wedge is moved toward the grids it forces the accelerator and screen grid support plates apart and hence the screen and accelerator grids attached to these plates are also separated. All materials used in the construction of this apparatus are capable of withstanding high temperatures. Graphite was used for both the grids and grid support plates to minimize the differential thermal expansion between these components that could cause grid warpage. The distance between the points at which the grids were attached to the support plates was also minimized to minimize the effects of grid warpage and deflection due to the attractive electrostatic forces between the grids. Initial alignment of the grids was accomplished manually by positioning and clamping each grid and then checking the alignment visually beneath a large illuminated magnifying glass. This alignment is maintained during operation by the boron nitride guideposts shown in Fig. 3. Electrical isolation is assured by the sheet of isomica between the screen grid support plate and the wedge. The wedge is mechanically connected to a micrometer used to measure and adjust its translation from the outside of the vacuum system.

Immediately after each period of data collection, while the source was still hot, the grid separation distance was reduced until the

ORIGINAL PAGE IS
OF POOR QUALITY

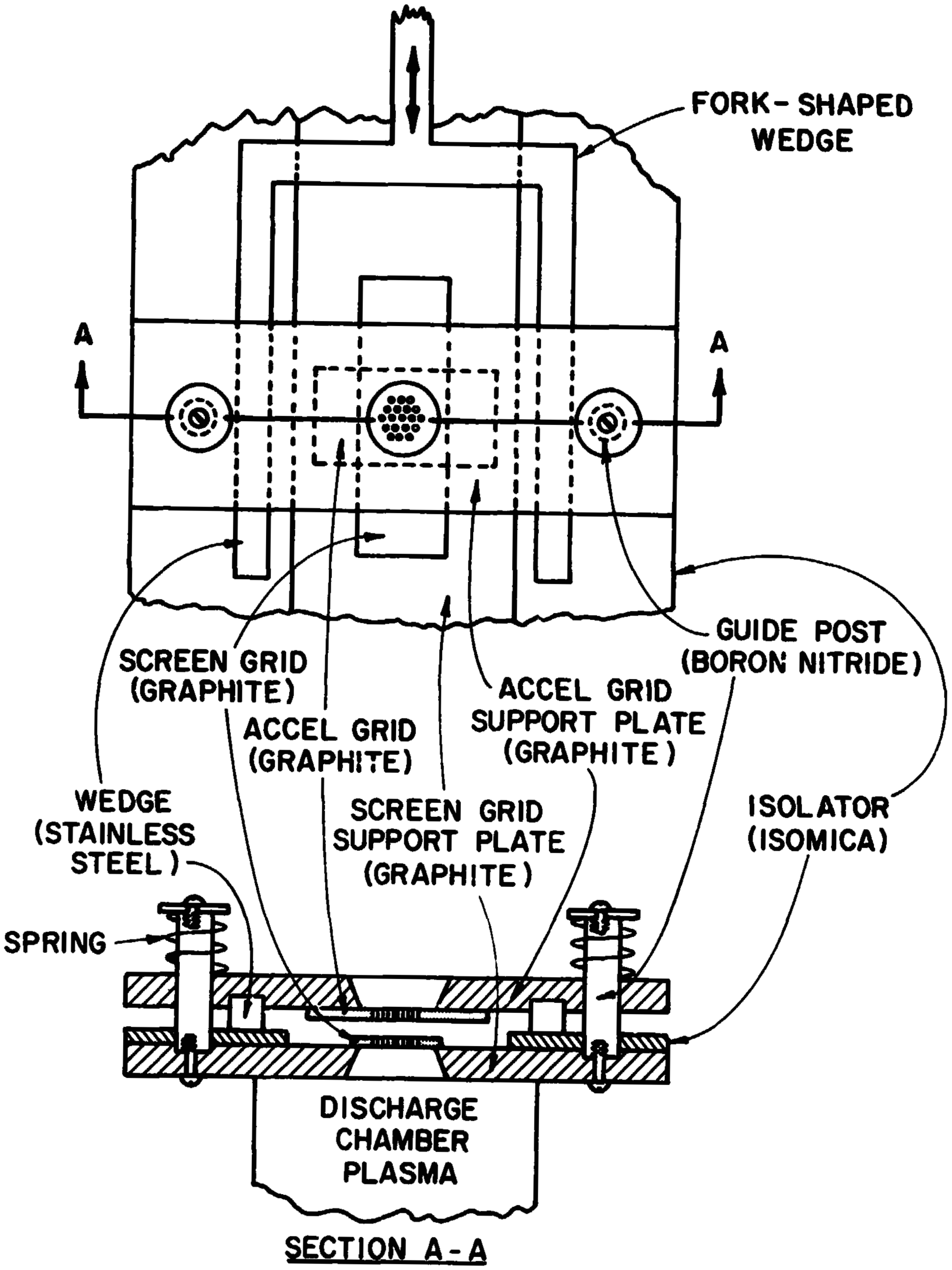

Figure 3. Variable Grid Spacing Apparatus

measured electrical resistance between the grids went essentially to zero. This reference point on the micrometer (assumed to correspond to zero separation) along with the geometry of the wedge could then be used to calculate the grid spacing from the micrometer readings recorded during the testing. Because this procedure for defining the reference point was conducted while the grids were hot, this further minimized any error of grid separation that might have been caused by thermal warpage.

Procedure

The ion extraction performance of each grid geometry was investigated over a large range of net-to-total accelerating voltages and grid separations. A summary of the parameters varied in these tests is provided in Table 1. The grid geometries have been normalized with respect to the screen hole diameter (d_s). Similarly, the discharge voltage (V_D) has been divided by the total accelerating voltage (V_T) to make it non-dimensional.

After allowing the source to warm up, data collection was begun with the accelerator system operating at a large grid separation and high ratio of net-to-total accelerating voltage, typically R = 0.8. The propellant flow rate was adjusted to the minimum flow rate at which the source operated stably over the full range of beam currents investigated. The conduct of the tests involved increasing the cathode emission current in steps to induce increases in the beam and impingement currents. These currents were recorded manually from high accuracy digital gauges at each step. This process continued until the impingement current reached a high value ($\tilde{>}$10% of the beam current). At this time, the cathode emission current was reduced to a low value

Table 1

Test Conditions

d_s (mm)	d_a/d_s	t_s/d_s	t_a/d_s	V_D/V_T	R
2.0	0.81	0.25	0.25	0.05	0.1 - 0.8
	*0.81	0.25	0.25	0.10	0.1 - 0.8
	0.81	0.25	0.25	0.15	0.1 - 0.8
	0.81	0.25	0.13	0.10	0.1 - 0.8
	0.81	0.25	0.38	0.10	0.1 - 0.8
	0.81	0.25	0.51	0.10	0.1 - 0.8
	0.81	0.13	0.25	0.10	0.1 - 0.8
	0.81	0.38	0.25	0.10	0.1 - 0.8
	0.66	0.25	0.25	0.10	0.1 - 0.8
	1.00	0.25	0.25	0.10	0.1 - 0.8
1.5	0.66	0.25	0.25	0.10	0.2, 0.5, 0.8
1.5	1.00	0.25	0.25	0.10	0.2, 0.5, 0.8
1.0	0.66	0.25	0.25	0.10	0.2, 0.5, 0.8
1.0	1.00	0.25	0.25	0.10	0.2, 0.5, 0.8
0.5	~0.81	0.25	0.25	0.15	0.2, 0.5, 0.8

*Standard Configuration

and the ratio of net-to-total accelerating voltage was lowered to the next value of interest. The procedure of increasing the beam and impingement currents was then repeated; keeping the propellant flow rate the same. After the range of net-to-total accelerating voltages of interest had been investigated, the grid separation was reduced slightly and the above procedure was repeated. Reductions in grid separations continued until very close grid separations were obtained. For all of the testing described here the magnet current was held constant at 12 amperes. This magnet current resulted in a magnetic field strength of approximately 35 gauss at the screen grid and 45 gauss near the upstream end of the discharge chamber. The bell jar pressure was primarily a function of the propellant flow rate and it varied within the range of 1.0 - 5.0 x 10^{-5} Torr for the tests. Also, unless stated otherwise, the discharge voltage was maintained at 45 volts.

The collection of backstreaming data for each grid geometry was accomplished by reducing the magnitude of the accelerator grid potential ($|V_A| = V_T - V_N$) while watching for the rather sudden increase in beam current that is indicative of electrons backstreaming into the discharge chamber. Care was taken to try to identify as closely as possible the exact accelerator potential at which even the slightest detectable increase in beam current was observed as a result of electron backstreaming. Beam current increases of one percent were generally sufficient to ensure the occurrence of electron backstreaming. At each test point, using the procedure just described, the accelerator grid voltage at which electron backstreaming initiated was double checked. As a general rule the magnitude of these voltages agreed to within one or two volts. The average of these accelerator grid voltages was used along with the net accelerating voltage (V_N) to calculate the backstreaming limit (R_{max}),

$$R_{max} = \frac{V_N}{V_N + |V_A|}\Bigg|_{Backstreaming} \quad . \tag{15}$$

Since the grid separation and grid geometry were known, the corresponding value of the effective length ($\ell_e/d_a \cdot \exp[t_a/d_a]$) could be calculated. It will be shown later that the electron backstreaming limit is somewhat dependent on beam current or normalized perveance per hole. However, because the value of the maximum allowable net-to-total accelerating voltage ratio (R_{max}) at the impingement limited perveance is probably of the greatest interest, most of the backstreaming data was collected at or near this operating condition. The net accelerating voltage was also observed to have a minor effect on electron backstreaming, but most of the backstreaming data presented here were obtained operating at a constant net accelerating voltage of 400 V.

Because of the potentially destructive nature of the electrical breakdown phenomenon, the electrical breakdown characteristics of each of the graphite grid pairs were measured after the perveance/impingement characteristics and electron backstreaming data had been obtained. The data were collected by establishing a given grid spacing with the ion source operating at a moderate beam current. The screen and accelerator voltage were then increased in magnitude until electrical breakdown occurred. These tests indicated that either the screen or accelerator voltage could be increased to induce breakdown, i.e. the magnitude of the electric field was the critical variable in determining when breakdown occurred. The electric field at electrical breakdown is defined then as the sum of the screen voltage (V_S) and the absolute value of the accelerator voltage (V_A) divided by the grid separation (ℓ_g)

$$E_{breakdown} = \frac{V_S + |V_A|}{\ell_g} \quad . \tag{16}$$

IV. EXPERIMENTAL RESULTS

Ion Extraction

Definition of Impingement-Limited Operation

Figure 4 displays a typical curve showing how impingement current (normalized to beam current) was observed to vary as a function of beam current. At low beam currents, the curve is horizontal and the ratio of impingement to beam current is constant at a baseline impingement level determined by the rate at which charge exchange ions* strike the accelerator grid. As the beam current is increased it is seen that the curve in Fig. 4 begins to depart from the baseline level and the impingement current begins to rise abruptly. This increase in impingement current above the baseline level is due to the direct impingement of high velocity ions on the accelerator grid. Instead of presenting all performance data in the form shown in Fig. 4, it is more convenient and more meaningful for comparison purposes to define an impingement-limited beam current, i.e. the beam current at which the direct accelerator grid impingement current becomes excessive. For this paper, the impingement-limited condition is said to occur when the onset of direct

---

*A charge exchange ion results from a slow moving neutral atom which gives up an electron to a beam ion. Because of this dependence on neutral density, the baseline impingement current is primarily a function of the background (bell jar) pressure.

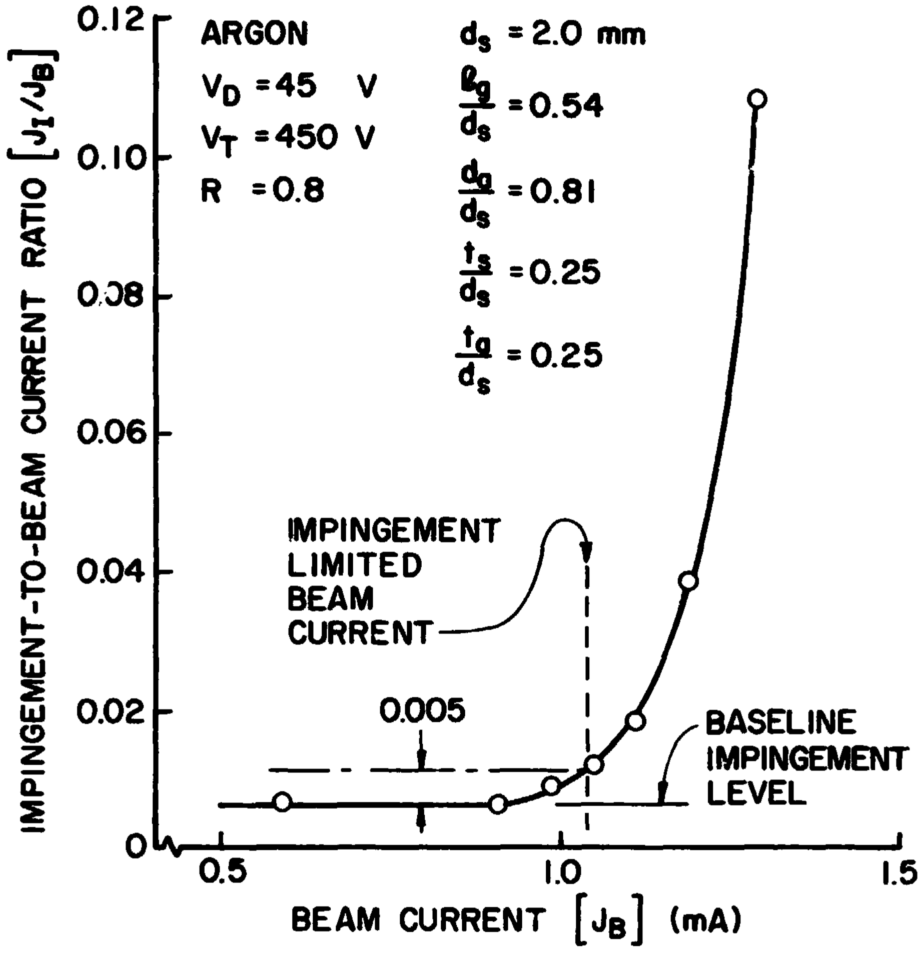

Figure 4. Characteristic Impingement-Limiting Curve

ion impingement results in an increment of 0.005 in the ratio of impingement to beam current above the baseline impingement level. The magnitude of this incremental increase, although somewhat arbitrary, was selected as a compromise between two competing considerations. First of all, it should be large enough to ensure that the increase in impingement current was indeed due to direct ion impingement and not a result of impingement current noise. On the other hand, because excessive direct ion impingement is undesirable, it should be as small as possible. The selected increment of 0.005 appeared to be an appropriate compromise which yielded consistent results. The beam current associated with this impingement-limited condition is denoted by the dashed line in Fig. 4.

For a given test, the total accelerating voltage, the grid separation distance and the hole size are known. The impingement-limited beam current can be therefore divided by the number of apertures to obtain the current per hole. The impingement-limited normalized perveance per hole can then be calculated using Eq. 7. The normalized perveance based on this definition will be used to make comparisons of the ion extraction capabilities of the various grid geometries investigated over a large range of operating conditions.

Effect of Net-to-Total Accelerating Voltage Ratio

When results like those of Fig. 4 are obtained over a range of separation distances and then impingement-limited normalized perveances are computed in the manner just described, one obtains curves like those shown in Fig. 5. In this figure, the impingement-limited normalized perveance per hole is plotted as a function of the grid separation normalized to the screen hole diameter for various ratios of the

ORIGINAL PAGE IS
OF POOR QUALITY

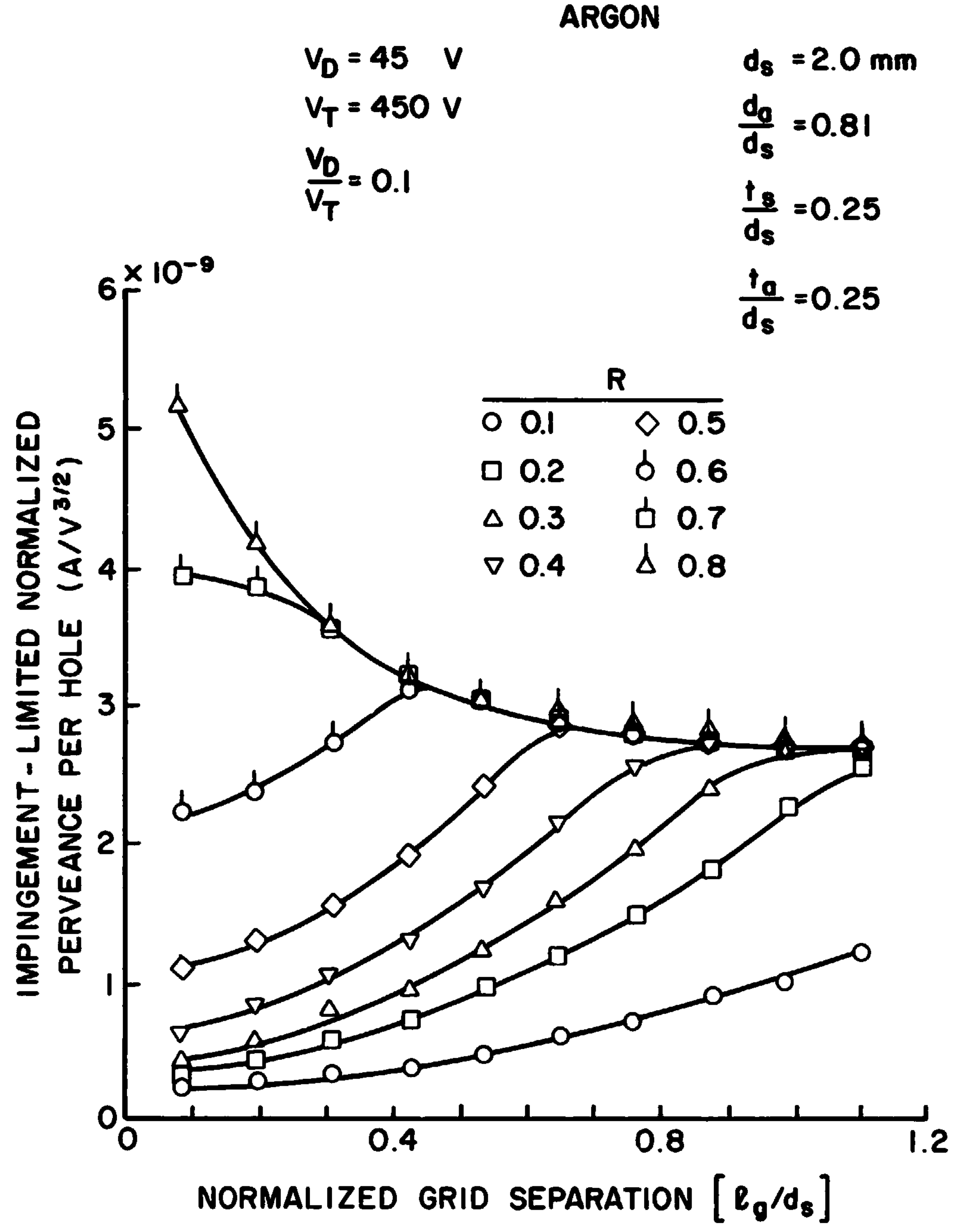

Figure 5. Effect of Net-to-Total Accelerat.ng Voltage Ratio on Ion Extraction Performance

net-to-total accelerating voltage ratio. Each of the curves in Fig. 5 corresponds to a different net-to-total accelerating voltage ratio (R). It is observed that at close grid separations increases in the ratio of net-to-total accelerating voltages always results in increased perveances (improved extraction performance). However, it is seen at larger grid separations that all the curves tend to converge to a single perveance. If the impingement-limited normalized perveance per hole was a perfect normalizing parameter over the complete range of grid separation and net-to-total accelerating voltage ratio, all of the curves would be coincident horizontal lines. Figure 5 shows that this tends to occur only at large grid separations. It is therefore argued that departures from this single value at close grid separations represent departures from the one-dimensional model on which the normalized perveance per hole is based. It is also believed that the reduction in perveance at low values of R is related to the poor focusing at lower values of R observed by Aston.[8] Although Aston reported large variations in beam divergence with R, his data did not indicate such a dramatic effect of R on the impingement-limited perveance per hole as that suggested by the results of Fig. 5. The main reason for this is considered to be due to the fact that Aston's investigation was conducted primarily at the larger grid separation ratios where single values of perveance are obtained.

In summary, the results shown in Fig. 5 indicate that the ion optics of two-grid accelerator systems are complex and are not adequately described by the one-dimensional model for space charge limited ion flow. In the one-dimensional model the acceleration length and potential difference through which the ions are accelerated are very well defined. Obviously, based on the results shown in Fig. 5 this does not appear to be true for two-grid accelerator systems, especially at smaller grid separation ratios. Also, in the one-dimensional model, ion trajectories are assumed to be one-dimensional. This is not a good assumption in the case of the two-grid accelerator system. Possible improvements to the one-dimensional model might be realized by selecting a new effective acceleration length. Such an effective acceleration length should represent a better physical description of the actual acceleration length encountered by the ions. For example, it might account for changes in the plasma sheath location that accompany changes in the extracted ion current density. It should still include the grid separation and also might include all or part of the grid thicknesses. Defining a new acceleration length was beyond the scope of this present study, however. As mentioned previously, a large body of experimental and theoretical ion extraction performance data already exist which utilize the present definition of the effective acceleration length (Eq. 6). Based on this historical usage, this effective acceleration length (ℓ_e) seemed to be the most appropriate for correlating the ion extraction performance data collected in this present work. It should be noted that regardless of the suggested improvements in the definition of the acceleration length, there would still be an effect of net-to-total accelerating voltage ratio on ion extraction performance at small grid separation ratios. Modeling the effect of the net-to-total accelerating voltage ratio on ion extraction performance represents a possible goal for future investigations.

The set of curves in Fig. 5 characterizes the ion extraction performance of the particular accelerator system geometry defined by the parameters d_a/d_s, t_s/d_s, t_a/d_s, d_s and ratio of discharge to total voltage (V_D/V_T) noted at the top of Fig. 5. The effect of variations in these parameters on the ion extraction performance will be considered in the following sections. Instead of trying to compare the ion extraction performance using all of the ratios of net-to-total accelerating voltage shown in Fig. 5, a high ratio (R = 0.8), a medium ratio (R = 0.5) and a low ratio (R = 0.2) have been selected to indicate general trends.

Effect of Discharge-to-Total Voltage Ratio

The effect of the ratio of discharge-to-total voltage on ion extraction performance is shown in Fig. 6. At large ratios of net-to-total accelerating voltage (R = 0.8) it is seen that lower ratios of discharge-to-total voltage result in increased perveances over the entire range of grid separations investigated. Similar trends hold true for the lower values of R, but it is observed that at closer grid separations the curves converge onto a single curve. In general though, lower ratios of discharge-to-total voltage result in improved ion extraction performance. This trend has been reported previously by Aston[8] and explored in more detail by Kaufman.[30] Kaufman[30] theorized that the relative effects of the discharge and total accelerating voltage on the plasma sheath cause the sheath to flatten out at high ratios of discharge-to-total voltage and thus result in the onset of impingement at lower perveances. Sheath profile data obtained by Aston[18] confirm this relative effect of discharge voltage on the contour of the sheath upstream of the screen hole.

It was of interest to determine whether or not the ion extraction performance data obtained at a particular ratio of discharge-to-total

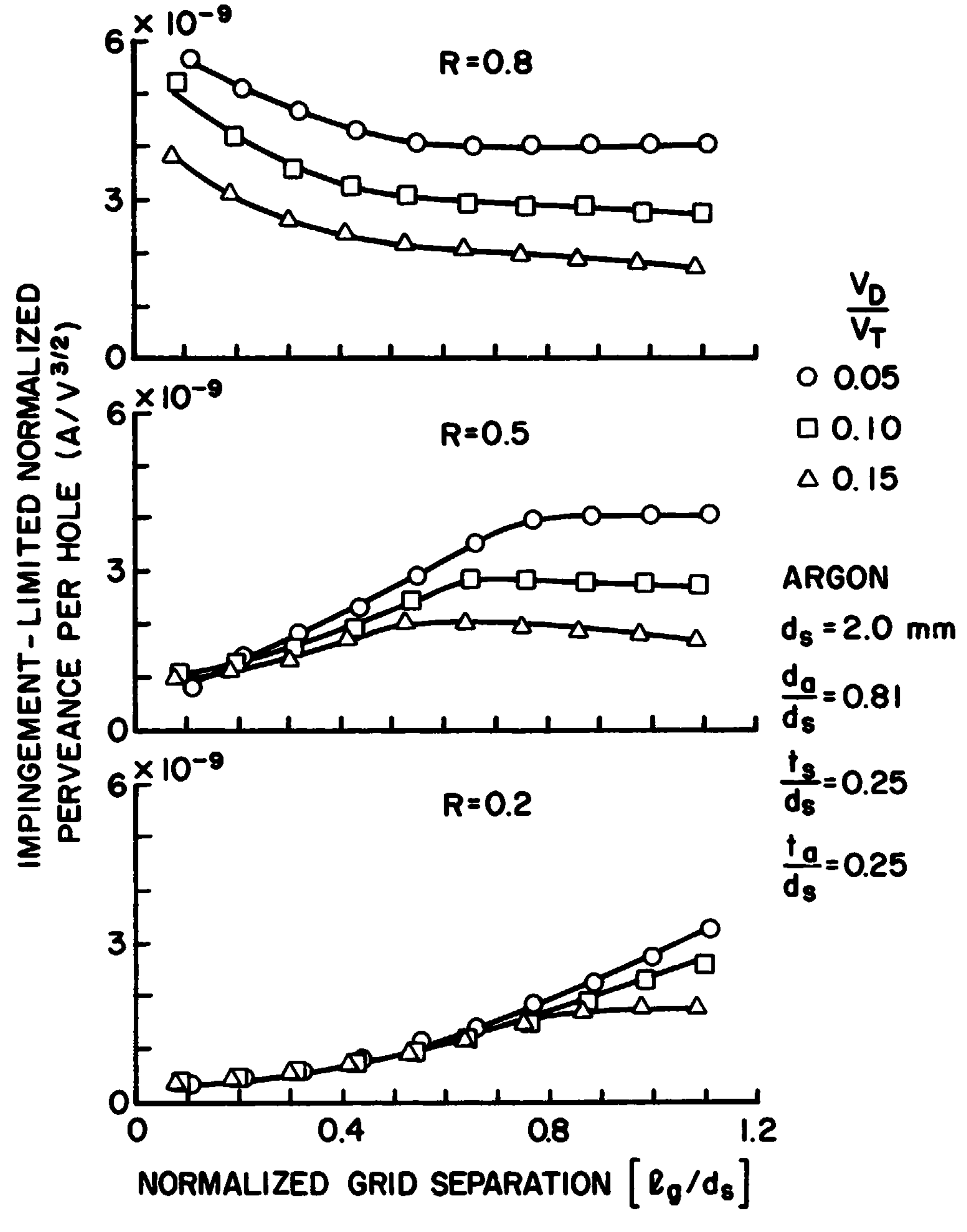

Figure 6. Effect of Discharge-to-Total Accelerating Voltage Ratio on Ion Extraction Performance

voltage was independent of the total accelerating voltage. If so, then the ion extraction performance data obtained at one total voltage would apply for any total voltage as long as the ratio of discharge-to-total voltage remained the same. To make this determination tests were conducted at total accelerating voltages of 350, 450, and 550 volts with the discharge voltage set in each case so the discharge-to-total accelerating voltage ratio was 0.1. Figure 7 shows the impingement-limited normalized perveance per hole data collected in these tests.

It is seen that the curves of constant net-to-total accelerating voltage ratios are relatively independent of the discharge and total accelerating voltages for this case where their ratio is held constant. Recently this invariance of the impingement-limited perveance with total voltage for a fixed geometry and discharge-to-total voltage ratio was verified in an independent investigation.[31]

Effect of Accelerator Aperture Diameter

In Fig. 8, the effect of variations in the accelerator hole diameter ratio (d_a/d_s) on impingement-limited perveance is shown. In general, it is observed that larger accelerator holes facilitate operation at higher perveances and therefore higher beam currents. The largest differences are seen over the entire range of grid separations for a net-to-total accelerating voltage ratio equal to 0.8. At this same net-to-total accelerating ratio of 0.8 it is observed that the curve for the largest accelerator hole diameter ratio (d_a/d_s = 1.0) does not extend to very low grid separations. It was not possible to operate at grid separation ratios below ~0.4 in this case because of the occurrence of electron backstreaming. It should be noted that some of the other geometries were near the electron backstreaming limit at

ORIGINAL PAGE IS
OF POOR QUALITY

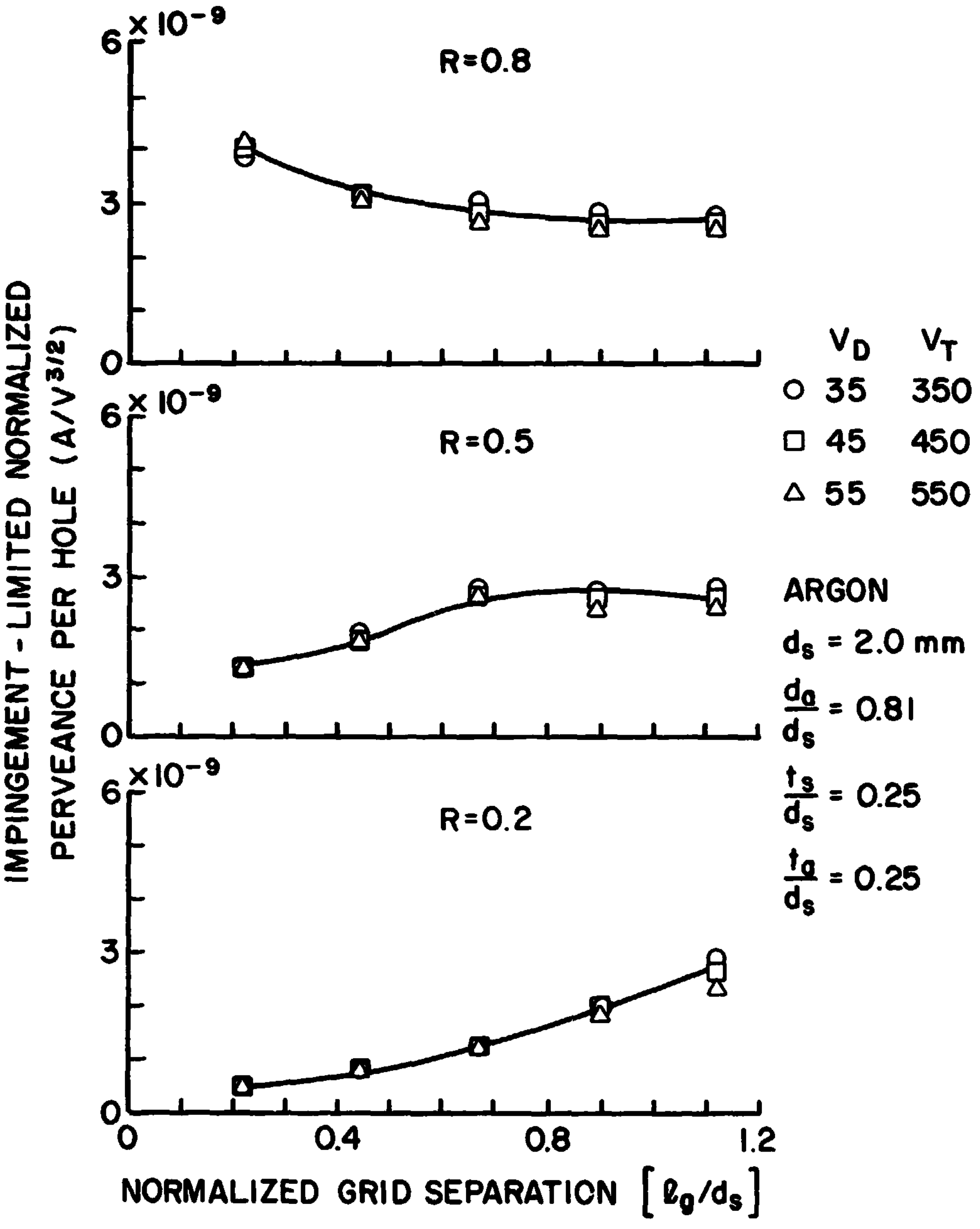

Figure 7. Effect of Total Voltage on the Ion Extraction Performance for a Specified Discharge-to-Total Voltage Ratio

ORIGINAL PAGE IS
OF POOR QUALITY

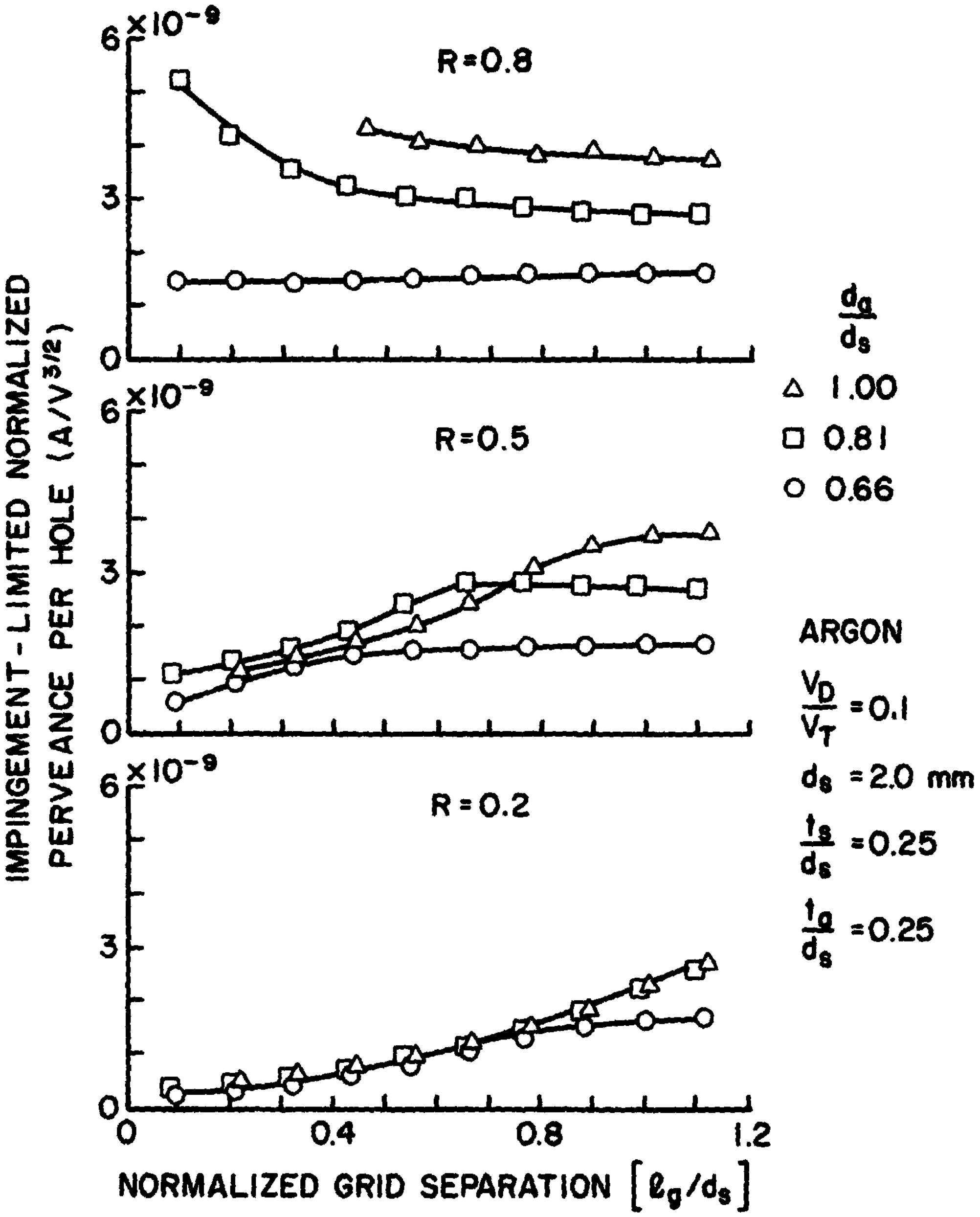

Figure 8. Effect of Accelerator Hole Diameter Ratio (d_a/d_s) on Ion Extraction Performance

very close grid separations when operating at a net-to-total accelerating voltage ratio of 0.8. However, it should be emphasized that caution was exercised not to include any data in the ion extraction performance results that might have been noticeably influenced by electron backstreaming.

The data of Fig. 8 also show for R = 0.8 that the perveance for the smallest accelerator hole diameter ratio (0.66) remained relatively constant as a function of grid separation instead of increasing to larger perveances of close grid separations as was the case for the medium ratio of $d_a/d_s = 0.81$. It is noteworthy that a similar trend to larger perveances at close grid separations was observed for the smallest accelerator hole diameter ratio ($d_a/d_s = 0.66$) but only at ratios of discharge-to-total voltage below the 0.1 value appropriate to the data of Fig. 8.

The trend of decreased ion extraction performance with decreased accelerator hole diameter was expected and has been reported in previous experimental and theoretical investigations.[5,8] There is, however, an exception that is of particular interest. At close grid separations for R = 0.5 it is seen that the impingement-limited perveance for the largest accelerator hole diameter ratio tested ($d_a/d_s = 1.0$) falls slightly below that for the medium ratio ($d_a/d_s = 0.81$). This is believed to be a real effect and will be discussed in greater detail in a later section.

Effect of Grid Thicknesses

Figure 9 shows the effect of accelerator grid thickness ratio on the impingement-limited perveance. The only significant effect on ion extraction performance is observed at close grid separations for a

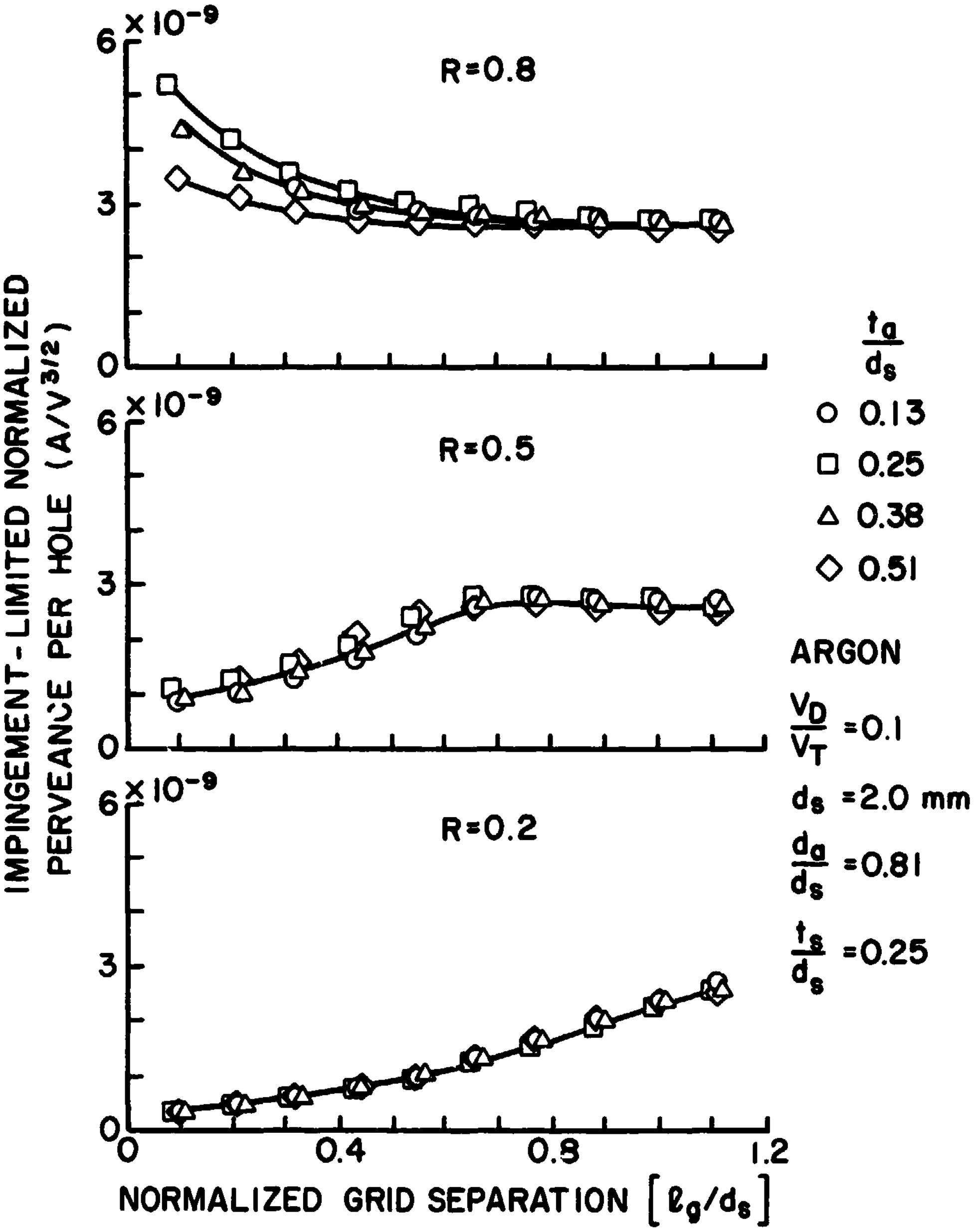

Figure 9. Effect of Accelerator Grid Thickness Ratio (t_a/d_s) on Ion Extraction Performance

net-to-total accelerating voltage ratio of 0.8. Even then, there is no consistent trend, except it is seen that the perveance levels of the thickest accelerator grid lies substantially below the others. This is consistent with the results obtained by Aston[8] who reported significant decreases in ion extraction performance only at fairly large ratios of accelerator grid thickness ($t_a/d_s \geq 0.6$).

Figure 10 shows the effect of screen grid thickness ratio on the impingement-limited perveance. At large grid separations and high R values it is seen that operation with thinner screen grids facilitates operation at higher perveances. For the medium and low ratios of net-to-total accelerating voltage ratio, however, this difference disappears at close grid separations. It is noteworthy that previous investigators operating at fixed grid separations have reported similar general trends of decreased perveance levels with increased relative screen grid thicknesses.[8,20]

Effect of Screen Grid Hole Size

A major consideration of this study was the investigation of the effect of operating with screen grid hole diameters below 2.0 mm on ion extraction performance. In Figures 11-13 the impingement-limited perveance levels obtained with screen grid hole diameters smaller than 2.0 mm are compared to those obtained with 2.0 mm diameter holes. Figures 11 and 12 compare the performance of 1.0, 1.5 and 2.0 mm diameter holes for the accelerator hole diameter ratios, of 0.66 and 1.00 respectively. These figures do not appear to show any consistent trends that would indicate a decrease in performance with decreasing hole size. Similarly, this observation has been verified recently in an independent investigation for screen grid hole diameters as small as

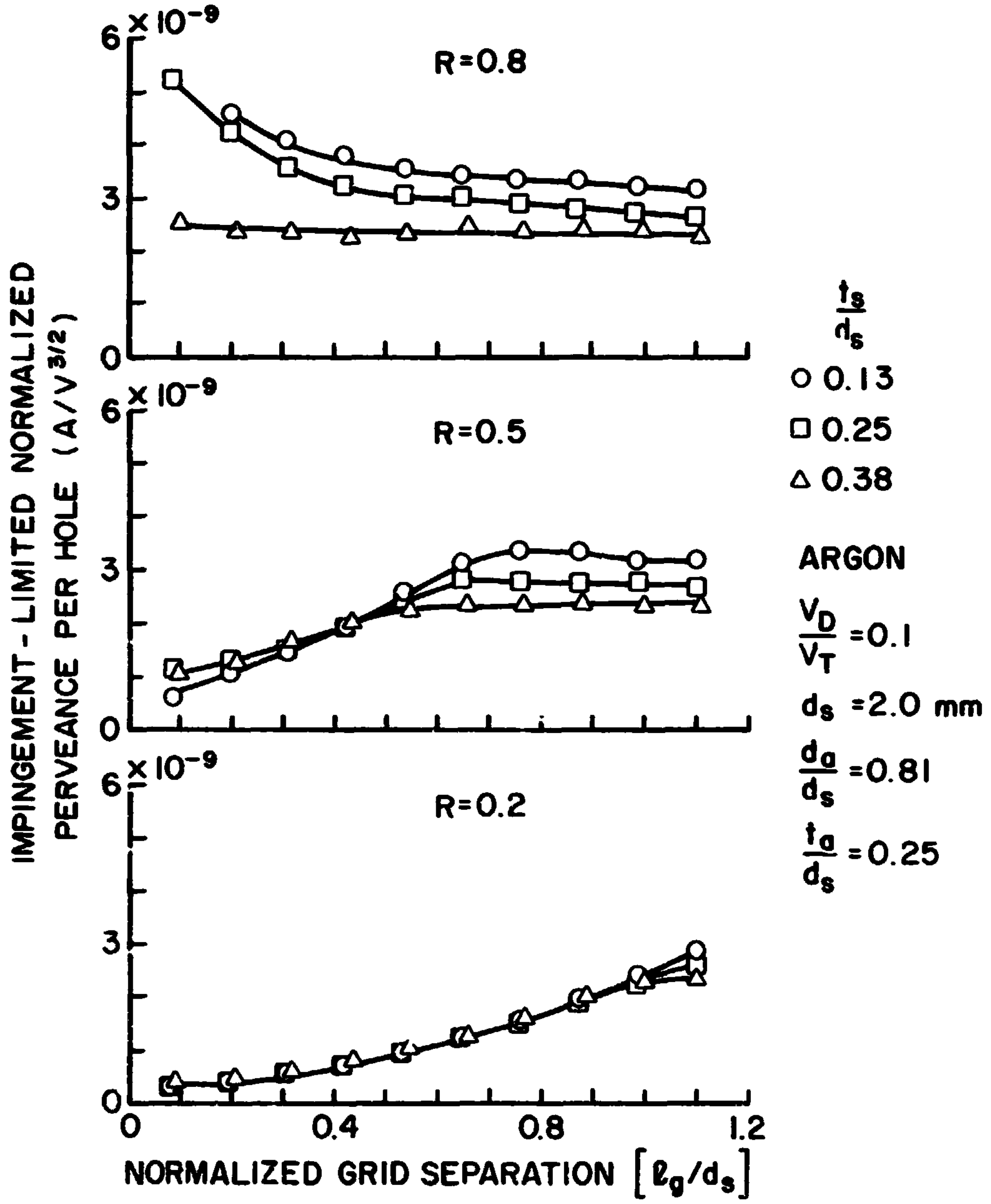

Figure 10. Effect of Screen Grid Thickness Ratio (t_s/d_s) on Ion Extraction Performance

ORIGINAL PAGE IS
OF POOR QUALITY

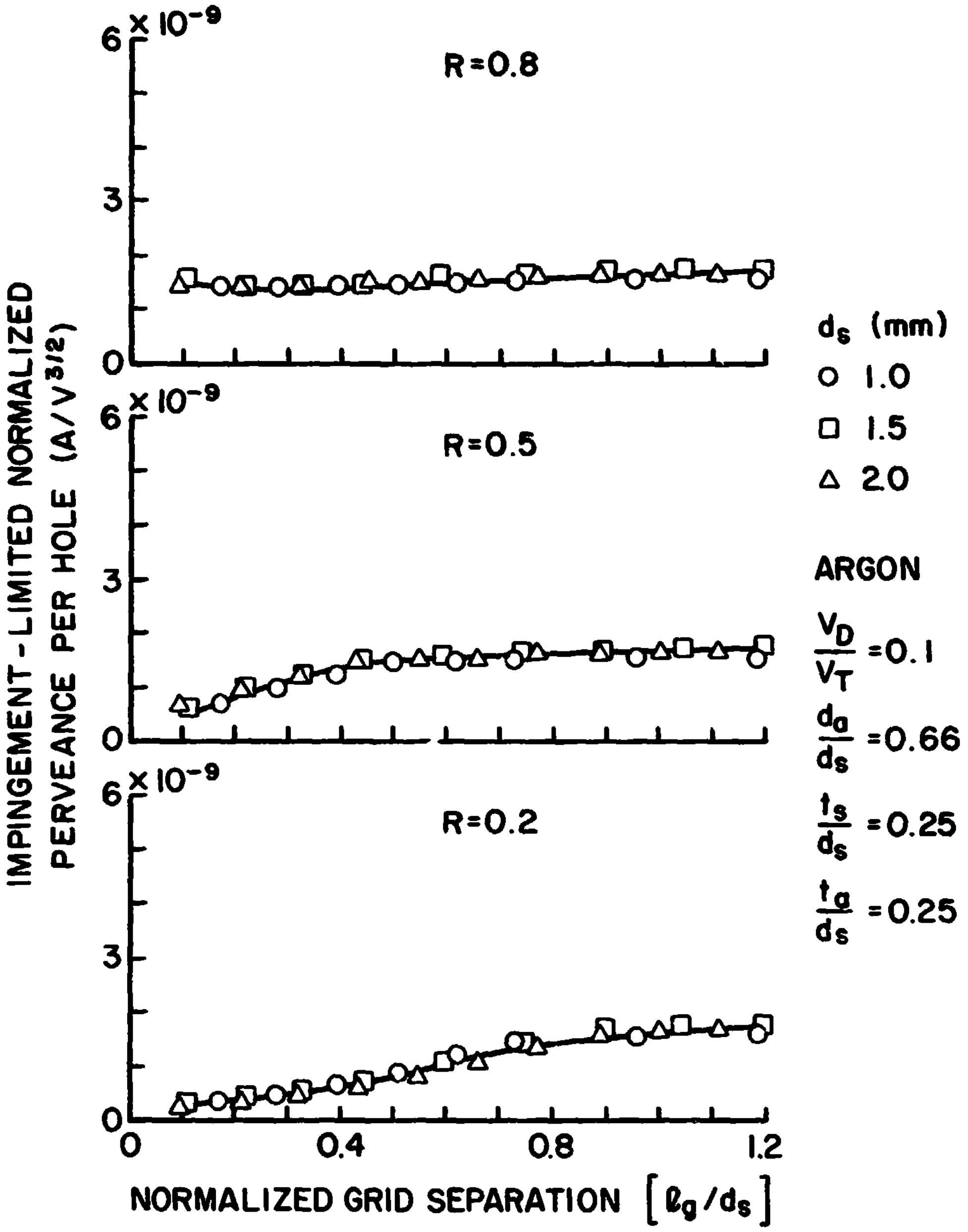

Figure 11. Effect of Screen Grid Hole Diameter on Ion Extraction Performance (small accelerator hole diameter ratio: $d_a/d_s = 0.66$)

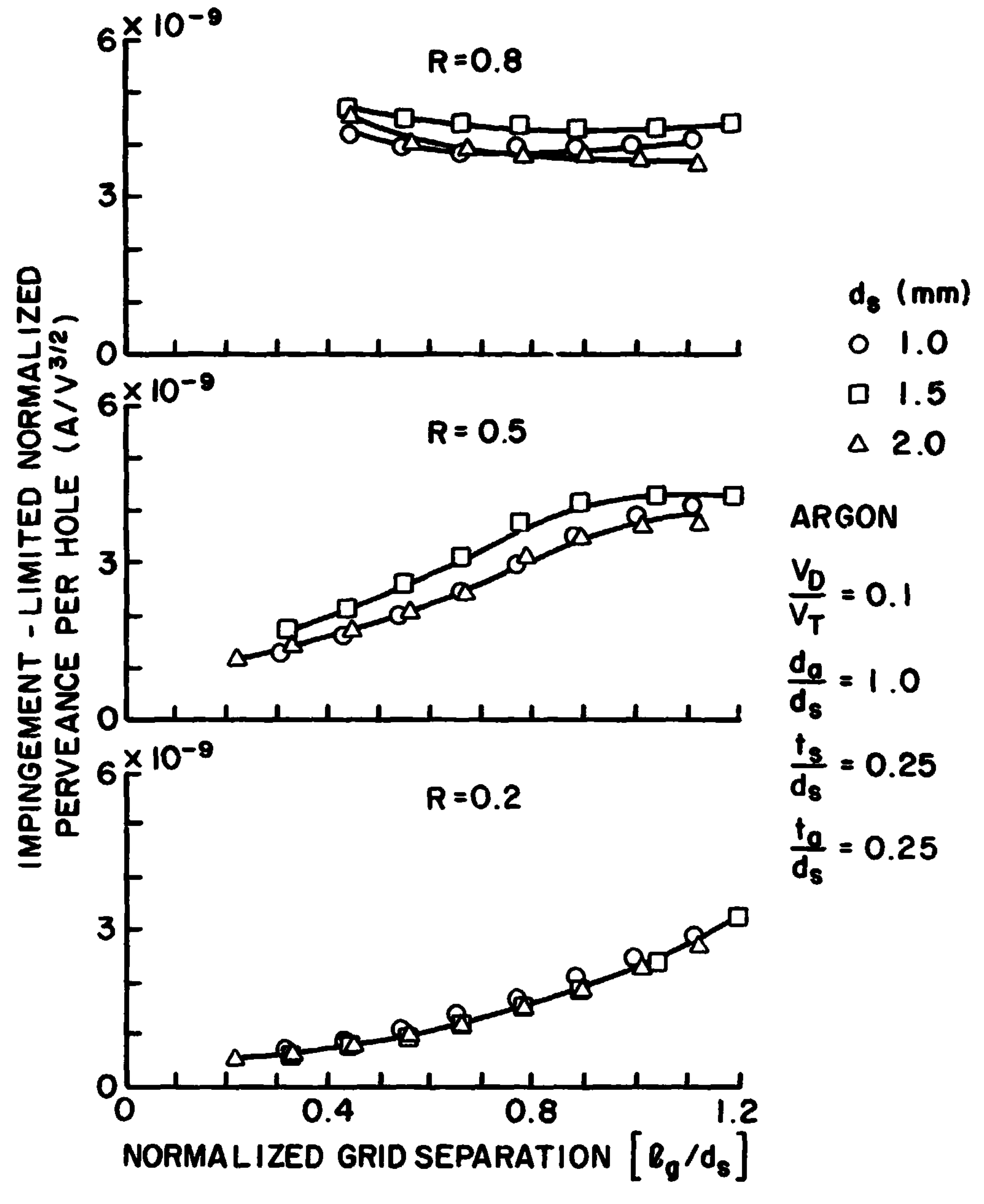

Figure 12. Effect of Screen Grid Hole Diameter on Ion Extraction Performance (large accelerator hole diameter ratio: d_a/d_s = 1.00)

ORIGINAL PAGE IS
OF POOR QUALITY

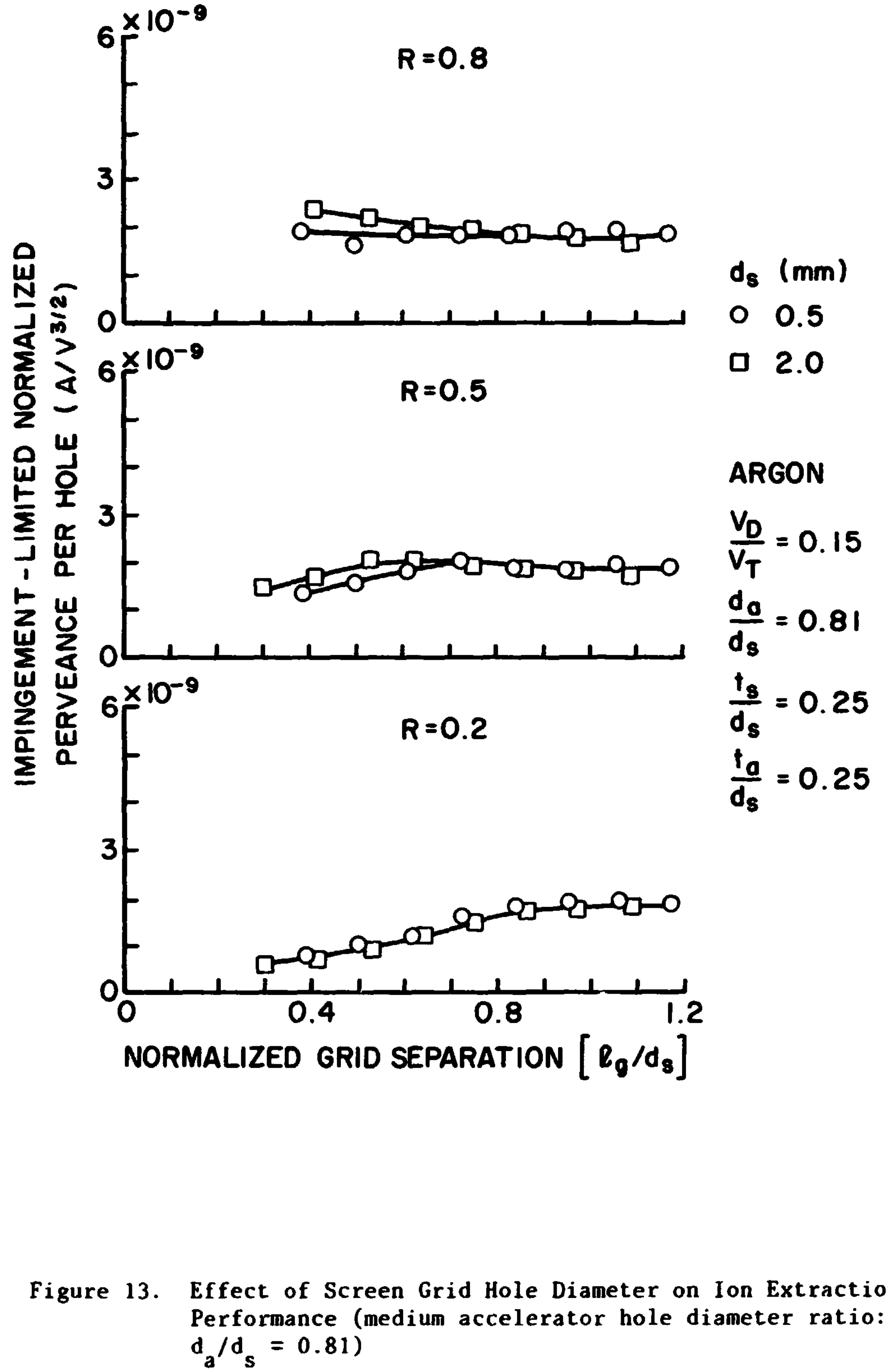

Figure 13. Effect of Screen Grid Hole Diameter on Ion Extraction Performance (medium accelerator hole diameter ratio: $d_a/d_s = 0.81$)

1.0 mm.[32] It should be noted that the grids with 1.0 mm and 1.5 mm diameter screen grid holes were manufactured and aligned in a similar fashion to those with 2.0 mm diameter holes. Using this conventional method of construction and alignment, attempts were made to extend the operation to screen grid hole diameters of 0.5 mm. These results suggested a decrease in ion extraction performance below the levels obtained for the larger diameter holes. The inability to align these smaller holes was suspected to be the cause of the poor performance. In order to ensure alignment, in a separate test the accelerator grids were ion machined in situ. This machining process yielded a slight spread (±0.05 mm) in accelerator hole diameters with an average diameter of 0.4 mm. In Fig. 13 the perveance levels obtained in this test are compared to those of the 2.0 mm diameter holes for an accelerator hole diameter ratio of 0.81 and a discharge-to-voltage ratio of 0.15. The similarity of perveance levels shown in Fig. 13 suggest that accelerator system operation without reductions in ion extraction performance is possible with screen grid hole diameters as small as 0.5 mm. This observation differs from what was expected based on previous experimental investigations that reported a decrease for screen grid hole diameters below 2.0 mm.[8,11-13] The reason for this disparity remains uncertain. However, based on the results and observations made during this investigation, certain possible explanations can be theorized.

It was noted above that only after hole alignment was ensured for the 0.5 mm diameter screen grid holes did the performance return to the levels obtained with the larger diameter holes. Based on this observation, it is proposed that misalignment of the screen and accelerator holes represents a possible explanation for the reductions in performance observed previously. It is also noteworthy that the conventional hole alignment technique used in this study differed somewhat from that of the previous investigations reporting reductions in performance for screen grid hole diameters below 2.0 mm. The variable grid spacing apparatus used in this study allowed the holes to be aligned with the grids touching and then later separated for testing. In the previous investigations, the grid systems required alignment of the holes with grids separated. This improvement in alignment technique might account for part of the reason why in this investigation normal grid operation could be extended to screen grid holes as small as 1 mm in diameter before encountering apparent alignment problems. Another consideration is that, except for the one conducted by Aston,[8] the other investigations were conducted with large diameter accelerator systems with thousands of holes. Their complexity makes the alignment of smaller holes more difficult. In any case, it should be emphasized that hole alignment is considered crucial to the success of operating with small screen hole diameters.

Another factor which was found to influence the ion extraction performance was the stability of the discharge chamber plasma. During a segment of the tests the discharge chamber was changed to a design that operated less stably (arc discharge noise being apparent on an oscilloscope). The onset of high impingement currents occured at lower perveance levels with this design than it did with the more stable one. In light of this observation, previous attempts to operate with smaller holes and higher current densities may have resulted in decreased performance due to unstable discharge chamber operating conditions.

As a final note, in this study when considering the ion extraction performance of the different screen grid hole diameters, only those results obtained with similar normalized grid geometries (ℓ_g/d_s, d_a/d_s, t_s/d_s, t_a/d_s) and similar operating conditions (V_D/V_T, R) were compared. This is important because it has been shown that the ion extraction performance is a function of those parameters.

Application to Design

Although the impingement-limited normalized perveance per hole is useful for correlating data, it is not easy to use directly to decide at what grid separation ratio and ratio of net-to-total accelerating voltage one should operate in order to maximize the beam current or beam current density for a specified net accelerating voltage. This information can, however, be obtained from curves similar to those shown in Fig. 5, if one assumes that for a particular ratio of discharge-to-total voltage these same curves would be obtained at other total accelerating voltage levels. Fortunately, this independence of the impingement-limited normalized perveance curves from the total accelerating voltage has been demonstrated (Fig. 7). Thus for source operation at the minimum flow rate required for stable operation, the impingement-limited normalized perveance per hole (P_I) is primarily a function of the net-to-total accelerating voltage ratio, the ratio of the discharge-to-total voltage and the grid geometry, i.e.

$$P_I = P_I \left(R, \frac{V_D}{V_T}, \frac{\ell_g}{d_s}, \frac{d_a}{d_s}, \frac{t_a}{d_s}, \frac{t_s}{d_s}\right) \qquad (17a)$$

or

$$\frac{J}{V_T^{3/2}} \left(\frac{\ell_e}{d_s}\right)^2 = P_I \left(R, \frac{V_D}{V_T}, \frac{\ell_g}{d_s}, \frac{d_a}{d_s}, \frac{t_a}{d_s}, \frac{t_s}{d_s}\right) \qquad (17b)$$

Dividing Eq. (17b) by $R^{3/2}$ and $\left(\frac{\ell_e}{d_s}\right)^2$, yields,

$$\frac{J}{V_N^{3/2}} = P_I \left(R, \frac{V_D}{V_T}, \frac{\ell_g}{d_s}, \frac{d_a}{d_s}, \frac{t_s}{d_s}, \frac{t_a}{d_s}\right) R^{-3/2} \left(\frac{\ell_e}{d_s}\right)^{-2} . \qquad (18)$$

The term on the left, which will be referred to as the impingement-limited current parameter, is useful because it facilitates a comparison of the maximum current per hole obtainable as a function of the net accelerating voltage as opposed to the total accelerating voltage. The reason for this is mainly due to the fact that the impingement-limited normalized perveance per hole is normalized with respect to the total accelerating voltage and not to the net accelerating voltage. Figure 14 shows a cross plot of data taken from Fig. 5 at three different grid separation ratios. In this figure the impingement-limited normalized perveance per hole is plotted as a function of the ratio of net-to-total accelerating voltage. This figure also includes additional data collected at net-to-total accelerating voltage ratios of 0.45, 0.55, 0.65 and 0.75. Using Eq. 18, the values of impingement-limited normalized perveance per hole found along the curves shown in Fig. 14 can be used to calculate the impingement-limited current parameter. The data of Fig. 14 have been replotted in Fig. 15 with the impingement-limited current parameter rather than the impingement-limited normalized perveance per hole as the dependent variable. Figure 15 shows the highest beam currents per hole are achieved at the lowest net-to-total accelerating voltage ratios and that the magnitudes of these currents are relatively independent of grid separation. At small grid separation ratios high current levels are also achieved at an optimum ratio of net-to-total accelerating voltage. The peaks in

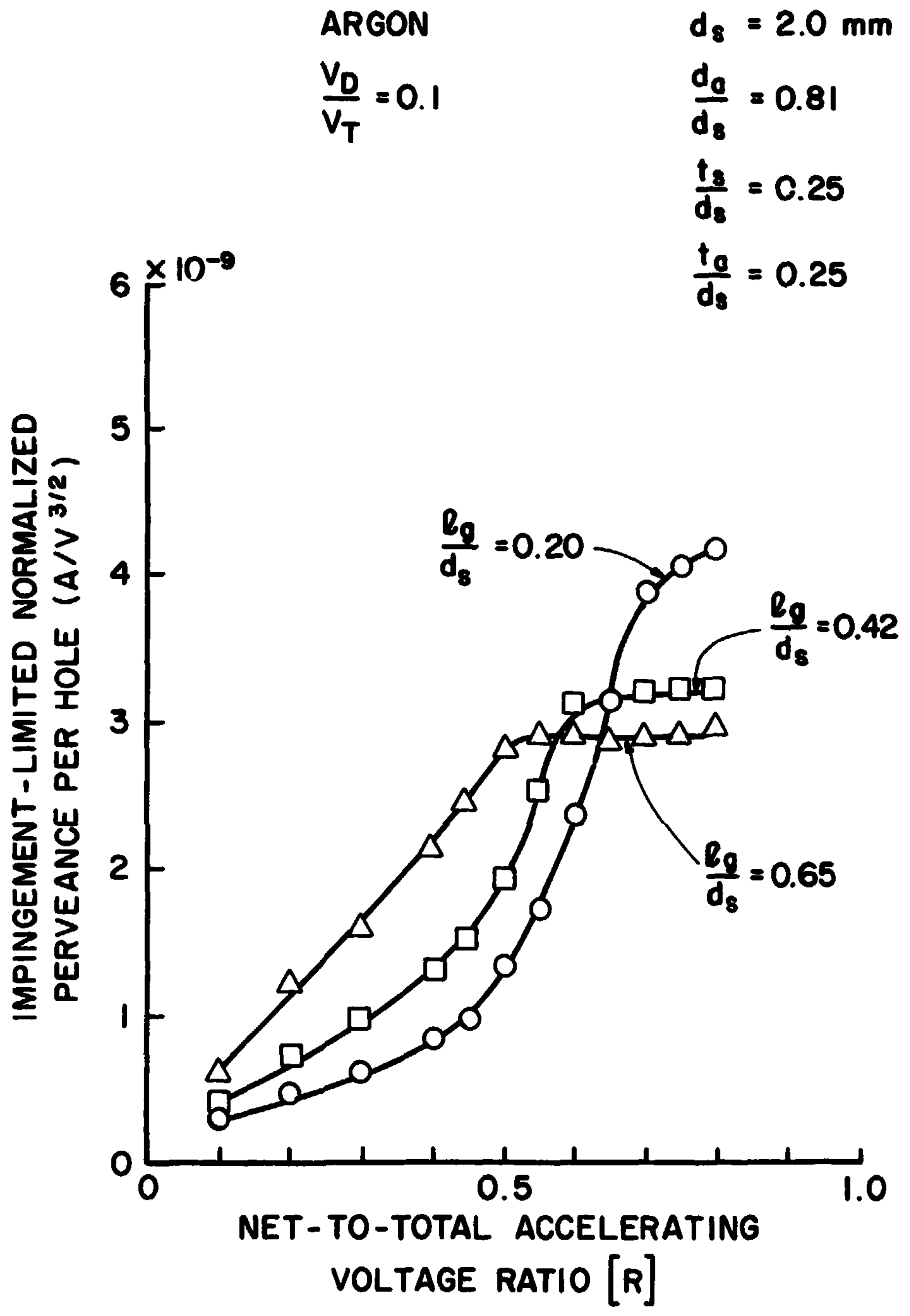

Figure 14. Cross Plot of Impingement-Limited Perveance as a Function of Net-to-Total Accelerating Voltage Ratio

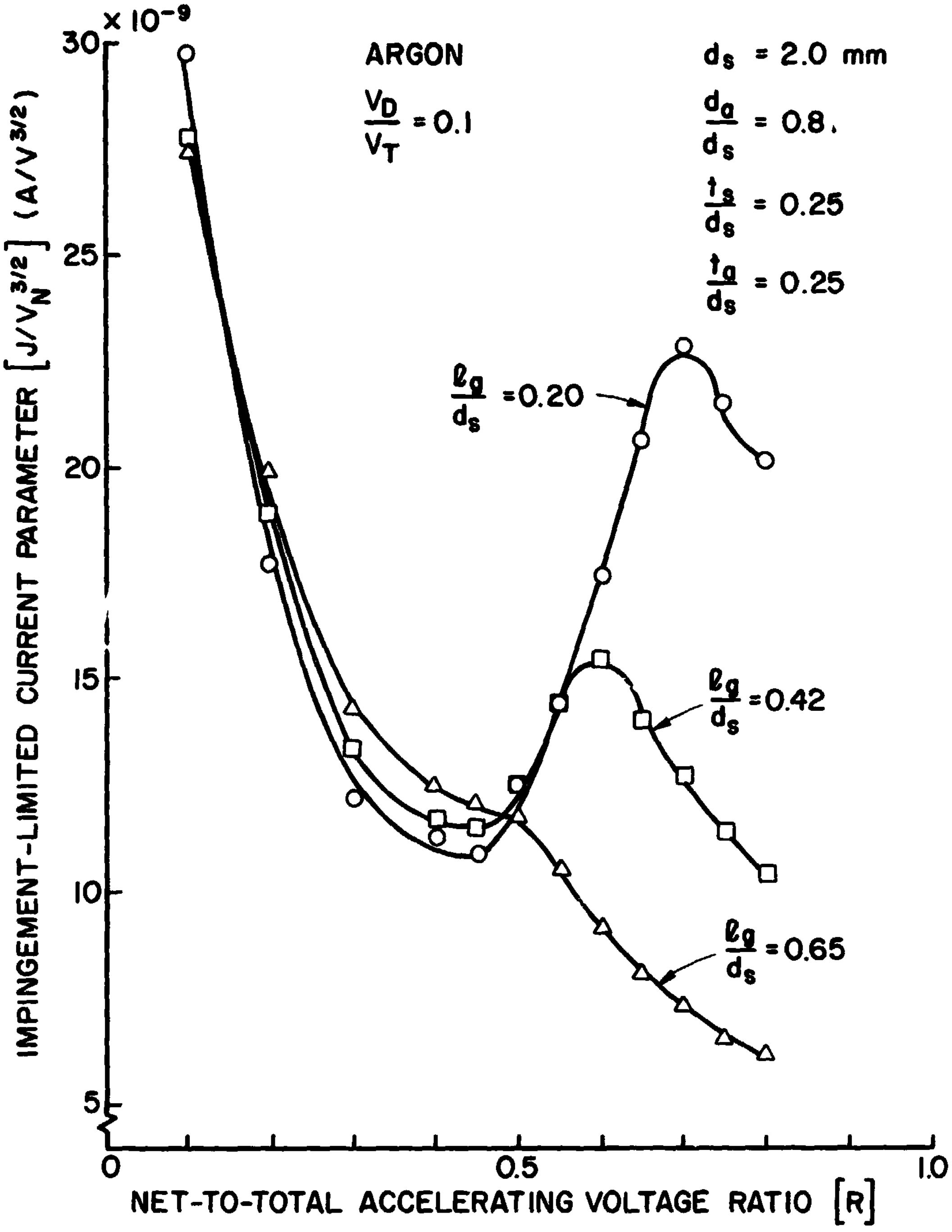

Figure 15. Comparison of Impingement-Limited Current Levels as a Function of Grid Separation and Net-to-Total Accelerating Voltage Ratio

the curves of Fig. 15 at these optimum R values represent the maximum currents achievable at close grid separations and high ratios of net-to-total accelerating voltage. It should be noted that even higher beam currents could presumably be realized at the peak by further reducing the grid separation and operating at R values above ~0.70 where the $\ell_g/d_s = 0.2$ curve peaks. The grid separation could presumably continue to be reduced until the onset of electron backstreaming or electrical breakdown occurred.

For operation at high beam current density levels the results of Fig. 15 seem to suggest the choice of operating at low ratios of net-to-total accelerating voltage or at high ratios of net-to-total accelerating voltage and small grid separation ratios. However, because of some other considerations, this observation is not as straight-forward as it may first appear. To illustrate, a design example using the results of Fig. 15 is considered.

The results of Fig. 15 suggest that similar values of the impingement-limited current paramter ($\sim 22.5 \times 10^{-9}$ A/V$^{3/2}$) would be obtained by operating either at the peak of the curve for $\ell_g/d_s = 0.2$ where $R \cong 0.7$ or at a net-to-total accelerating voltage ratio of 0.15. The interesting thing to note about operation at $R = 0.15$ is that for the range of normalized grid separation appropriate to Fig. 15 ($0.2 < \ell_g/d_s < 0.65$) the impingement-limited current parameter appears to be independent of the grid separation ratio. Because of manufacturing and mechanical design constraints, one of the first dimensions usually specified in the design of a large diameter accelerator system is the grid separation distance necessary to maintain a minimum span-to-gap ratio. Under the constraint of maintaining this design limited grid separation distance, operation at larger grid separation ratios could be accomplished by selecting smaller screen grid holes. These smaller screen grid holes would facilitate more holes per unit area of the grids and thus higher beam current densities. In the particular case under consideration here, for a fixed grid separation distance, an increase in the grid separation ratio from 0.2 to 0.65 translates roughly into a screen hole diameter three times as small. Since the area of the hole scales with the square of hole diameter, this means that approximately nine times as many holes could fit into the same size accelerator system and, as a result, a nine fold increase in current density could be achieved. From the standpoint of obtaining higher densities, the preceding comparison suggests that when the grid separation distance is fixed, it is advantageous to operate with smaller holes at low ratios of net-to-total accelerating voltage and large grid separation ratios as opposed to high ratios of net-to-total accelerating voltage and small grid separation ratios. This statement presumes that the impingement-limited current parameter is not a function of screen grid hole size. Because the impingement-limited current parameter is based directly on the impingement-limited normalized perveance per hole, it is argued that the observed invariance with hole size demonstrated in these tests for perveance therefore applies similarly to the impingement-limited current parameter.

Besides current density, there are still other considerations that need to be addressed when trying to decide between operating at a high value of R or at a low value of R. When operating two-grid accelerator systems at low ratios of net-to-total accelerating voltage one observes:

1) Higher total voltages. For a fixed net accelerating voltage lower ratios of net-to-total accelerating correspond to higher total voltages. To avoid electrical breakdown these higher total voltages may require operation at larger grid separations. It is conceivable that eventually these increased grid separations would result in decreased beam current per hole. This would tend to reduce the increased current densities noted above for operation at low ratios of net-to-total accelerating voltage and large grid separation ratios.

2) More divergent beams. Aston[8,9] found that decreasing the net-to-total accelerating voltage ratio generally increases overall ion beam divergence. These more divergent beams result in a thrust loss due to off-axis velocity components of the ions.

3) Rapid rise to excessive impingement. At very low ratios of net-to-total accelerating voltage ($R < 0.3$), the rate of increase to high impingement levels with increases in beam current was observed in these tests to be more dramatic than it was at higher ratios. This increased sharpness of the "knee" on the characterstic impingement-limited curve (Fig. 4) could present problems for a thruster operating near the impingement limit because a small fluctuation in thruster operating conditions might cause a dramatic and undesirable increase in impingement current.

4) Higher baseline levels of impingement. In Fig. 16, representative data showing how the baseline ratio of impingement-to-beam current was observed to increase with decreasing

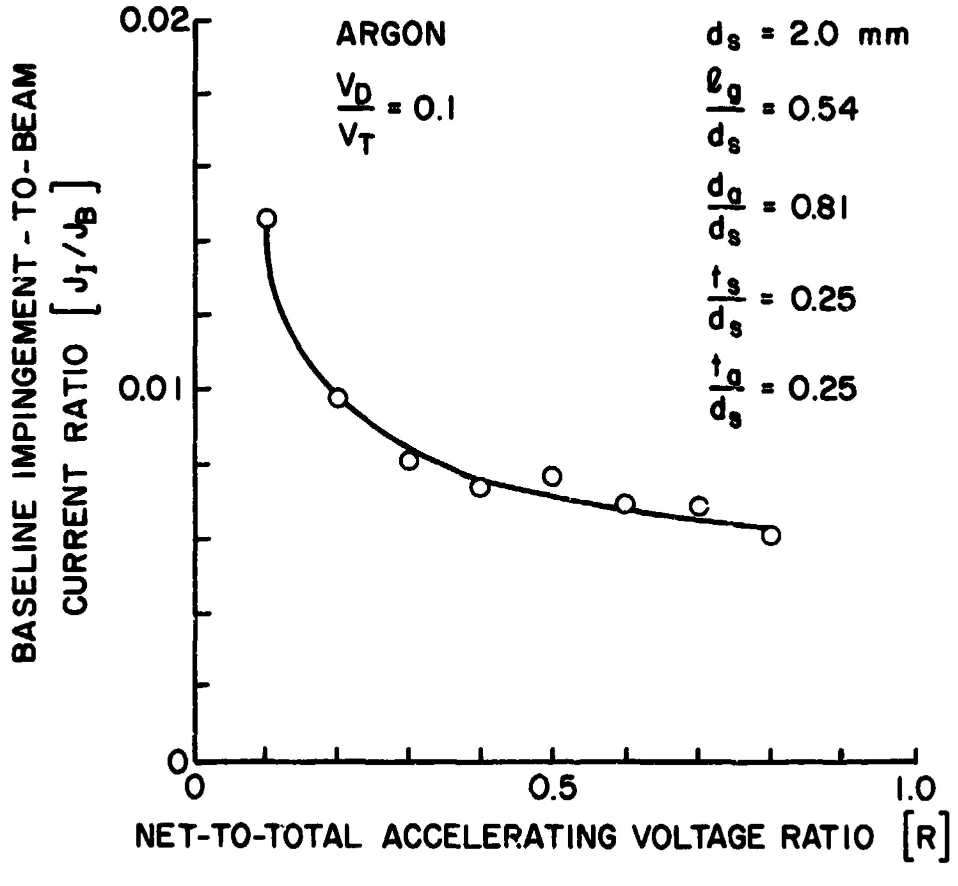

Figure 16. Effect of Net-to-Total Accelerating Voltage Ratio on the Baseline Impingement Level

ratios of net-to-total accelerating voltage is shown. The increase in baseline impingement current levels is not believed to be attributable to increases in bell jar pressure because it remained the same for all of the data shown in Fig. 16. Part of the increase in impingement current observed at the lower values of R can be attributed, however, to larger collisional cross sections for charge exchange. Using the empirical relationship developed by Robinson[33] for the charge exchange cross section of argon, calculations show that changing from a net accelerating voltage of 315 V (R = 0.8), to 45 V (R = 0.1) would only result in a 20% increase in the charge exchange cross section. Although, it is in the right direction, this increase in cross section only accounts for a small fraction of the increase in impingement current suggested by the data shown in Fig. 16. The reason for the remainder of the increase in impingement current remains uncertain. It is speculated that at the very low ratios of net-to-total accelerating voltage, the ion focusing has deteriorated to the point where a measurable amount of direct ion impingement is evidenced at all beam current levels. If this is so, then decreased thruster efficiency and decreased accelerator grid lifetimes would be expected.

5) Higher energy charge exchange ions. As the ratio of net-to-total accelerating voltage is reduced the negative potential on the accelerator grid increases. This results in an increase in the energies of charge exchange ions striking the

accelerator grid. These higher energy ions would result in increased erosion rates and shorter accelerator grid lifetimes.

All of these disadvantages must be weighed against the advantage of obtaining higher beam current densities by operating with low ratios of net-to-total accelerating voltage and large grid separation ratios as compared to operating at high ratios of net-to-total accelerating voltage and small grid separation ratios. The only perceived disadvantage to operating at high ratios of net-to-total accelerating voltage as opposed to low ratios is the greater likelihood of electron backstreaming at higher ratios.

The usefulness of the impingement-limited current parameter as a design tool is further demonstrated in Fig. 17. In this figure the impingement-limited current parameter is plotted as a function of the ratio of net-to-total accelerating voltage for three different accelerator hole diameter ratios operating at the same normalized grid separation. The most interesting point to be made concerning the results shown in Fig. 17 is that at larger ratios of net-to-total accelerating voltage the highest impingement-limited current levels are obtained not with the largest accelerator hole diameter but rather with the second largest. This is an important result because it is preferable from the discharge chamber viewpoint to operate with smaller accelerator grid holes in order to minimize the loss of unionized propellant. Heretofore, it was generally accepted that grids should be operated with the largest possible accelerator grid holes ($d_a/d_s = 1.0$) to achieve the highest beam currents. Hence, the objectives for high beam currents and low neutral propellant loss were in conflict. However, the results

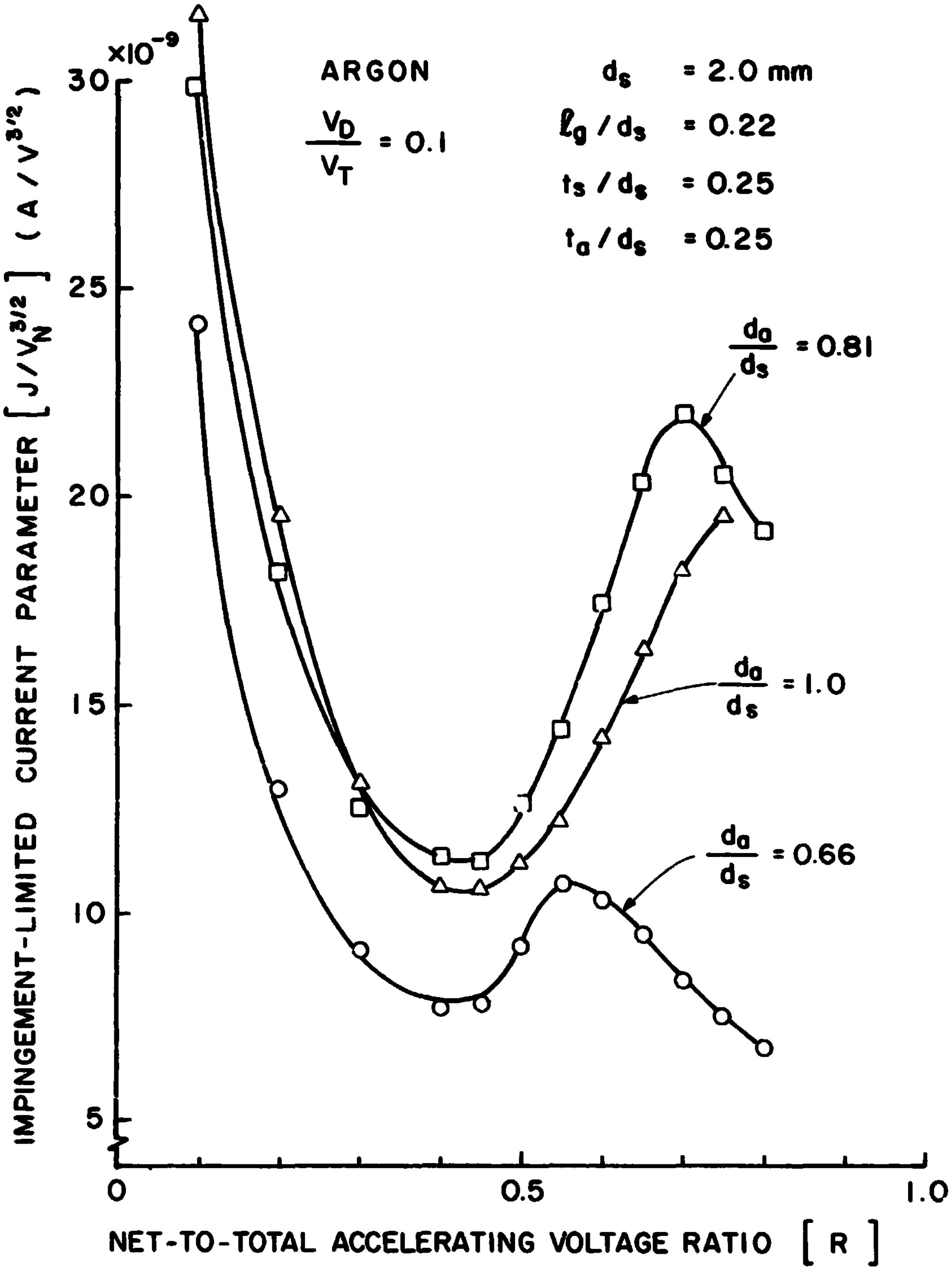

Figure 17. Comparison of Impingement-Limited Current Levels as a Function of Accelerator Hole Diameter Ratio and Net-to-Total Accelerating Voltage Ratio

of Fig. 17 suggest that at small grid separations ratios and medium to high ratios of R, it is sometimes unnecessary and even self-defeating to try and achieve higher beam currents by utilizing very large accelerator hole diameter ratios ($d_a/d_s = 1.0$). It should be noted that the data point for $d_a/l_s = 1.0$ and $R = 0.8$ was not included in Fig. 17 because of the occurrence of electron backstreaming.

The observed reduction in impingement-limited current for the accelerator hole diameter ratio of unity is inconsistent with the trend toward higher current levels that are generally expected for larger accelerator hole diameter ratios. It is postulated that increases in the accelerator grid hole diameter ratio cause the potential difference between the center of the accelerator grid hole and the accelerator grid proper to become larger. This results in increased defocusing in the region of the accelerator grid. It is argued that at close grid separations with large accelerator holes this reduced ion focusing is communicated upstream into the screen grid hole in a manner that causes the onset of direct ion impingement at reduced beam currents.

In earlier sections the effects of variations in accelerator system geometry and operating conditions on the impingement-limited perveance were examined at selected ratios of net-to-total accelerating voltage ($R = 0.2$, 0.5, 0.8). It should be noted, however, that a complete tabular listing of the experimental results for the entire range of ratios investigated, from $R = 0.1$ to 0.8 for 2.0 mm diameter screen holes can be found in Appendix B. The data contained in Appendix B represent design data which can be used to make comparisons similar to those shown in Figs. 15 and 17. Because the ion extraction performance was demonstrated to be relatively independent of the screen grid hole size, it is argued that the data contained in Appendix B can be applied to any screen grid hole size as long as the normalized geometrical parameters are the same.

Other Considerations

The effects of variations in accelerator system geometries and operating conditions considered thus far in this thesis represent the main focus of this investigation. There are, however, some other effects and considerations that should be taken into account when considering ion extraction performance results and their application to accelerator system design.

As mentioned previously, for the data analysis used herein, the impingement limit was based on a very modest increase in impingement current above the baseline level. To be precise, it was defined at the point where direct ion impingement of the accelerator grid resulted in an increment of 0.005 in the ratio of impingement-to-beam current above the baseline impingement level, ($\delta(J_I/J_B) = 0.005$). Because this definition was somewhat arbitrary, it is worthwhile to consider the sensitivity of the results to this definition. Figure 18 shows how allowing operation of higher levels of direct ion impingement generally resulted in increased perveance levels. It is seen, however, that the shapes of the curves at each ratio of net-to-total accelerating voltage remain qualitatively the same. The proximity of the curves to one another gives a rough indication of the relative sharpness of the "knee" on the impingement-limiting curve. The proximity of the curves shown for a net-to-total accelerating voltage ratio of 0.2 verify the statement made earlier concerning the rapid rise to excessive impingement levels observed for very low values of R. It was also observed

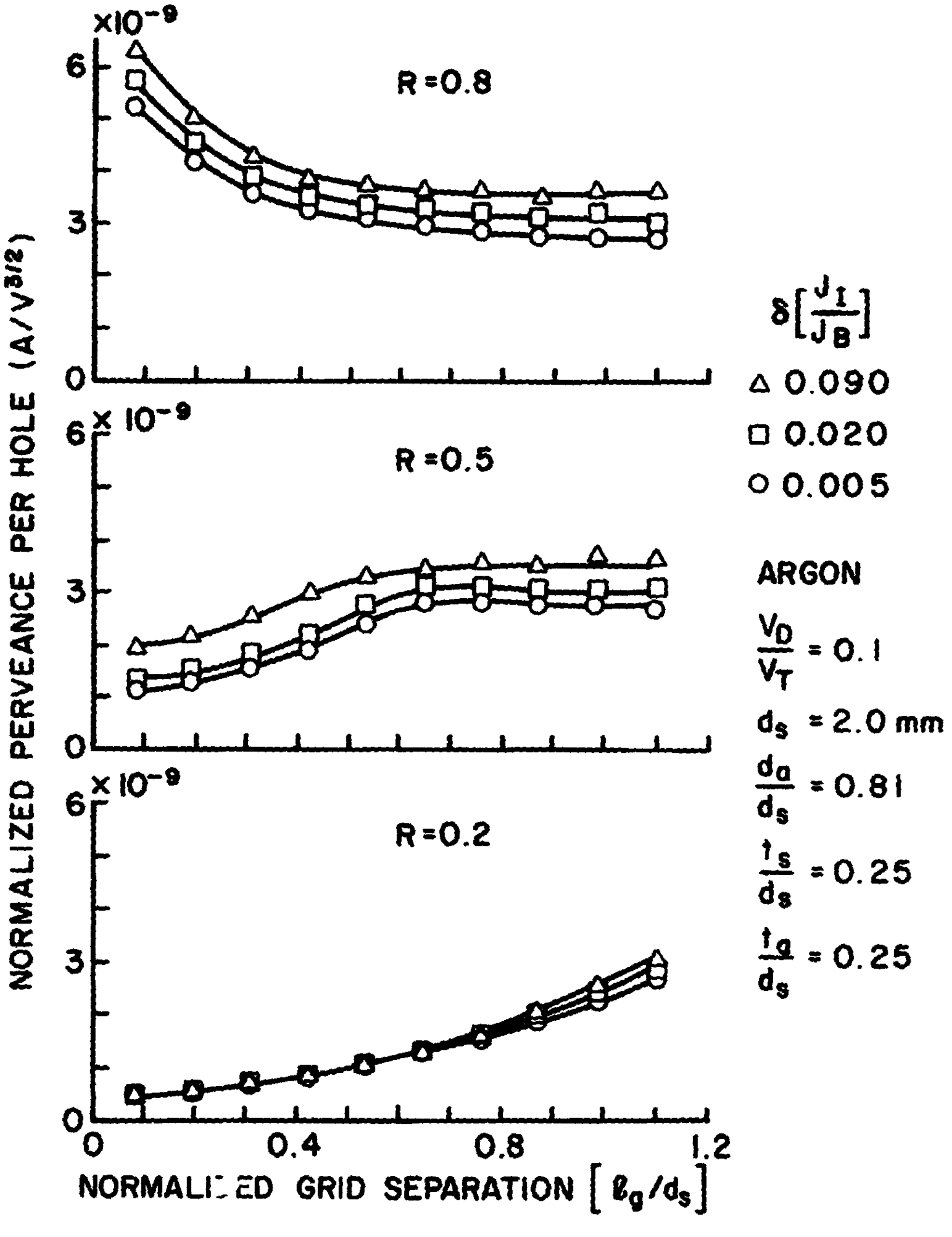

Figure 18. Effect of Changes in the Definition of the Impingement-Limited Operating Conditions on the Ion Extraction Performance Results

during these experiments that impingement versus beam current curves obtained with smaller ratios of discharge-to-total voltage characteristically had sharper knees. The most important point to make concerning the results of Fig. 18 is that the obtainable perveance levels are somewhat dependent on the definition of the impingement limit. Consequently, knowledge of how impingement-limited operation is defined is important when applying ion extraction performance results to accelerator system design.

Figure 19 shows the effect of propellant flow rate on the impingement-limited normalized perveance per hole. Each of the flow rates shown represents a multiple of the minimum propellant flow rate required to maintain stable source operation over a complete range of beam currents. The circular symbols represent the minimum required flow rate which was also the standard flow rate used throughout this investigation. It is seen from Fig. 19 that for the most part increases in the flow rate by a factor of 2 and 3 did not have a dramatic effect on the ion extraction performance. An interesting distinction, however, can be made between the results obtained for a net-to-total accelerating voltage ratio 0.5 and those results obtained for the ratio of 0.8. At close grid separation for $R = 0.8$ it is seen that increases in flow rate resulted in decreased perveance levels, while the opposite appears to occur for $R = 0.5$.

During the early part of this investigation other factors related to the discharge chamber operation were determined to influence the ion extraction performance. One of the parameters identified was the cleanliness of the anode surface. Before measures were taken to ensure the cleanliness of the anode surface, fairly large unexplained fluctuations

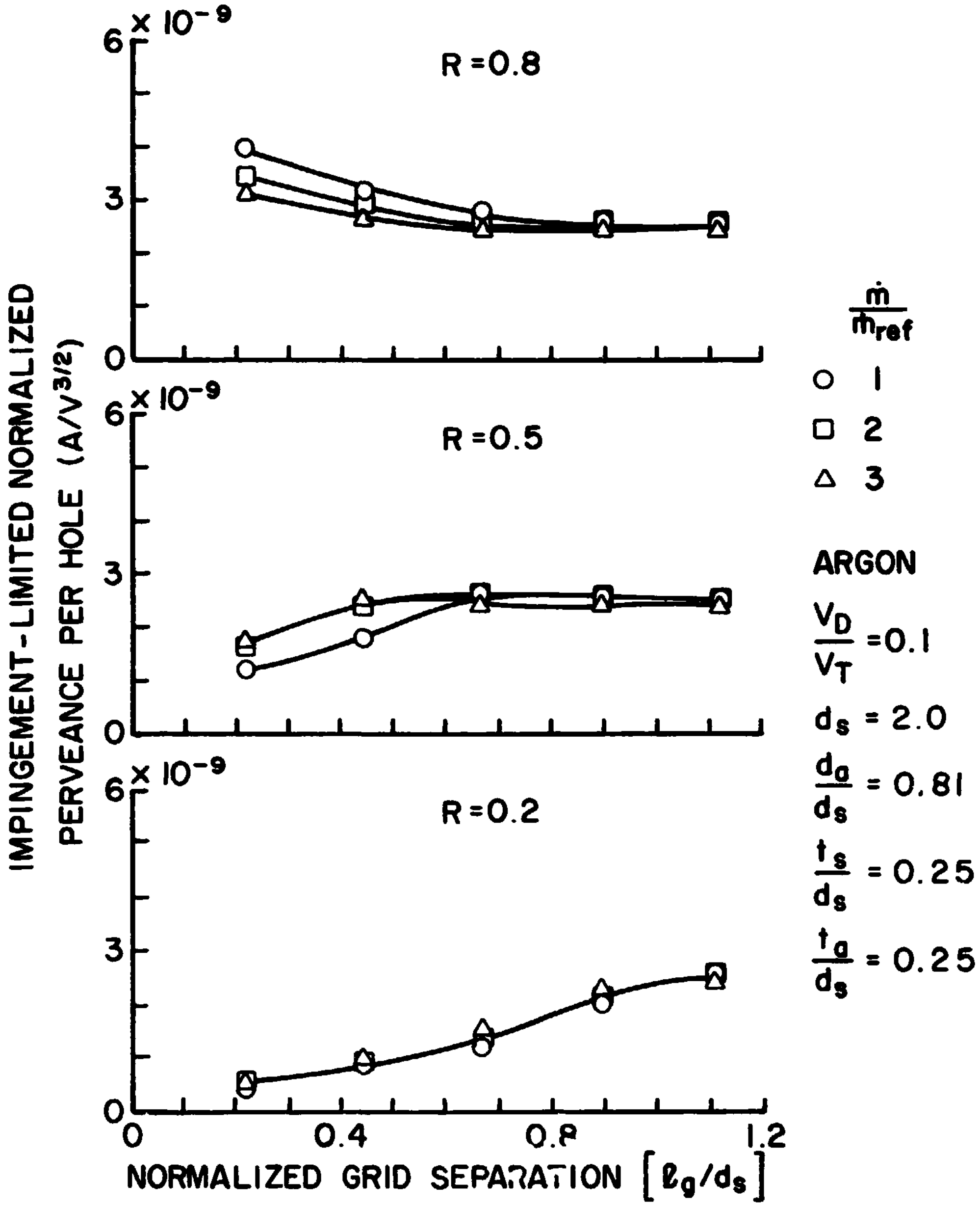

Figure 19. Effect of Propellant Flow Rate on Ion Extraction Performance

in the impingement-limited perveance would result. The results of Fig. 20 give an indication of the magnitude of the observed fluctuations in the impingement-limited normalized perveance per hole for a net-to-total accelerating voltage of 0.8. After implementing procedures to ensure a clean anode surface at the start of each experiment, the reproducibility of the ion extraction data improved to the level suggested by Fig. 21. Another discharge chamber related effect was the reduction in impingement limited perveance levels observed with a less stable discharge.

Considering the effects of the aforementioned discharge chamber parameters on ion extraction performance, the application of the ion extraction performance results of this investigation to thrusters incorporating different discharge chamber designs might be questioned. Because considerable effort was taken to minimize the changes in these discharge chamber parameters during the investigation of the effects of variations in the accelerator system geometries and operating conditions, it is reasoned that those results are self-consistent and that similar qualitative conclusions based on those results would be drawn regardless of the discharge chamber design. However, it is believed that slight quantitative differences can be expected between different discharge chamber designs. The exact mechanisms by which each of these different discharge chamber parameters affect the ion extraction performance are not presently understood and their investigation were beyond the scope of this present study. Changes in the discharge chamber design or operating conditions may cause changes in the bulk plasma properties such as plasma potential, electron temperature, and the ratio of primary to Maxwellian electron densities. These changes,

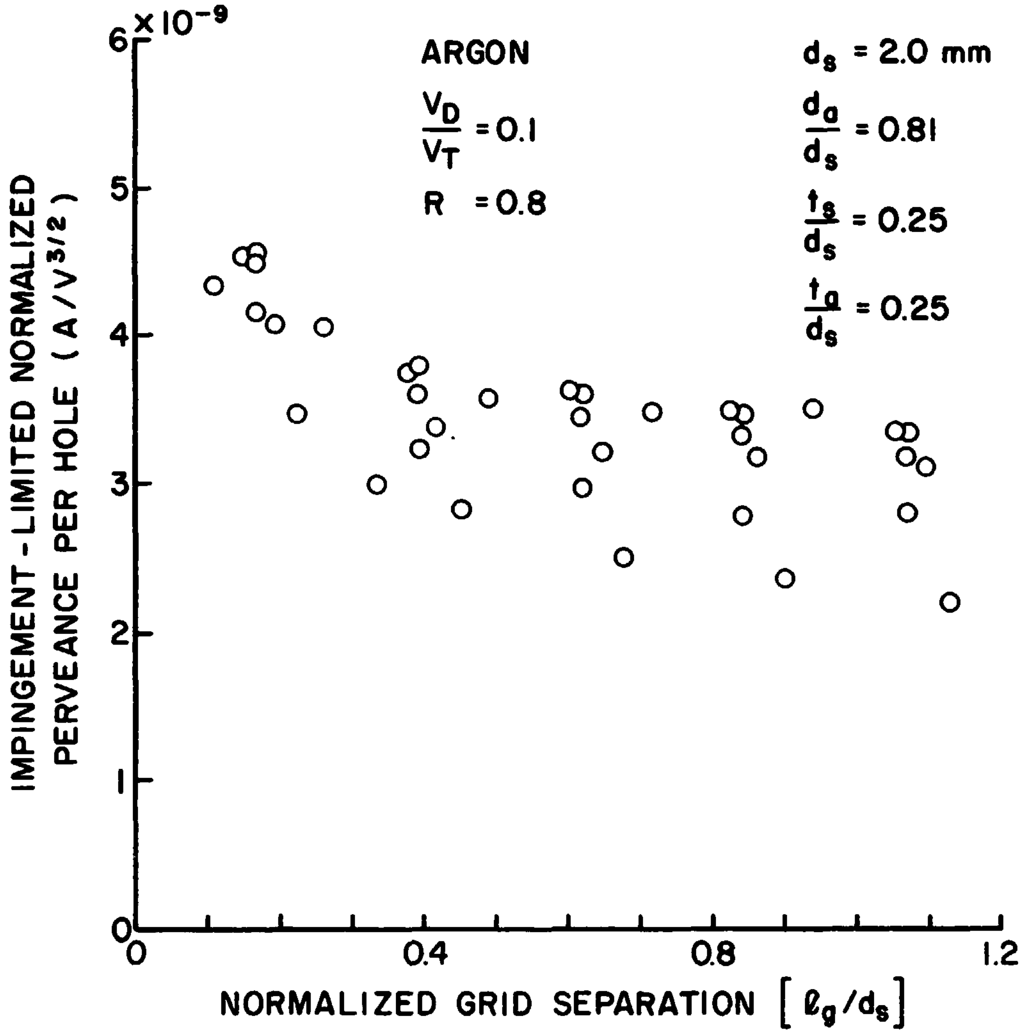

Figure 20. Characteristic Scatter in Ion Extraction Performance Results Before Implementing Improved Experimental Technique

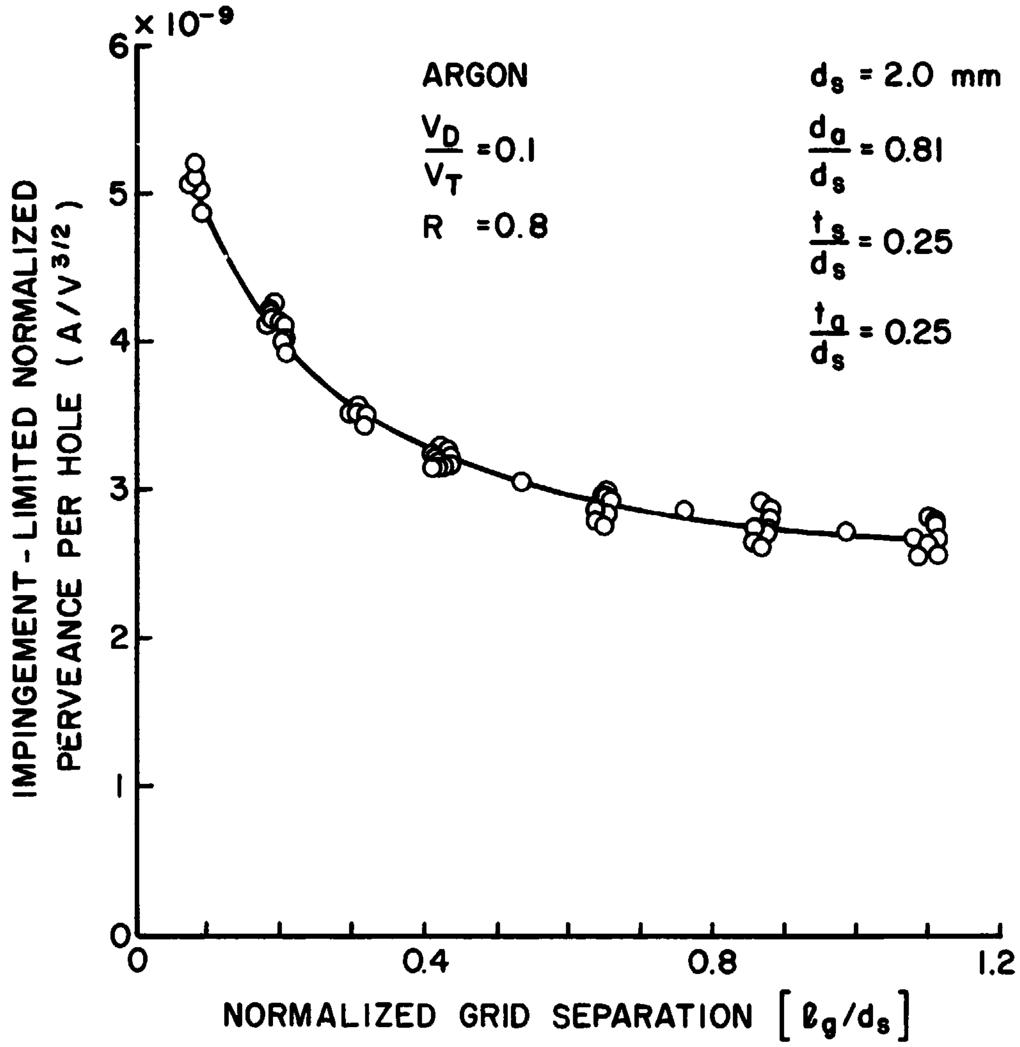

Figure 21. Characteristic Scatter in Ion Extraction Performance Results After Implementing Improved Experimental Technique

in turn, alter the shape of the screen grid hole plasma sheath which affects the ion focusing. It is proposed that understanding these mechanisms more thoroughly represents a potential area of investigation for future studies.

Electron Backstreaming

Because the variable grid spacing apparatus facilitated operation over a wide range of grid separations, this apparatus was found to be well suited for measuring the electron backstreaming characteristics of the various grid pairs used in this investigation. The effect of the ion beam current or perveance on the electron backstreaming limit (R_{max}) is shown in Fig. 22 where these quantities are plotted for three different grid separations. The data of Fig. 22 were obtained with the standard grid geometry. It is seen that at each grid separation lower perveance levels facilitate operation at higher ratios of net-to-total accelerating voltage before electron backstreaming occurs. This effect is even more pronounced at closer grid separations. The data points at the maximum perveance for each of the curves in Fig. 22 represents operation near the impingement-limited condition. Most of the experimental electron backstreaming data in this study were collected with the accelerator system operating near this impingement limit because it represents the worst case and also because ion thrusters would typically operate near that condition. In Fig. 23 the effect of variations in the net accelerating voltage on the backstreaming limit are shown as a function of the normalized grid separation. It is seen that only at close separations and net accelerating voltages below 400 V do changes in net accelerating voltage cause a significant change in the backstreaming limit. The effects of variations in the net accelerating

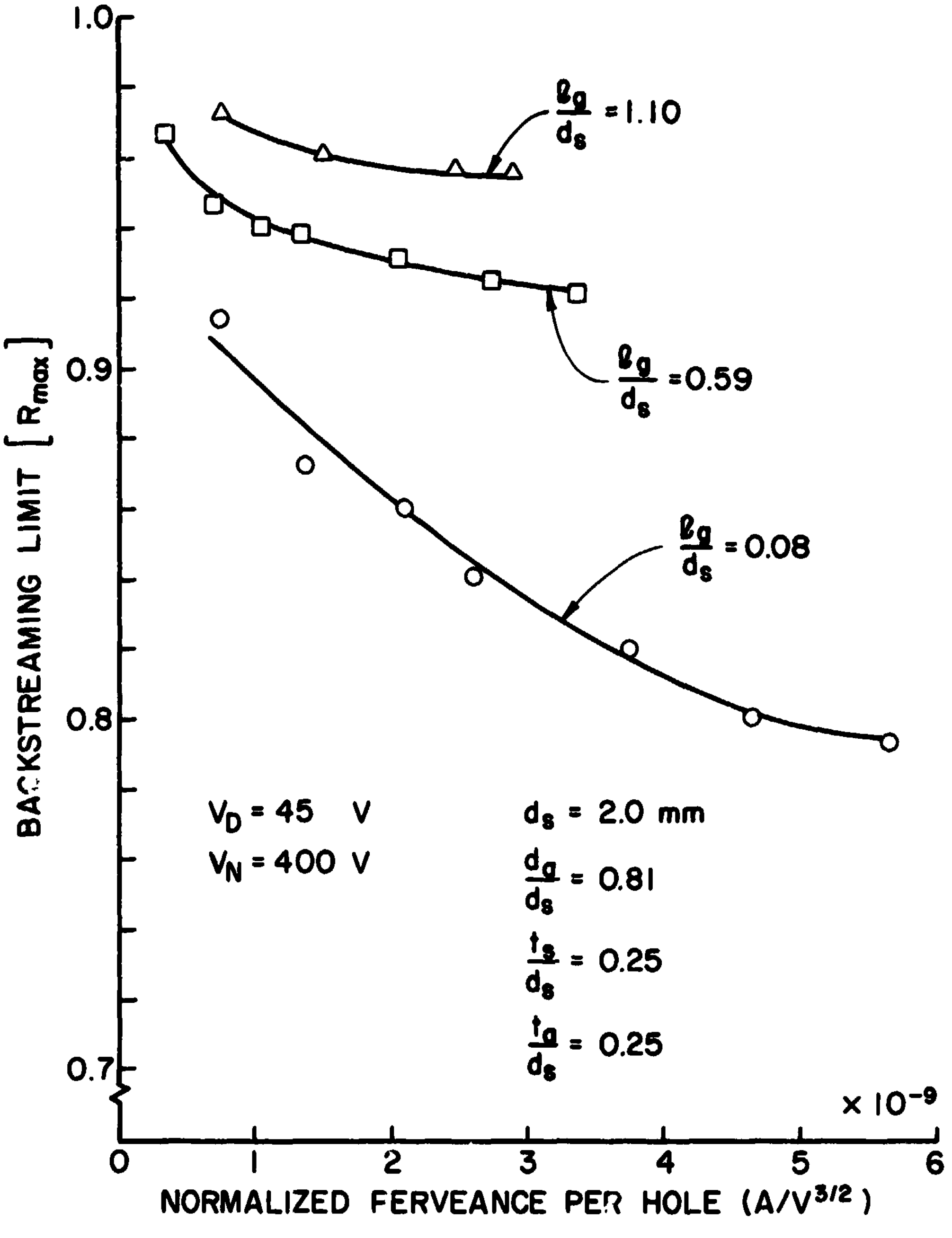

Figure 22. Effect of Perveance on Electron Backstreaming Limit

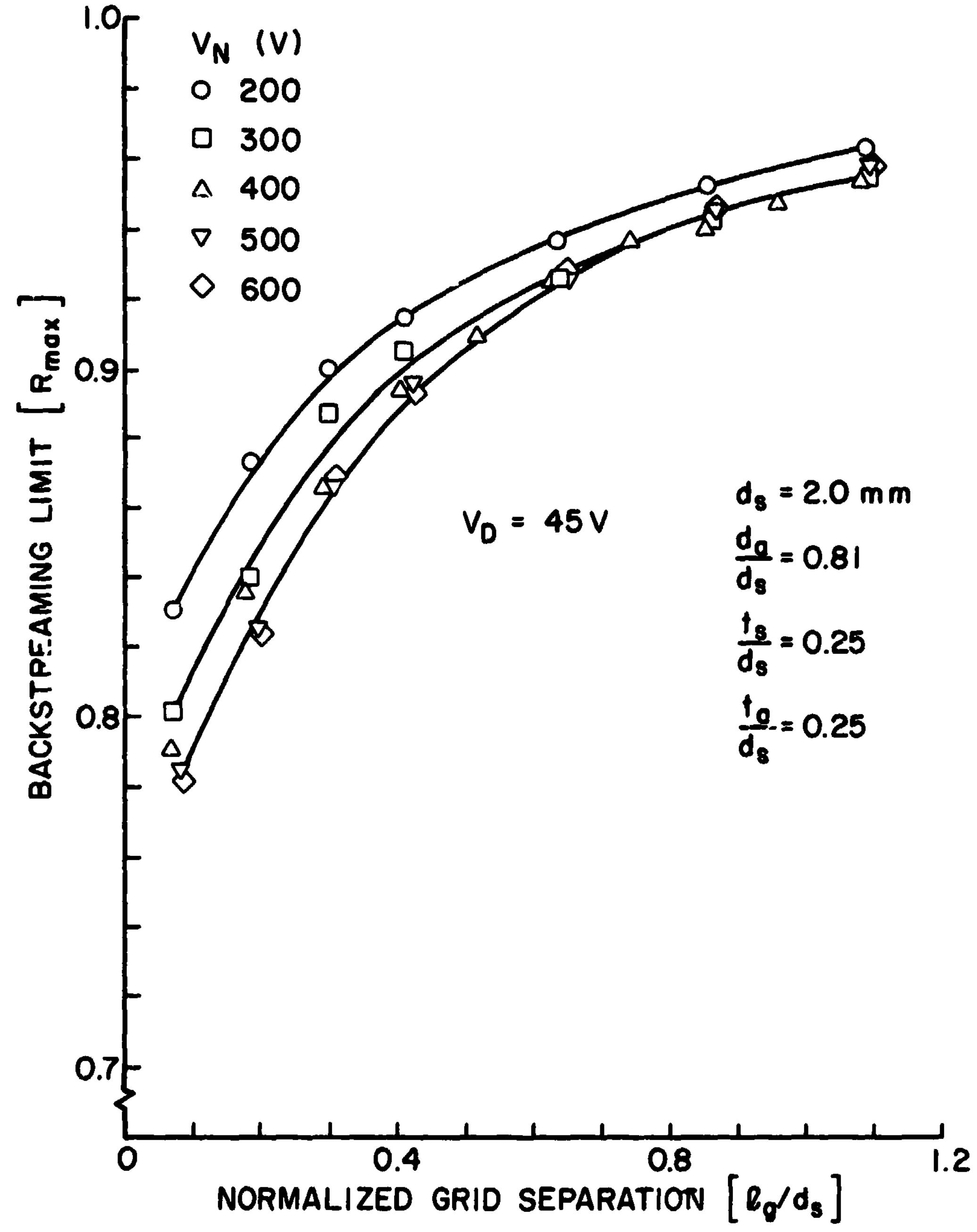

Figure 23. Effect of Net Accelerating Voltage on Electron Backstreaming Limit Operating Near the Impingement Limit

voltage on the electron backstreaming limit are not believed to be caused so much by the voltage changes themselves as by the induced changes in impingement-limited perveance levels. Smaller net accelerating voltages correspond to smaller total accelerating voltages. These smaller total accelerating voltages result in higher discharge-to-total voltages and it was demonstrated earlier in this work that higher ratios of discharge-to-total voltage generally result in lower levels of impingement-limited perveance. This indirect effect of the net accelerating voltage on electron backstreaming may explain in part why the effect of net accelerating voltages on electron backstreaming is more pronounced at lower accelerating voltages. For lower net accelerating voltages equivalent changes in the net accelerating voltage produce larger changes in the ratio of discharge-to-total voltage than they would at higher net accelerating voltages. Assuming that changes in the ratio of discharge-to-total voltage cause proportional changes in perveance, these larger changes in the discharge-to-total voltage ratio would produce larger changes in the perveance and therefore have a greater effect on backstreaming. Another contributing factor is suggested by the results of Fig. 22 where it is observed that the effect of perveance on the backstreaming limit appears to be more pronounced at lower perveance levels. Because lower net accelerating voltages generally result in lower perveance levels, it is reasoned that the electron backstreaming limit would be expected to be more sensitive to changes in the net accelerating voltage at low net accelerating voltages than it would at high net accelerating voltages. It is noteworthy that this reduced effect of perveance on backstreaming at higher perveances is in general agreement with results obtained by Kaufman using numerical techniques.[5]

All of the experimental electron backstreaming data obtained with the different grid geometries for a screen grid hole diameter of 2.0 mm are correlated in Fig. 24. These data were obtained at a net accelerating voltage of 400 V operating at beam currents near the impingement limit. In Fig. 24 the backstreaming limit, R_{max}, is plotted as a function of the effective normalized length mentioned previously. Considering the wide range of geometries included in the data of Fig. 24, the effective length, $\ell_e/d_a \cdot \exp[t_a/d_a]$, appears to correlate the backstreaming data reasonably well. Because the data were collected over a wide range of operating conditions and because the geometric effects seem to be reflected properly in the effective length parameter, Fig. 24 can be used as a design curve. Accelerator system operation without electron backstreaming could be expected by operating in the area below and to the right of the experimental curve or above it would probably allow electron backstreaming to occur; remembering, of course, that reduced perveance levels would permit operation at slightly higher ratios of net-to-total accelerating voltage than those indicated in Fig. 24. Accordingly, those changes in the discharge or net accelerating voltage that cause reductions in the impingement-limited perveance levels would be expected to shift the design curve up toward higher ratios of net-to-total accelerating voltage. However, based on arguments presented previously in this section, changes resulting in higher perveance levels would not be expected to change the position of the curve significantly. As a matter of information, it should be mentioned that during these tests the screen grid hole size was also determined to have a minor effect on electron backstreaming. It was observed that grid pairs utilizing smaller screen grid

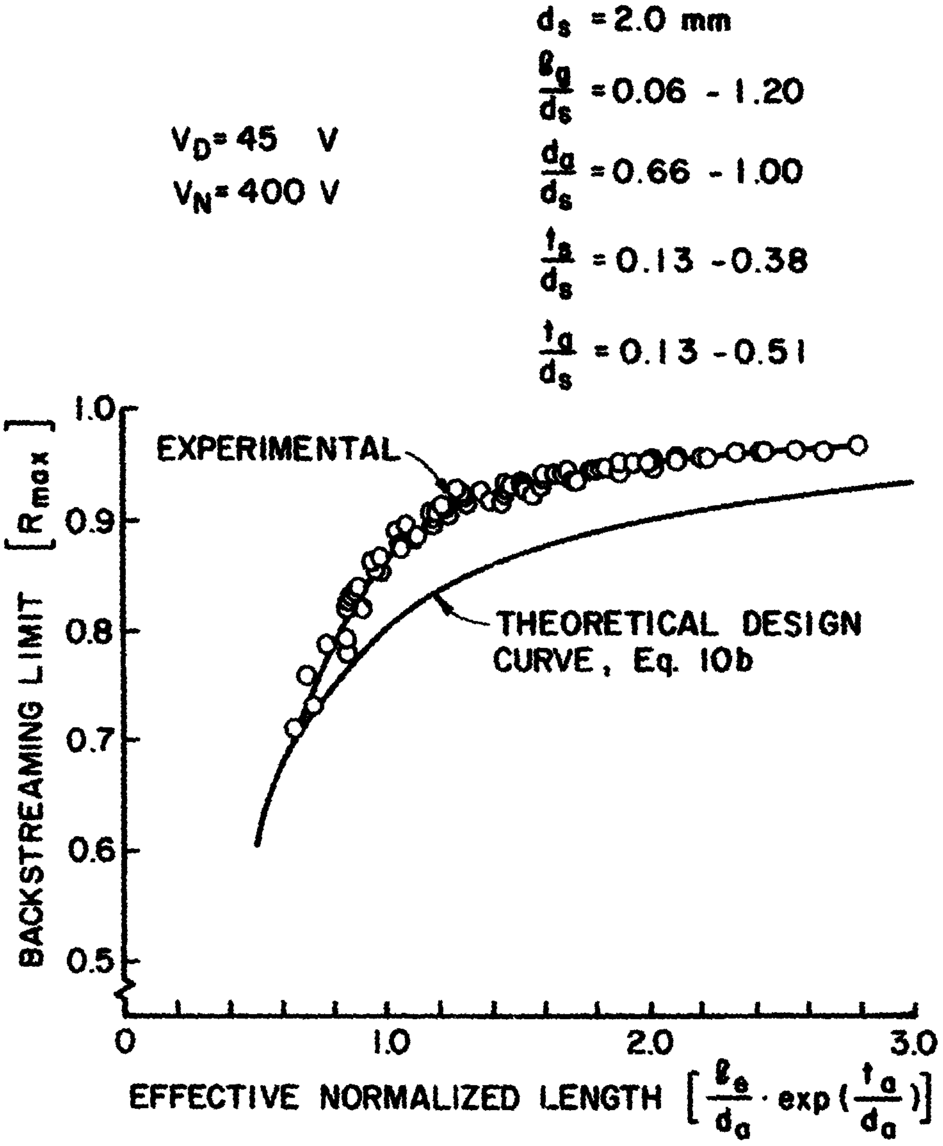

Figure 24. Correlation of Electron Backstreaming Limits for all 2.0 mm Diameter Screen Grid Aperture Geometries Operating Near the Impingement Limit

holes tended to allow operation at slightly higher ratios of net-to-total accelerating voltage before electron backstreaming occurred. It was also observed that the magnitude of increases in the electron backstreaming limit only became significant (above the spread of data shown in Fig. 24) for screen hole diameters below 1.5 mm. The explanation for this effect with hole size remains uncertain at this time. It is possible this trend toward higher backstreaming limits with decreasing hole size might be related to an increase in grid webbing area between the holes which accompanied reductions in screen hole diameter in the present experiments. This occurred because the hole-to-hole spacing was held fixed while the diameter varied. It is also possible that this observed effect of hole size on backstreaming might somehow be related to the plasma sheath thickness downstream of the accelerator grid. It is speculated that possibly the distance between the accelerator grid and neutralization surface did not scale proportionally with the dimensions of the smaller grid geometries.

In Fig. 24 a comparison is made to the theoretical design curve proposed by Kaufman.[5] Qualitatively, the experimental and theoretical curves have the same shape. At values of the effective normalized length above ~0.8 the theoretical curve is seen to be more conservative. It should be noted that, to the author's knowledge, the experimental results of Fig. 24 represent the most extensive experimental investigation of electron backstreaming to date. A tabular listing of all the experimental data shown in Fig. 24 can be found in Appendix C.

Electrical Breakdown

Electrical breakdown tests were conducted on each of the different screen and accelerator grid pairs used in this investigation. The electrical breakdown characteristics of each of the different grid pairs, although sometimes dramatically different from one another, were observed to be fairly constant over the range of grid separations investigated ($\ell_g \lesssim 0.25$ mm). The only significant trend observed with accelerator system geometry is shown in Fig. 25 where the electrical field at electrical breakdown is plotted as a function of the screen grid thickness. This figure shows that the thicker screen grids ($t_s \geq 0.5$ mm) facilitated operation at larger electrical fields than those obtained with thinner screen grids. It might be expected that the thinner grids were deflected more due to the electrostatic and thermal loads encountered and this resulted in the lower observed electric fields. Deflection analysis calculations confirmed this suspicion and showed that deflection of grids due to electrostatic attraction may have indeed caused the lower electric field at breakdown with the thinner grids. Computations showed a 0.25 mm thick grid would deflect 0.029 mm while a 0.50 mm grid would deflect 0.0036 mm and a 0.75 mm grid would deflect 0.0011 mm at a total accelerating voltage of 450 volts and a grid separation of 0.1 mm. It should be noted that an improvement to the grid support system was made prior to testing of the thinnest grid for which data are shown in Fig. 25 ($t_s = 0.13$ mm). This improvement involved moving the support points of the grid hold down system closer to the grid apertures. This may account for part of the reason why the trend toward lower electric fields with decreased grid thickness did not continue for the thinner grids.

In view of this possible grid deflection, the validity of the ion extraction performance results obtained with the thinner grids might be questioned. Computations showed that grid deflection due to electrostatic forces becomes substantial only at the closest grid separations.

ORIGINAL PAGE IS
OF POOR QUALITY

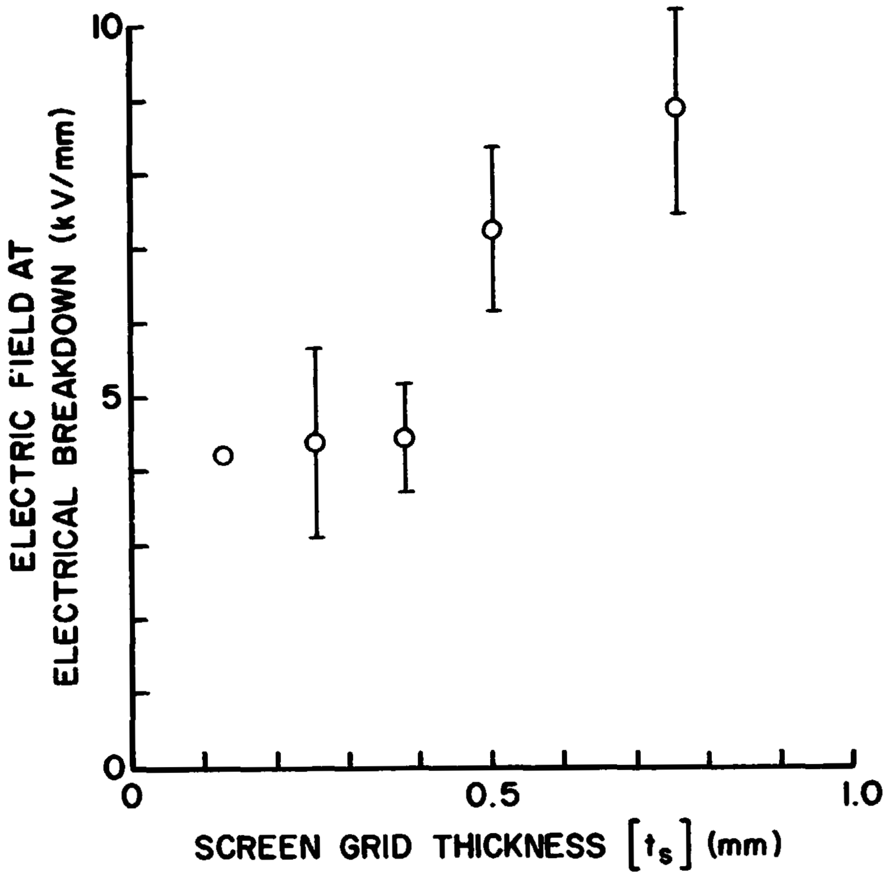

Figure 25. Effect of Screen Grid Thickness on Electric Field Stress at Electrical Breakdown

For example, increasing the grid separation from 0.1 mm to 0.25 mm for the 0.25 mm thick grid operating at a total voltage of 450 V would reduce the deflection from 0.029 mm to 0.0045 mm. Therefore, it is argued that the majority of the ion extraction results were unaffected by grid deflection. In any case, it should be emphasized that although the grid deflection may have affected the electrical breakdown results, it is felt that they did not affect the ion extraction performance results sufficiently to change the conclusions based on those results.

All of the electrical breakdown data obtained in this investigation occurred at electric fields higher than 2 kV/mm. A limit of 2 kV/mm has been accepted generally for many years as a design criterion for ion thruster accelerator systems. Most of the existing electrical breakdown data for ion thrusters suggest, however, that a limit of 2 kV/mm is probably conservative.[25-29] It appears that the results of this investigation support that observation since the majority of electrical breakdown data obtained lie substantially above 2 kV/mm. It should be emphasized that the results obtained in this study were for graphite grids and argon propellant. Other grid materials and propellants might be expected to give somewhat different results. Finally, it should be noted that no special effort was made to ensure the quality of the finishes on the grid surface and it is believed that this may have caused some of the scatter in the elec cal breakdown limits encountered in these tests. A tabular list all the electrical breakdown data obtained can be found in Appendi .

An appreciation of the importance of operating with large electric fields and small screen grid holes to realize increased current densities can be gained by considering Fig. 26. This figure shows the

ORIGINAL PAGE IS
OF POOR QUALITY

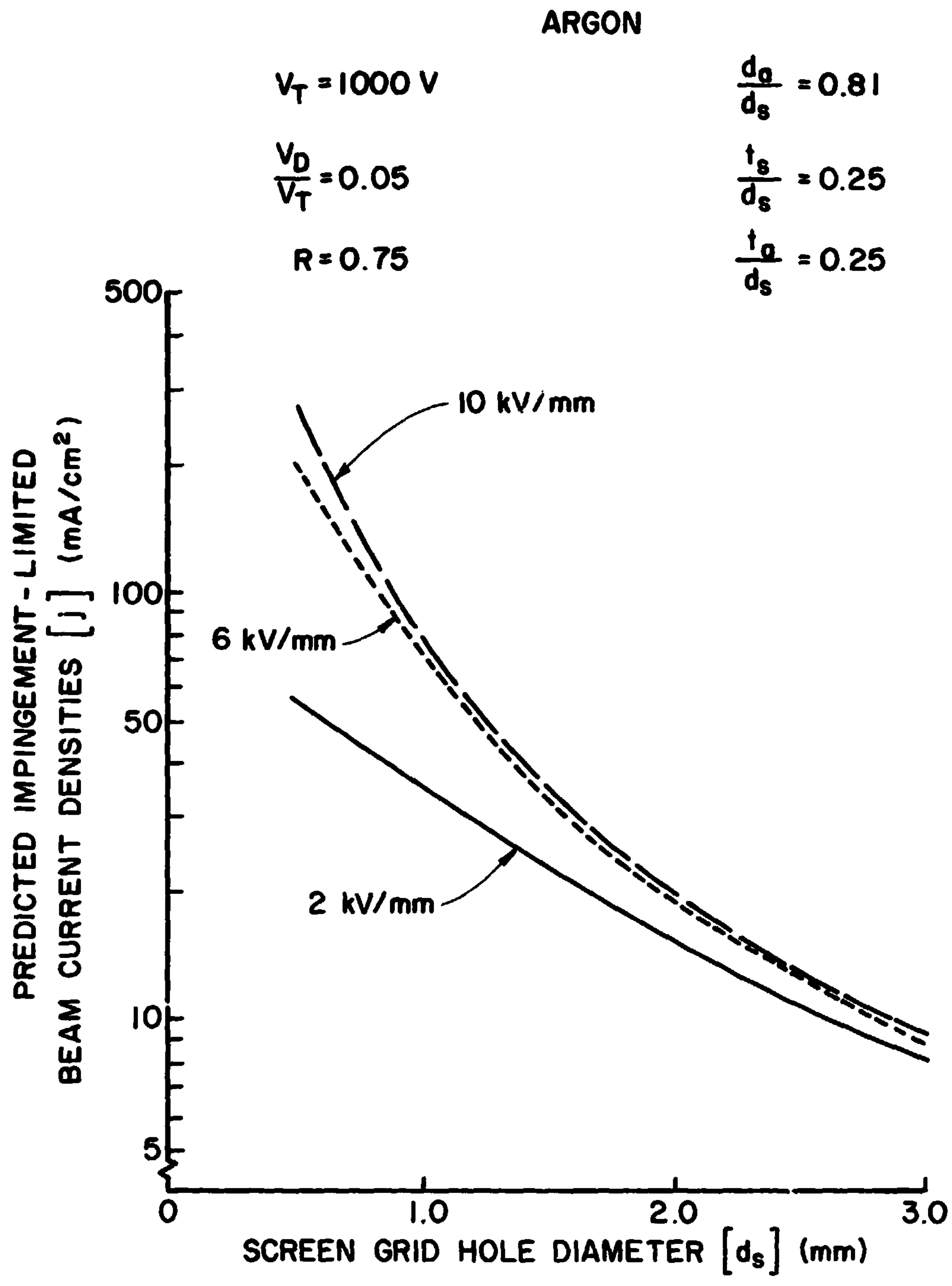

Figure 26. Comparison of Predicted Current Density Levels as a Function of Electrical Breakdown Limit and Screen Grid Hole Diameter for a Total Accelerating Voltage of 1000 V

projected levels of impingement-limited current densities that one might expect as a function of the screen grid hole diameter and maximum allowed electric field. The current density levels shown in Fig. 26 were calculated by scaling the impingement-limited perveance values obtained with the 2.0 mm diameter screen grid hole for a discharge-to-total voltage ratio of 0.05 and a net-to-total accelerating voltage ratio of 0.75. It should be noted that the current densities of Fig. 26 pertain to a total accelerating voltage of 1000 V and were calculated by dividing the impingement-limited beam current per hole expected at that voltage by the area of the screen grid hole. Fig. 26 shows that for large screen grid holes, increases in the maximum allowable electric fields would not yield substantial increases in current density. This does not hold true, however, for the smaller screen grid hole diameters where large increases in current density levels are suggested by the difference between the curves for 2 kV/mm and 6 kV/mm. Also, it is seen in Fig. 26 that for the range of screen grid hole diameters considered therein, operating at electric fields above 6 kV/mm would not be expected to produce substantial increases in current densities. Although the results suggested by Fig. 26 are based n experimental results, it should be mentioned that similar qualitative conclusions could have been drawn using a simple Child's law analysis to predict expected current densities as a function of hole size and electric field strength.

V. CONCLUSIONS

An apparatus has been developed which is well suited to the evaluation of the impingement-limited ion extraction capabilities, the electron backstreaming and electrical breakdown characteristics of two-grid accelerator systems. The following conclusions are drawn based on this study of these phenomena.

1) The basic relationships defining the current extraction capabilities of ion optic systems appear to be valid for screen grid hole diameters as small as 0.5 mm. It is expected that these relationships would be valid for even smaller holes provided the accelerator systems is mechanically sound and proper hole alignment and grid separation are maintained. Also, the ion source must be capable of supplying a high current density to the accelerator system while maintaining a stable discharge.
2) The results show the ion extraction performance of two-grid accelerator systems is a function of the net-to-total accelerating voltage ratio and grid separation ratio. Tests show at large grid separation ratios the impingement-limited perveance per hole at which the grids can be operated is relatively independent of the net-to-total accelerating voltage ratio. At small grid separation ratios, however, it was found that the impingement-limited perveance levels increased as the ratio of net-to-total accelerating voltage

increased. When the impingement-limited normalized perveance per hole is plotted over a large range of net-to-total accelerating voltage ratios, as a function of grid separation ratio, the resulting set of curves characterize the ion extraction performance of a particular accelerator system geometry described by the accelerator hole diameter ratio (d_a/d_s), the screen grid thickness ratio (t_s/d_s), and the accelerator grid thickness ratio (t_a/d_s). Results also show that these characteristic performance curves are dependent on the ratio of the discharge-to-total voltage (V_D/V_T) but appear to be independent of the total accelerating voltage. Tests show that impingement-limited normalized perveance per hole at which the grids can be operated degrades as the ratio of discharge-to-total accelerating voltage increases.

3) Using the data from a set of characteristic performance curves, an empirical model of the current that can be extracted from a grid aperture as a function of net-to-total accelerating voltage ratio and grid separation ratio is developed. This model shows that high beam current per hole levels are realized at a specified net accelerating voltage at low net-to-total accelerating voltage levels for all grid separation ratios. The model also suggests, however, that at small grid separation ratios there is another high beam current per hole operating point. This high beam current condition is realized at an optimum net-to-total accelerating voltage ratio in the range R = 0.5 to 0.8.

4) As expected, results show a general trend toward higher perveance levels with increases in the accelerator hole diameter ratio (d_a/d_s). However, in this study an interesting exception to this trend has been observed. When operating in the range of medium to high ratios of net-to-total accelerating voltage ratio at small grid separation ratios, results show that the current levels obtained with an accelerator hole diameter ratio of $d_a/d_s = 1.0$ actually fell below the levels obtained with a smaller accelerator hole diameter ratio, $d_a/d_s = 0.81$. This observation implies that an optimum accelerator hole diameter ratio exists. Grid operation at accelerator hole diameter ratios larger than this supposed optimum ratio would result in decreased impingement-limited perveance levels.

5) This work resulted in a large body of experimental data which can be used in the design of high beam current density accelerator systems. An example of how the ion extraction performance data might be used for design is discussed in Appendix A.

6) The electron backstreaming data obtained in this study resulted in a simple design curve which can be used to design accelerator systems in such a fashion as to avoid electron backstreaming.

7) Electrical fields greater than 2 kV/mm were obtained before electrical breakdown occurred between the pairs of graphite grids tested. This limit of 2 kV/mm is considered somewhat conservative since the average electric field at electrical breakdown was near 6 kV/mm.

Future work should focus on the effect of variations in discharge chamber conditions on ion extraction performance. Also, because of the importance of operating at higher electric fields in order to take full advantage of the increased current densities obtainable with smaller screen grid holes, a more detailed investigation of the electrical breakdown phenomenon is recommended.

REFERENCES

1. Lockwood, D. L., Michelson, W., and Hamza, V., "Analytical Space-Charge Flow and Theoretical Electrostatic Rocket Engine Performance," 1st Electric Propulsion Conference, Berkeley, Calif., March 14-16, 1962.

2. Hyman, J., Eckhardt, W. O., Knechtli, R. C., and Buckey, C. R., "Formation of Ion Beams from Plasma Sources: Part 1," AIAA Journal, Vol. 2, Oct. 1964, pp. 1739-1748.

3. Bogart, C. D. and Richley, E. A., "A Space Charge Flow Computer Program," NASA Tech. Note TN-D3394, 1966.

4. Lathem, W. C., "Ion Accelerator Designs for Kaufman Thrusters," Journal of Spacecraft and Rockets, Vol. 6, Nov. 1969, p. 1237.

5. Kaufman, H. R., "Accelerator System Solution for Broad-Beam Ion Sources," AIAA Journal, Vol. 15, July 1977, pp. 1025-1034.

6. Alterburg, W., Freisinger, J., Hauser, J., Seibert, N., and Loeb, H. W., "Beam Formation in RF-Ion Thrusters," AIAA Paper No. 75-426, New Orleans, La., 1975.

7. Aston, G. and Kaufman, H. R., "The Ion-Optics of a Two-Grid Electron Bombardment Thruster," AIAA Paper No. 76-1029, Key Biscayne, Fl., 1976.

8. Aston, G., Kaufman, H. R. and Wilbur, P. J., "Ion Beam Divergence Characteristics of Two-Grid Accelerator Systems," AIAA Journal, Vol. 16, No. 5, May 1978, pp. 516-524.

9. Aston, G. and Kaufman, H. R., "Ion Beam Divergence Characteristics of Three-Grid Accelerator Systems," AIAA Journal, Vol. 17, No. 1, Jan. 1979, pp. 64-70.

10. Homa, J. H. and Wilbur, P. J., "Ion Beamlet Vectoring by Grid Translation," AIAA Paper No. 82-1895, Nov. 1982.

11. Kerslake, W. R. and Paulik, E. V., "Additional Studies of Screen and Accelerator Grids for Electron-Bombardment Ion Thrusters," NASA Technical Note D-1411, 1963.

12. Rawlin, V. K., Banks, B. A., and Byers, D. C., "Dished Accelerator Grids on 30-cm Ion Thruster," Journal of Spacecraft and Rockets, Vol. 10, Jan. 1973, pp. 29-35.

13. Rawlin, V. K., "Studies of Dished Accelerator Grids for 30-cm Ion Thrusters," AIAA Paper No. 73-1086, Oct./Nov., 1973.

14. Whealton, J. H. and Tsai, C. C., "Influence of Chrometic Aberrations on Space Charge Ion Optics," Review of Scientific Instruments, Vol. 49, No. 4, April 1978, pp. 495-498.

15. Whealton, J. H., Jaeger, E. F., and Whitson, J. C., "Optics of Ion Beams of Arbitrary Perveance Extracted from a Plasma," Journal of Computational Physics, Vol. 27, 1978, pp. 32-41.

16. Wooten, J. W., Whealton, J. H., McCollough, D. H., McGaffrey, R. W., Akin, J. E., and Drooks, L. J., "Ion Extraction and Optics in 3D," Journal of Computational Physics, Vol. 43, 1981, pp. 95-111.

17. Child, C. D., "Discharge from Hot CaO," Physical Review, Vol. 32, 1911, pp. 492-511.

18. Aston, G. and Wilbur, P. J., "Ion Extraction from a Plasma," Journal of Applied Physics, Vol. 52, No. 4, April 1981.

19. Spangenberg, K. R., Vacuum Tubes, 1948, pp. 348-349.

20. Kaufman, H. R., "Technology of Electron Bombardment Thrusters," Advances in Electronics and Physics, Vol. 36, Academic Press Inc., San Francisco, 1974.

21. Cobine, J. D., Gaseous Conductors: Theory and Engineering Applications, 1st Ed., Dover Publications Inc., New York, 1958, p. 164.

22. Kilpatrick, W. D., "Criterion for Vacuum Sparking Designed to Include Both rf and dc," Review of Scientific Instruments, Vol. 28, No. 10, October, 1957, pp. 824-826.

23. Coupland, J. R., Green, T. S., Hammond, D. P., and Riv'ere. A. C., "A Study of Ion Beam Intensity and Divergence Obtained from a Single Aperture Three Electrode Extraction System," Review of Scientific Instruments, Vol. 44, No. 9, September 1973.

24. Green, T. S., Inst. Phys. Conf., Ser. 54, Bristol, 1980, p. 271.

25. Kersiake, W. R., "Charge-Exchange Effects on the Accelerator Impingement of an Electron-Bombardment Ion Rock t," NASA Tech. Note TN D-1657, May 1963.

26. Byers, D. C., "An Experimental Investigation of a High-Voltage Electron-Bombardment Ion Thruster," J. Electrochem. Soc., Vol. 116, Jan. 1969, pp. 9-17

27. Beattie, J. R., and Poeschel, R. L., "Extended Performance Thruster Technology Evaluation," AIAA Paper 78-666, April 1978.

28. Rawlin, V. K., "Extended Operating Range of the 30-cm Ion Thruster with Simplified Power Processor Requirements," AIAA Paper No. 81-0692, April 1981.

29. Aston, G., "Ion Accelerator Systems for High Power 30-cm Thruster Operation," AIAA Paper No. 82-1893, Nov. 1982.

30. Kaufman, H. R., "Ion Source Design for Industrial Applications," AIAA Journal, Vol. 20, No. 6, June 1982, pp. 745-760.

31. Brophy, J. R., "Effect of Screen Grid Potential on Perveance," appears in "Advanced Ion Thruster Research," NASA CR-168340, Feb. 1984.

32. Tsuchiya, I. and Masuzawa, T., "Study on Low Energy Ion-milling Equipment," International Ion Engineering Congress, Kyoto, Japan, September 12-16, 1983, pp. 765-770.

33. Robinson, R. S., "Physical Processes in Directed Ion Beam Sputtering," NASA CR-159567, March 1979, p. 51.

APPENDIX A

A Design Example

The purpose of this design example is to illustrate a possible technique for using the ion extraction performance data obtained in this study. To do this, the following design problem is posed:

Given a maximum design electric field of 4 kV/mm and a desired net accelerating voltage of 500 volts, determine what ratio of net-to-total accelerating voltage yields the highest beam current density. Also, examine the effect of screen grid hole size on impingement-limited current density.

For this particular example, the ion extraction performance data collected with the standard grid geometry ($d_a/d_s = 0.81$, $t_s/d_s = 0.25$ and $t_a/d_s = 0.25$) operating at discharge-to-total voltage ratio of 0.05 will be used. The appropriate experimental data are found on the first page of Appendix B.

Because the desired net accelerating voltage has been specified, selection of a ratio of net-to-total accelerating voltage determines the total voltage,

$$V_T = \frac{V_N}{R} \quad . \tag{A-1}$$

Under the design constraint of not exceeding a maximum electric field, this total voltage at each value of R can be used to determine the minimum grid separation allowed

$$\ell_g = \frac{V_S + |V_A|}{E_{max}} = \frac{V_T - V_D}{E_{max}} = \frac{V_T\left(1 - \frac{V_D}{V_T}\right)}{E_{max}} \qquad \text{(A-2a)}$$

or

$$\ell_g = \frac{\frac{V_N}{R}\left(1 - \frac{V_D}{V_T}\right)}{E_{max}} \; . \qquad \text{(A-2b)}$$

Substitution of the known quantities for this design example into Eq. A-2b yields the following expression

$$\ell_g = \frac{\frac{500}{R}\,(1 - 0.05)}{4000} = \frac{0.119}{R} \qquad \text{(A-3)}$$

where ℓ_g has the units millimeters. Figure A.1 shows how the grid separation is observed to vary as a function of R according to Eq. A-3.

To use the ion extraction performance data, it is still necessary to select a screen grid hole diameter (d_s). For now, a screen hole diameter of 2.0 mm will be assumed. With the screen hole diameter specified, for each value of R the respective value of the minimum normalized grid separation (ℓ_g/d_s) is now also defined

$$\frac{\ell_g}{d_s} = \frac{0.119}{d_s \cdot R} = \frac{0.06}{R} \; . \qquad \text{(A-4)}$$

With the two independent variables, R and ℓ_g/d_s, thus defined, it is now possible to use the ion extraction performance curves to determine the impingement-limited normalized perveance per hole (P_I). At each ratio of net-to-total accelerating voltage, the respective perveance (P_I) can be used to calculate the current density (j)* where

---

*All of the current densities referred to in this appendix and elsewhere in the thesis are based on the screen grid hole area, i.e. the current density is defined as the current per hole divided by the area of the screen grid hole.

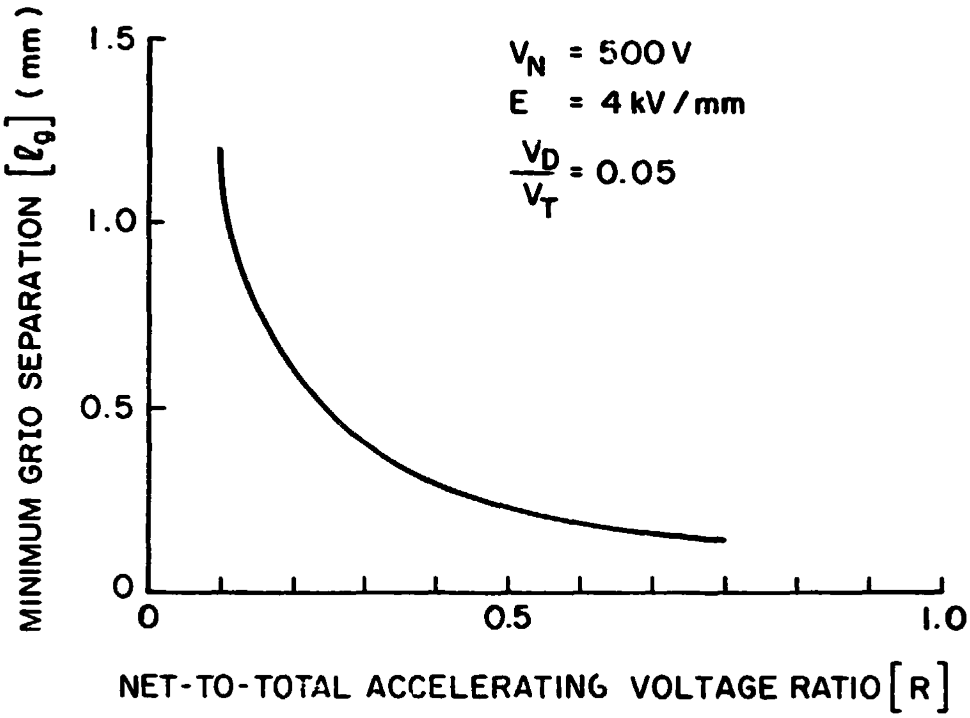

Figure A.1. Minimum Grid Separation Variation

$$j = \frac{P_I \cdot V_T^{3/2}}{\frac{\pi}{4} d_s^2 \left(\frac{\ell_e}{d_s}\right)^2} \times 10^5 \qquad \text{(A-5a)}$$

or

$$j = \frac{P_I \cdot \left(\frac{V_N}{R}\right)^{3/2}}{\frac{\pi}{4} (d_s)^2 \left[\left(\frac{\ell_g}{d_s}\right)^2 + 0.25\right]} \times 10^5 \ . \qquad \text{(A-5b)}$$

Here, j has units mA/cm^2 and d_s is expressed in millimeters. There is another factor that needs to be considered, namely when to determine the maximum current density obtainable at each value of R. The current density appropriate to the minimum normalized grid separation does not always result in the highest current density for each value of R. This is because in some cases the impingement-limited current density decreases (contrary to usual situation) as the grid separation is reduced below a certain value of normalized grid separation. A typical example of this effect is shown in Fig. A.2 where the impingement-limited current density is plotted as a function of normalized grid separation for R = 0.5. It should be mentioned that the operating conditions and normalized grid geometries appropriate to Fig. A.2 pertain to the present design example. For this design example the value of the minimum normalized grid separation for R = 0.5 is 0.12. Figure A.2 shows that higher current densities could be obtained by operating at normalized grid separations larger than 0.12. Of particular interest here is the maximum current density shown in Fig. A.2. For those values of R where higher current densities can be obtained by operating at normalized grid separation ratios larger than the minimum grid separation ratio, the value of the maximum obtainable current density should be used for comparison purposes. If higher currents

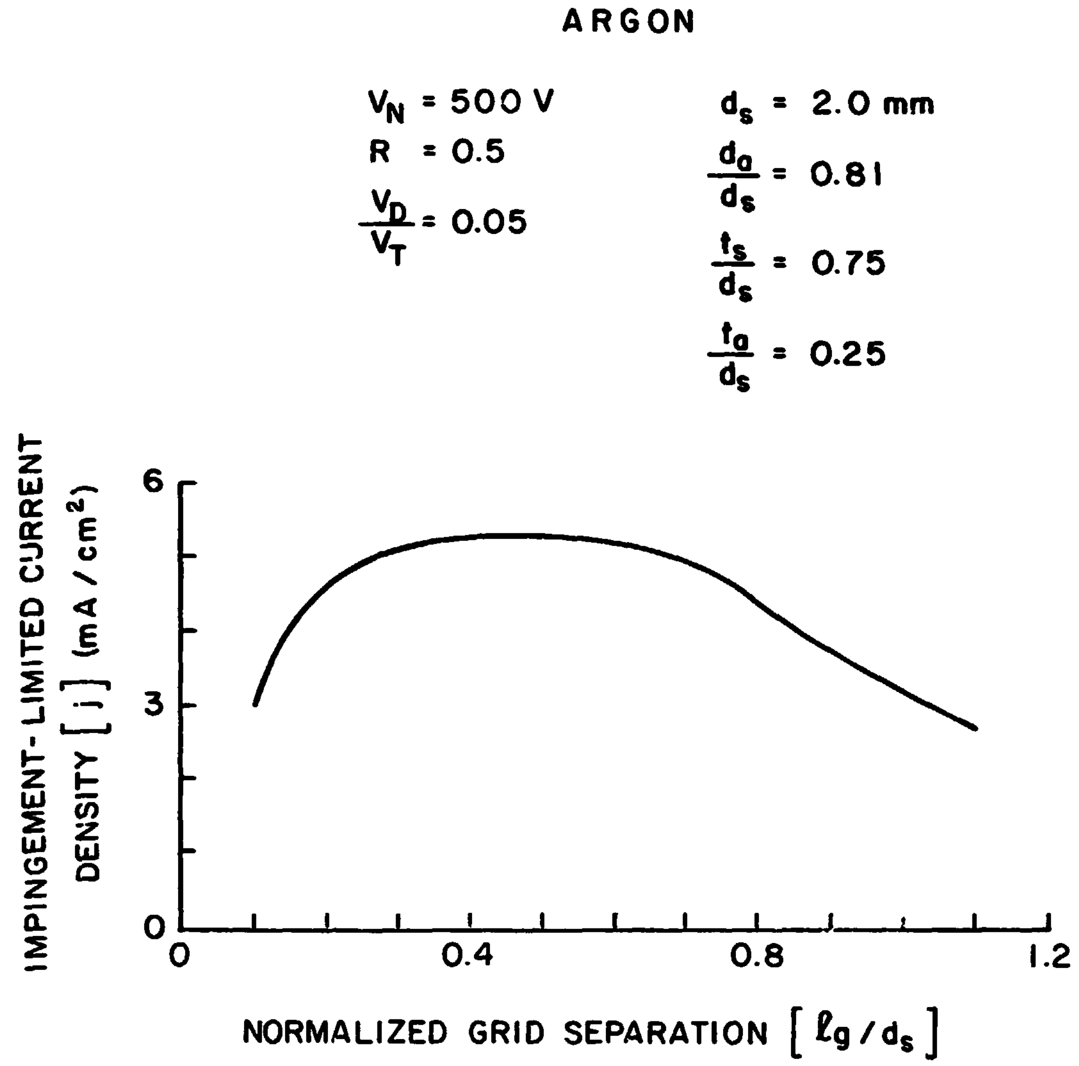

Figure A.2. Impingement-Limited Current Density as a Function of Normalized Grid Separation for R = 0.5

cannot be obtained at larger normalized grid separation ratios, the current density associated with the minimum grid separation ratio is used. The current densities determined in the aforementioned fashion for various values of net-to-total accelerating voltage ratio are shown plotted in Fig. A.3. This figure shows that the highest current densities would be expected at very low ratios of net-to-total accelerating voltage. It also shows, however, that high beam current densities can be obtained at the higher ratios of net-to-total accelerating voltage. The choice between these two high beam current density operating conditions, very low values of R or high values of R, should be based on several considerations. First of all, there are the disadvantages of operating at very low ratios of R discussed earlier (pgs. 48 to 51). There is, however, an advantage to operating at lower values of R that needs to be discussed. Because of their higher total voltages smaller ratios of net-to-total accelerating voltage necessitate operation at larger grid separations. Using present grid manufacturing techniques, these larger grid separations facilitate operation with [illegible] diameter discharge chambers which are generally considered to be capable of producing ion beams more efficiently than smaller diameter discharge chambers. If at some point in the future smaller diameter thrusters can be designed to produce ion beams as efficiently as large diameter thrusters, then this advantage of operating at very low values of R could be negated. Another possibility is that maybe at some point in the future an improvement in grid design will allow accelerator systems of any desired diameter to be constructed with very close grid separations.

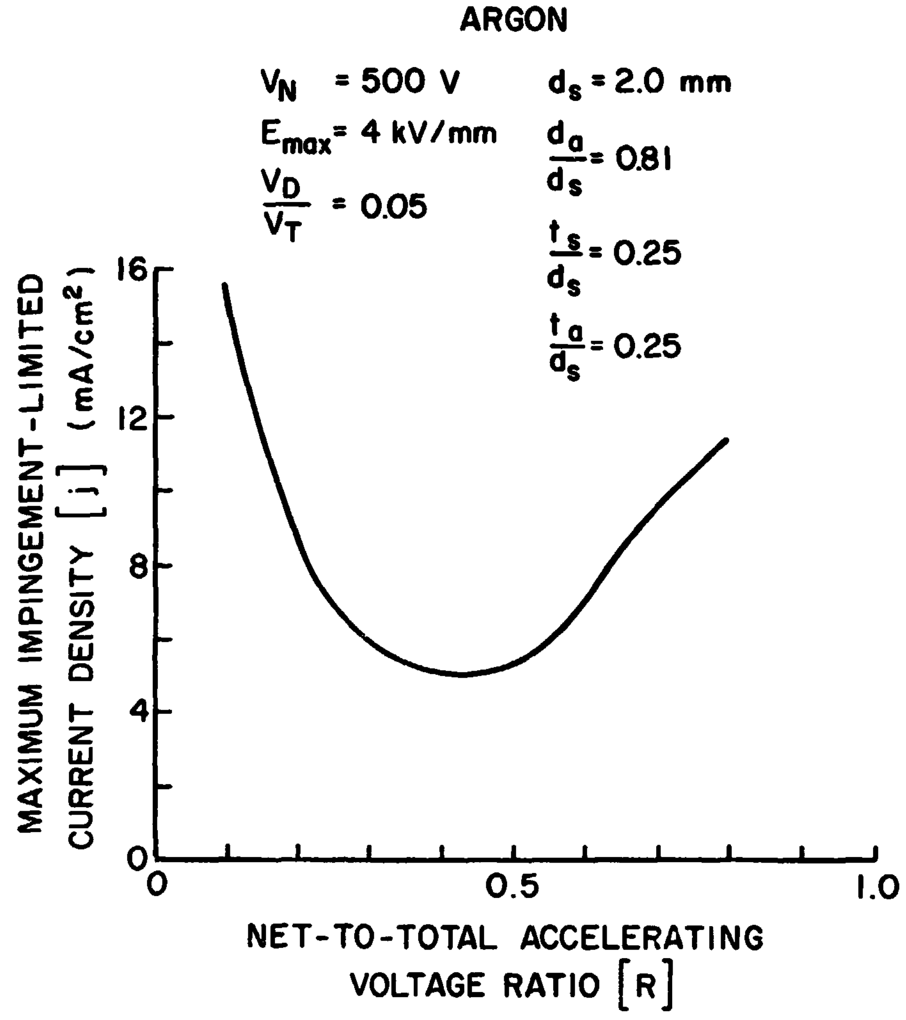

Figure A.3. Maximum Impingement-Limited Current Densities Predicted for a Screen Aperture Diameter of 2.0 mm

It should be mentioned that the higher ratios of net-to-total accelerating voltage shown in Fig. A.3 were checked for the possible occurrence of electron backstreaming. Based on the design curve shown in Fig. 24, the net-to-total accelerating voltage ratio of 0.8 was found to be near the electron backstreaming limit. After incorporating a safety factor to ensure grid operation free of electron backstreaming, operation at a ratio of net-to-total accelerating voltage less than R = 0.75 is recommended.

Curves similar in nature to that shown in Fig. A.3 can be obtained by repeating the above procedure for other screen grid hole diameters. In Fig. A.4 a comparison of the predicted current densities obtainable with screen grid hole diameter smaller than 2.0 mm is made. Fig. A.4 shows that smaller screen grid hole diameters facilitate operation at higher beam current densities. From a practical standpoint, mechanical design considerations and the need for efficient ion beam production will most likely limit the extent to which the screen grid hole diameter can be reduced. One reason for this is that to maintain similar normalized grid thicknesses (t_s/d_s, t_a/d_s) as the hole size is reduced, the grid thicknesses must also be reduced. These reduced grid thicknesses mean less mechanical strength and in general shorter grid lifetimes. Using present accelerator system designs, reduced strength necessitates smaller diameter accelerator systems and smaller thrusters. A possible alternative to this would be to maintain the same grid thicknesses as the screen grid hole size is reduced. One problem with this alternative is that the results of Fig. 10 show that increases in the screen grid thickness ratio generally result in reduced perveance levels. Another problem is that increases in the screen grid thickness

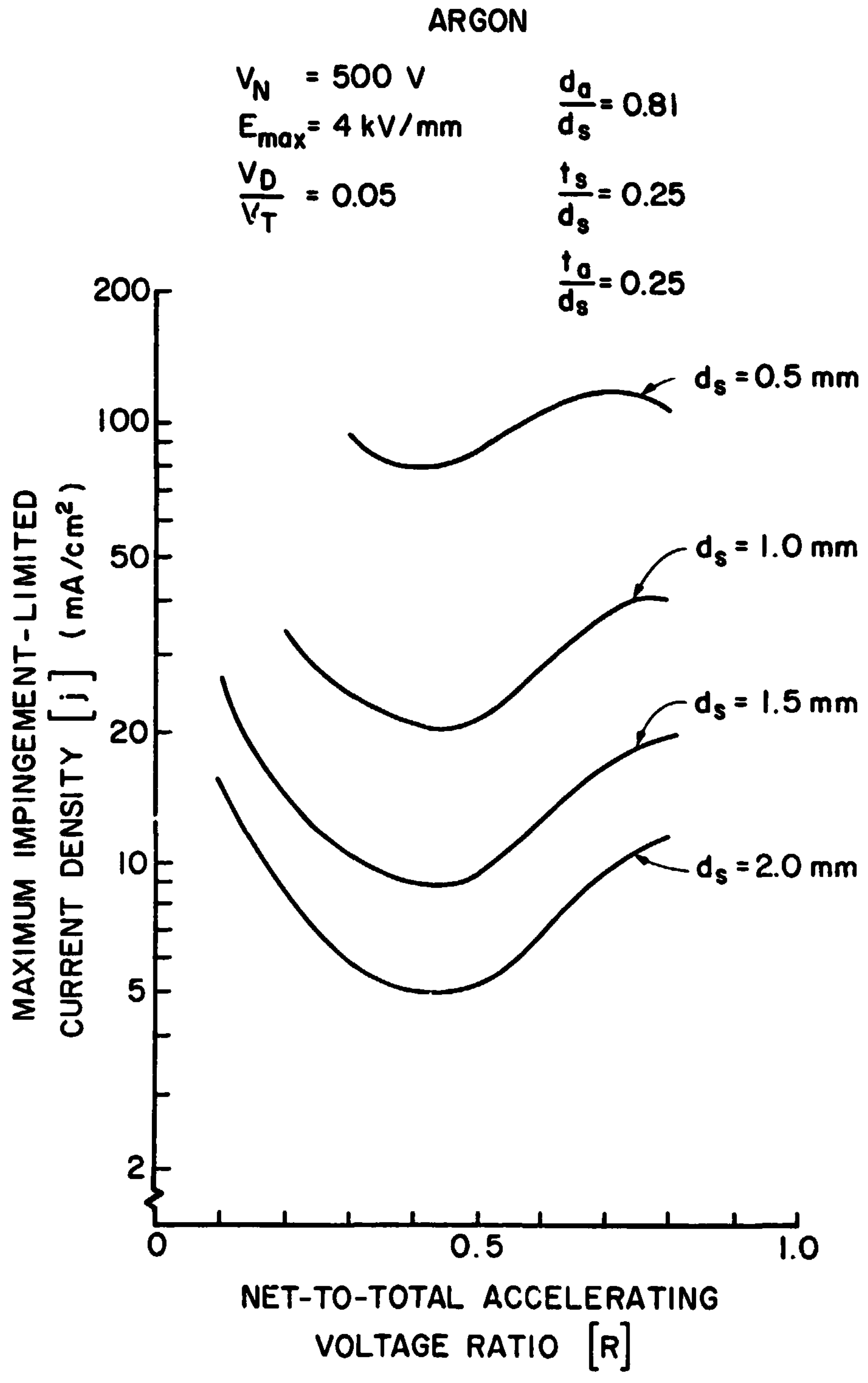

Figure A.4. Comparison of the Maximum Impingement-Limited Current Densities Predicted for Different Screen Grid Hole Diameters ratio cause significant reductions in beam ion production efficiency.[20] Also, from a mechanical design viewpoint, the increased precision required to maintain proper hole alignment for the smaller holes might limit the extent to which the screen grid hole size can be reduced.

As a final note, in this design example the ratio of discharge-to-total voltage is artificially maintained at a value of 0.05. This facilitated the use of only one set of experimental data. However, in practice, the discharge voltage is usually held fixed and does not vary with changes in total voltage. In this operating mode, the expected current densities would differ slightly from those shown in Figs. A.3 and A.4. The reason for this is that it has been demonstrated that changes in the discharge-to-total voltage ratio generally effect changes in the impingement-limited perveance levels (Fig. 6). Based on the results shown in Fig. 6, slightly higher beam current densities would be expected for operation at discharge-to-total voltage ratios less than the value appropriate to Fig. 28 ($V_D/V_T = 0.05$). Similarly, slightly lower beam current densities would be expected at discharge-to-total voltage ratios greater than 0.05. For a fixed discharge voltage, this effect of the discharge-to-total voltage ratio on beam current densities would tend to favor the lower values of R where higher total voltages are observed.

APPENDIX B

Impingement-Limited Perveance Data

Grid Geometry: $d_s = 2.0$ mm, $d_a/d_s = 0.81$, $t_s/d_s = 0.25$, $t_a/d_s = 0.25$

Operating Conditions: $V_D = 45$ V, $V_T = 900$ V

Impingement-Limited Normalized Perveance Per Hole

$[J/V_T^{3/2} (\frac{\ell_e}{d_s})^2]$ (nanopervs/hole)

$\frac{\ell_g}{d_s}$	R: 0.10	0.20	0.30	0.40	0.45	0.50	0.55	0.60	0.65	0.70	0.75	0.80
1.11	1.97	3.22	3.95	3.96	3.99	3.99	4.00	3.98	4.01	4.05	4.02	4.02
1.00	1.65	2.70	3.45	3.96	3.98	4.02	3.98	3.98	4.00	4.01	4.03	4.03
0.89	1.42	2.20	2.85	3.67	3.95	3.98	3.97	4.00	3.98	4.01	4.04	4.00
0.77	1.13	1.78	2.29	3.03	3.55	3.95	3.97	4.00	3.98	4.01	4.04	4.03
0.66	0.95	1.40	1.84	2.47	2.93	3.51	3.95	4.01	4.02	4.02	4.02	4.03
0.55	0.78	1.10	1.41	1.94	2.35	2.89	3.57	3.99	4.07	4.08	4.09	4.08
0.43	0.59	0.80	1.03	1.46	1.80	2.27	2.90	3.65	4.19	4.29	4.30	4.33
0.32	0.44	0.61	0.75	1.01	1.33	1.81	2.38	3.03	3.86	4.44	4.62	4.60
0.21	0.35	0.47	0.58	0.74	0.89	1.37	1.98	2.66	3.51	4.25	4.94	5.10
0.11	0.27	0.36	0.45	0.56	0.66	0.84	1.75	2.36	3.19	4.05	4.99	5.62

Standard Configuration

Grid Geometry: $d_s = 2.0$ mm, $d_a/d_s = 0.81$, $t_s/d_s = 0.25$, $t_a/d_s = 0.25$

Operating Conditions: $V_D = 45$ V, $V_T = 450$ V

Impingement-Limited Normalized Perveance Per Hole

$[J/V_T^{3/2} (\frac{\ell_e}{d_s})^2]$ (nanopervs/hole)

$\frac{\ell_g}{d_s}$	R: 0.10	0.20	0.30	0.40	0.45	0.50	0.55	0.60	0.65	0.70	0.75	0.80
1.10	1.21	2.56	2.65	2.65	2.65	2.65	2.66	2.73	2.66	2.64	2.69	2.70
0.99	0.98	2.26	2.65	2.69	2.69	2.74	2.70	2.71	2.69	2.71	2.70	2.72
0.87	0.88	1.84	2.39	2.76	2.75	2.75	2.73	2.79	2.76	2.79	2.82	2.76
0.76	0.71	1.46	1.94	2.54	2.74	2.79	2.80	2.83	2.82	2.81	2.82	2.85
0.65	0.59	1.20	1.58	2.14	2.46	2.82	2.90	2.88	2.86	2.89	2.88	2.97
0.54	0.46	0.94	1.24	1.66	1.94	2.41	2.94	3.04	3.02	3.04	3.06	3.06
0.42	0.38	0.73	0.95	1.28	1.50	1.91	2.53	3.11	3.17	3.22	3.21	3.21
0.31	0.32	0.60	0.79	1.03	1.21	1.56	2.03	2.73	3.36	3.54	3.52	3.54
0.20	0.27	0.46	0.58	0.83	0.95	1.29	1.70	2.35	3.13	3.87	4.05	4.17
0.09	0.23	0.36	0.46	0.60	0.75	1.11	1.55	2.26	3.05	3.95	4.72	5.20

Grid Geometry: $d_s = 2.0$ mm, $d_a/d_s = 0.81$, $t_s/d_s = 0.25$, $t_a/d_s = 0.25$

Operating Conditions: $V_D = 45$ V, $V_T = 300$ V

Impingement-Limited Normalized Perveance Per Hole

$[J/V_T^{3/2} (\frac{\ell_g}{d_s})^2]$ (nanopervs/hole)

$\frac{\ell_g}{d_s}$	R: 0.10	0.20	0.30	0.40	0.45	0.50	0.55	0.60	0.65	0.70	0.75	0.80
1.09		1.74	1.73	1.77	1.73	1.65	1.70	1.66	1.69	1.73	1.70	1.64
0.98		1.74	1.76	1.77	1.77	1.77	1.76	1.74	1.77	1.78	1.74	1.78
0.86		1.68	1.81	1.86	1.87	1.83	1.85	1.83	1.84	1.85	1.87	1.83
0.75		1.46	1.79	1.88	1.88	1.91	1.88	1.92	1.89	1.90	1.91	1.91
0.64		1.14	1.46	1.83	1.99	1.98	1.99	2.01	2.01	2.01	1.99	2.02
0.52		0.88	1.14	1.48	1.76	1.99	2.10	2.09	2.11	2.12	2.11	2.14
0.41		0.71	0.91	1.18	1.40	1.71	2.15	2.30	2.32	2.32	2.35	2.35
0.30		0.54	0.69	0.90	1.09	1.37	1.83	2.38	2.52	2.54	2.55	2.60
0.19		0.44	0.57	0.72	0.87	1.12	1.51	2.16	2.81	3.09	3.07	3.11
0.07		0.37	0.48	0.63	0.76	0.99	1.33	2.03	2.81	3.49	3.83	3.85

ORIGINAL PAGE IS
OF POOR QUALITY

C-2

Grid Geometry: $d_s = 2.0$ mm, $d_a/d_s = 0.81$, $t_s/d_s = 0.25$, $t_a/d_s = 0.13$

Operating Conditions: $V_D = 45$ V, $V_T = 450$ V

Impingement-Limited Normalized Perveance Per Hole

$[J/V_T^{3/2} (\frac{\ell_e}{d_s})^2]$ (nanopervs/hole)

$\frac{\ell_g}{d_s}$	R:	0.10	0.20	0.30	0.40	0.45	0.50	0.55	0.60	0.65	0.70	0.75	0.80
1.11		1.38	2.69	2.70	2.69	2.70	2.70	2.67	2.68	2.69	2.71	2.69	2.67
1.00		1.17	2.33	2.71	2.78	2.72	2.72	2.73	2.72	2.72	2.73	2.73	2.70
0.89		0.97	2.03	2.44	2.68	2.72	2.71	2.64	2.75	2.74	2.73	2.71	2.76
0.77		0.81	1.64	2.01	2.41	2.69	2.75	2.74	2.74	2.72	2.77	2.75	2.74
0.66		0.65	1.30	1.57	1.90	2.18	2.54	2.70	2.77	2.75	2.74	2.75	2.79
0.55		0.51	0.96	1.20	1.49	1.70	2.09	2.56	2.82	2.80	2.82	2.84	2.88
0.43		0.41	0.79	0.97	1.16	1.36	1.63	2.12	2.68	2.92	2.95	2.91	2.94
0.32		0.34	0.62	0.75	0.91	1.08	1.29	1.70	2.29	2.89	3.16	3.16	3.16
0.21		0.28	0.48	0.57	0.73	0.87	1.04	1.38	1.93	2.60	3.26	3.58	--
0.10		0.26	0.38	0.45	0.56	0.66	0.86	1.17	1.67	2.40	3.15	--	--

Grid Geometry: $d_s = 2.0$ mm, $d_a/d_s = 0.81$, $t_s/d_s = 0.25$, $t_a/d_s = 0.38$

Operating Conditions: $V_D = 45$ V, $V_T = 450$ V

Impingement-Limited Normalized Perveance Per Hole

$[J/V_T^{3/2} (\frac{\ell_e}{d_s})^2]$ (nanopervs/hole)

$\frac{\ell_g}{d_s}$	R: 0.10	0.20	0.30	0.40	0.45	0.50	0.55	0.60	0.65	0.70	0.75	0.80
1.12	1.43	2.56	2.59	2.57	2.55	2.61	2.61	2.59	2.57	2.60	2.61	2.63
1.01	1.16	2.40	2.64	2.64	2.60	2.65	2.65	2.70	2.62	2.65	2.65	2.65
0.90	0.94	1.99	2.51	2.66	2.70	2.66	2.70	2.70	2.72	2.68	2.69	2.71
0.78	0.79	1.62	2.09	2.54	2.69	2.73	2.74	2.76	2.76	2.77	2.77	2.75
0.67	0.68	1.31	1.65	2.09	2.40	2.71	2.83	2.87	2.84	2.85	2.87	2.85
0.56	0.56	1.02	1.29	1.63	1.90	2.25	2.73	2.90	2.88	2.92	2.89	2.92
0.45	0.45	0.80	1.00	1.29	1.50	1.77	2.20	2.75	3.01	3.01	3.03	2.99
0.33	0.36	0.60	0.76	1.00	1.14	1.40	1.74	2.34	2.99	3.19	3.22	3.26
0.22	0.31	0.46	0.59	0.77	0.93	0.99	1.50	1.94	2.62	3.34	3.58	3.61
0.11	0.26	0.37	0.47	0.60	0.71	0.90	1.31	1.83	2.54	3.32	4.01	4.37

Grid Geometry: $d_s = 2.0$ mm, $d_a/d_s = 0.81$, $t_s/d_s = 0.25$, $t_a/d_s = 0.51$

Operating Conditions: $V_D = 45$ V, $V_T = 450$ V

Impingement-Limited Normalized Perveance Per Hole

$[J/V_T^{3/2} (\frac{\ell_e}{d_s})^2]$ (nanopervs/hole)

$\frac{\ell_g}{d_s}$	R:	0.10	0.20	0.30	0.40	0.45	0.50	0.55	0.60	0.65	0.70	0.75	0.80
1.11		1.19	2.50	2.46	2.50	2.50	2.47	2.46	2.52	2.46	2.52	2.48	2.47
1.00		0.97	2.37	2.48	2.52	2.46	2.48	2.49	2.51	2.48	2.49	2.53	2.49
0.89		0.85	2.03	2.42	2.56	2.58	2.56	2.57	2.58	2.56	2.55	2.57	2.56
0.77		0.68	1.63	2.09	2.51	2.59	2.57	2.56	2.57	2.58	2.59	2.59	2.58
0.66		0.59	1.29	1.65	2.09	2.46	2.58	2.57	2.58	2.58	2.58	2.67	2.61
0.55		0.47	1.02	1.28	1.70	2.05	2.45	2.62	2.64	2.63	2.63	2.61	2.63
0.43		0.39	0.79	1.00	1.28	1.60	2.04	2.53	2.68	2.70	2.73	2.74	2.73
0.32		0.33	0.60	0.78	1.00	1.27	1.60	2.11	2.66	2.83	2.85	2.85	2.88
0.21		0.27	0.47	0.58	0.77	0.97	1.29	1.71	2.23	2.83	3.05	3.10	3.11
0.10		0.24	0.37	0.46	0.59	0.71	1.00	1.46	2.02	2.58	3.14	3.42	3.46

Grid Geometry: d_s = 2.0 mm, d_a/d_s = 0.81, t_s/d_s = 0.13, t_a/d_s = 0.25

Operating Conditions: V_D = 45 V, V_T = 450 V

Impingement-Limited Normalized Perveance Per Hole

$[J/V_T^{3/2} (\frac{\ell_e}{d_s})^2]$ (nanopervs/hole)

$\frac{\ell_g}{d_s}$	R: 0.10	0.20	0.30	0.40	0.45	0.50	0.55	0.60	0.65	0.70	0.75	0.80
1.10	1.28	2.78	3.16	3.14	3.12	3.13	3.12	3.12	3.16	3.13	3.13	3.16
0.99	1.06	2.35	3.00	3.17	3.20	3.20	3.24	3.23	3.21	3.19	3.22	3.19
0.87	0.87	1.92	2.48	3.09	3.26	3.29	3.33	3.28	3.29	3.33	3.34	3.33
0.76	0.74	1.55	1.99	2.62	3.04	3.34	3.34	3.39	3.39	3.35	3.41	3.39
0.65	0.61	1.26	1.60	2.08	2.53	3.09	3.33	3.38	3.35	3.39	3.38	3.41
0.54	0.50	0.96	1.24	1.63	1.96	2.55	3.21	3.48	3.49	3.52	3.50	3.52
0.42	0.40	0.72	0.89	1.23	1.51	1.94	2.65	3.35	3.67	3.73	3.73	3.76
0.31	0.33	0.55	0.68	0.90	1.13	1.47	2.01	2.84	3.56	3.98	3.98	4.05
0.20	0.27	0.40	0.49	0.64	0.75	1.04	1.62	2.33	3.16	3.92	4.38	4.53
0.09	0.19	0.29	0.36	0.45	0.52	0.61	0.83	1.88	2.96	3.73	4.45	--

Grid Geometry: $d_s = 2.0$ mm, $d_a/d_s = 0.81$, $t_s/d_s = 0.38$, $t_a/d_s = 0.25$

Operating Conditions: $V_D = 45$ V, $V_T = 450$ V

Impingement-Limited Normalized Perveance Per Hole

$[J/V_T^{3/2} (\frac{\ell_e}{d_s})^2]$ (nanopervs/hole)

$\frac{\ell_g}{d_s}$	R: 0.10	0.20	0.30	0.40	0.45	0.50	0.55	0.60	0.65	0.70	0.75	0.80
1.11	1.30	2.30	2.34	2.30	2.33	2.36	2.32	2.32	2.31	2.34	2.34	2.34
1.00	1.09	2.26	2.35	2.34	2.35	2.35	2.35	2.35	2.36	2.38	2.36	2.36
0.89	0.91	1.93	2.33	2.36	2.38	2.35	2.39	2.39	2.37	2.40	2.41	2.42
0.77	0.73	1.57	2.03	2.32	2.35	2.36	2.35	2.34	2.37	2.38	2.39	2.36
0.66	0.62	1.26	1.64	2.10	2.30	2.33	2.32	2.32	2.33	2.35	2.36	2.40
0.55	0.51	1.04	1.33	1.78	2.02	2.25	2.27	2.30	2.29	2.29	2.30	2.33
0.43	0.40	0.79	1.04	1.35	1.66	2.01	2.19	2.22	2.23	2.27	2.25	2.25
0.32	0.32	0.63	0.81	1.08	1.29	1.66	2.06	2.23	2.28	2.29	2.31	2.34
0.21	0.27	0.49	0.61	0.84	1.00	1.30	1.77	2.20	2.33	2.34	2.33	2.36
0.10	0.24	0.41	0.51	0.66	0.80	1.02	1.41	2.00	2.40	2.52	2.56	2.55

Grid Geometry: $d_s = 2.0$ mm, $d_a/d_s = 0.66$, $t_s/d_s = 0.25$, $t_a/d_s = 0.25$

Operating Conditions: $V_D = 45$ V, $V_T = 450$ V

Impingement-Limited Normalized Perveance Per Hole

$[J/V_T^{3/2} (\frac{\ell_e}{d_s})^2]$ (nanopervs/hole)

$\frac{\ell_g}{d_s}$	R: 0.10	0.20	0.30	0.40	0.45	0.50	0.55	0.60	0.65	0.70	0.75	0.80
1.11	1.05	1.68	1.65	1.65	1.67	1.66	1.67	1.69	1.67	1.66	1.68	1.62
1.00	0.90	1.66	1.67	1.65	1.64	1.64	1.66	1.69	1.64	1.66	1.65	1.63
0.89	0.77	1.56	1.65	1.60	1.64	1.61	1.62	1.64	1.62	1.62	1.60	1.62
0.77	0.62	1.32	1.57	1.60	1.60	1.60	1.61	1.61	1.60	1.60	1.60	1.58
0.66	0.52	1.04	1.32	1.53	1.56	1.56	1.56	1.57	1.58	1.58	1.58	1.57
0.55	0.41	0.79	1.03	1.33	1.50	1.51	1.50	1.54	1.53	1.51	1.52	1.51
0.43	0.33	0.60	0.78	1.03	1.25	1.44	1.47	1.49	1.48	1.48	1.48	1.45
0.32	0.27	0.46	0.58	0.77	0.93	1.23	1.43	1.45	1.46	1.47	1.47	1.43
0.21	0.22	0.33	0.43	0.56	0.68	0.93	1.28	1.43	.47	1.45	1.44	1.43
0.10	0.18	0.25	0.32	0.41	0.50	0.63	0.92	1.36	1.44	1.44	1.44	1.44

Grid Geometry: $d_s = 2.0$ mm, $d_a/d_s = 1.00$, $t_s/d_s = 0.25$, $t_a/d_s = 0.25$

Operating Conditions: $V_D = 45$ V, $V_T = 450$ V

Impingement-Limited Normalized Perveance Per Hole

$[J/V_T^{3/2} (\frac{\ell_e}{d_s})^2]$ (nanopervs/hole)

$\frac{\ell_g}{d_s}$	R: 0.10	0.20	0.30	0.40	0.45	0.50	0.55	0.60	0.65	0.70	0.75	0.80
1.12	1.40	2.71	3.22	3.63	3.72	3.75	3.69	3.71	3.74	3.74	3.79	3.74
1.01	1.17	2.27	2.72	3.24	3.56	3.77	3.72	3.76	3.76	3.75	3.79	3.77
0.90	0.97	1.87	2.24	2.68	3.13	3.56	3.79	3.79	3.87	3.86	3.81	3.90
0.78	0.79	1.53	1.82	2.21	2.56	3.11	3.49	3.66	3.79	3.76	3.75	3.80
0.67	0.64	1.20	1.46	1.77	2.08	2.41	3.04	3.64	3.89	3.92	3.94	3.97
0.56	0.52	0.98	1.18	1.45	1.69	2.05	2.58	3.18	3.71	4.12	4.06	4.07
0.45	0.42	0.79	0.95	1.19	1.39	1.73	2.15	2.75	3.33	3.94	4.17	4.28
0.33	0.34	0.62	0.77	0.95	1.13	1.39	1.76	2.28	2.88	3.52	4.06	--
0.22	0.30	0.52	0.64	0.80	0.95	1.17	1.48	1.98	2.56	3.19	3.79	--

APPENDIX C

Electron Backstreaming Data

For all data contained in this Appendix:

$d_s = 2.0$ mm $\qquad V_D = 45$ V $\qquad V_N = 400$ V

	$\frac{\ell_g}{d_s}$	$J/V_T^{3/2}\,(\frac{\ell_e}{d_s})^2$ (nanopervs/hole)	R_{max}	$\frac{\ell_e}{d_a} \cdot \exp(\frac{t_a}{d_a})$
	1.08	3.01	0.953	2.01
	0.97	3.07	0.947	1.84
$\frac{d_a}{d_s} = 0.81$	0.86	3.08	0.940	1.68
	0.74	3.10	0.936	1.51
$\frac{t_s}{d_s} = 0.25$	0.63	3.31	0.924	1.36
	0.52	3.41	0.909	1.22
$\frac{t_a}{d_s} = 0.25$	0.41	3.55	0.894	1.09
(Standard Configuration)	0.29	3.98	0.866	0.98
	0.18	4.64	0.836	0.90
	0.07	5.69	0.791	0.85
	1.09	2.91	0.936	1.74
	0.98	3.08	0.928	1.59
$\frac{d_a}{d_s} = 0.81$	0.87	2.94	0.921	1.45
	0.76	3.01	0.912	1.31
$\frac{t_s}{d_s} = 0.25$	0.64	3.10	0.900	1.18
	0.53	3.25	0.883	1.05
$\frac{t_a}{d_s} = 0.13$	0.42	3.52	0.859	0.94
	0.30	3.68	0.827	0.85
	0.19	4.32	0.780	0.77
	0.08	4.33	0.737	0.73

	$\frac{\ell_g}{d_s}$	$J/V_T^{3/2} \left(\frac{\ell_e}{d_s}\right)^2$ (nanopervs/hole)	R_{max}	$\frac{\ell_e}{d_a} \cdot \exp\left(\frac{t_a}{d_a}\right)$
	1.11	2.64	0.960	2.41
	1.00	2.98	0.955	2.20
$\frac{d_a}{d_s} = 0.81$	0.89	3.08	0.950	2.01
	0.77	3.00	0.945	1.82
$\frac{t_s}{d_s} = 0.25$	0.66	3.17	0.940	1.64
	0.55	3.19	0.931	1.46
$\frac{t_a}{d_s} = 0.38$	0.43	3.27	0.920	1.31
	0.32	3.62	0.901	1.17
	0.21	4.17	0.881	1.07
	0.10	4.91	0.851	1.01
	1.10	2.62	0.964	2.79
	0.99	2.69	0.962	2.56
$\frac{d_a}{d_s} = 0.81$	0.87	2.66	0.958	2.33
	0.76	2.78	0.954	2.11
$\frac{t_s}{d_s} = 0.25$	0.65	2.85	0.951	1.89
	0.54	2.95	0.943	1.69
$\frac{t_a}{d_s} = 0.51$	0.42	2.94	0.933	1.51
	0.31	3.06	0.925	1.36
	0.20	3.45	0.906	1.24
	0.09	4.23	0.890	1.17

	$\frac{\ell_g}{d_s}$	$J/V_T^{3/2}\ (\frac{\ell_e}{d_s})^2$ (nanopervs/hole)	R_{max}	$\frac{\ell_e}{d_a} \cdot \exp(\frac{t_a}{d_a})$
	1.11	3.46	0.946	2.06
	1.00	3.77	0.941	1.88
$\frac{d_a}{d_s} = 0.81$	0.89	3.79	0.935	1.72
	0.77	3.91	0.928	1.55
$\frac{t_s}{d_s} = 0.13$	0.66	3.94	0.916	1.40
	0.55	3.98	0.901	1.25
$\frac{t_a}{d_s} = 0.25$	0.43	4.41	0.881	1.12
	0.32	4.79	0.852	1.00
	0.21	5.47	0.817	0.92
	0.10	5.82	0.775	0.86
	1.14	2.52	0.956	2.11
	1.03	2.58	0.951	1.94
$\frac{d_a}{d_s} = 0.81$	0.92	2.63	0.946	1.77
	0.81	2.63	0.940	1.60
$\frac{t_s}{d_s} = 0.38$	0.69	2.72	0.933	1.44
	0.58	2.78	0.923	1.29
$\frac{t_a}{d_s} = 0.25$	0.47	2.73	0.908	1.16
	0.36	2.94	0.892	1.04
	0.24	3.33	0.859	0.94
	0.13	3.70	0.832	0.87
	0.07	3.86	0.819	0.85

ORIGINAL PAGE IS
OF POOR QUALITY

	$\frac{\ell_g}{d_s}$	$J/V_T^{3/2}\ (\frac{\ell_e}{d_s})^2$ (nanopervs/hole)	R_{max}	$\frac{\ell_e}{d_a} \cdot \exp(\frac{t_a}{d_a})$
	1.09	1.75	0.962	2.66
	0.98	1.77	0.959	2.44
$\frac{d_a}{d_s} = 0.66$	0.86	1.79	0.955	2.22
	0.75	1.87	0.950	2.01
$\frac{t_s}{d_s} = 0.25$	0.64	1.88	0.945	1.80
	0.52	1.84	0.936	1.61
$\frac{t_a}{d_s} = 0.25$	0.41	1.99	0.927	1.44
	0.30	1.86	0.914	1.30
	0.19	1.76	0.901	1.19
	0.07	1.94	0.883	1.13
	1.11	4.23	0.919	1.57
	0.98	4.32	0.912	1.44
$\frac{d_a}{d_s} = 1.00$	0.89	4.07	0.908	1.31
	0.77	4.34	0.893	1.19
$\frac{t_s}{d_s} = 0.25$	0.66	4.50	0.874	1.07
	0.55	4.72	0.852	0.96
$\frac{t_a}{d_s} = 0.25$	0.43	4.96	0.824	0.85
	0.32	4.94	0.785	0.77
	0.21	4.52	0.758	0.70
	0.10	3.69	0.711	0.66

APPENDIX D

Electric Breakdown Data

d_s (mm)	$\frac{d_a}{d_s}$	$\frac{t_s}{d_s}$	$\frac{t_a}{d_s}$	ℓ_g (mm)	$E_{BREAKDOWN}$ (kV/mm)
2.0	0.81	0.25	0.25	0.16	8.03
↓	↓	↓	↓	0.11	8.17
↓	↓	↓	↓	0.07	8.71
↓	↓	↓	↓	0.02	9.76
↓	↓	↓	0.13	0.17	8.81
↓	↓	↓	↓	0.12	8.07
↓	↓	↓	↓	0.07	6.99
↓	↓	↓	↓	0.03	6.31
↓	↓	↓	0.38	0.13	6.90
↓	↓	↓	↓	0.09	6.60
↓	↓	↓	↓	0.04	8.11
↓	↓	↓	0.51	0.18	8.31
↓	↓	↓	↓	0.13	7.68
↓	↓	↓	↓	0.09	7.46
↓	↓	↓	↓	0.04	7.17
↓	↓	0.13	0.25	0.19	3.77
↓	↓	↓	↓	0.14	3.27
↓	↓	↓	↓	0.10	2.73
↓	↓	↓	↓	0.05	2.01
↓	↓	0.38	↓	0.16	9.00
↓	↓	↓	↓	0.12	8.35
↓	↓	↓	↓	0.07	7.32
↓	↓	↓	↓	0.03	10.58
↓	0.66	0.25	↓	0.16	8.03

d_s (mm)	$\frac{d_a}{d_s}$	$\frac{t_s}{d_s}$	$\frac{t_a}{d_s}$	ℓ_g (mm)	$E_{BREAKDOWN}$ (kV/mm)
2.0	0.66	0.25	0.25	0.11	8.17
↓	↓	↓	↓	0.07	8.71
↓	↓	↓	↓	0.02	9.76
↓	1.00	↓	↓	0.15	6.35
↓	↓	↓	↓	0.10	5.95
↓	↓	↓	↓	0.06	5.25
↓	↓	↓	↓	0.01	7.01
1.5	0.66	↓	↓	0.22	4.76
↓	↓	↓	↓	0.18	4.19
↓	↓	↓	↓	0.13	4.01
↓	↓	↓	↓	0.09	3.36
↓	↓	↓	↓	0.04	3.85
↓	1.00	↓	↓	0.19	5.13
↓	↓	↓	↓	0.15	4.47
↓	↓	↓	↓	0.10	4.30
↓	↓	↓	↓	0.06	4.35
↓	↓	↓	↓	0.01	5.95
1.0	0.66	↓	↓	0.19	5.85
↓	↓	↓	↓	0.14	5.48
↓	↓	↓	↓	0.10	5.15
↓	↓	↓	↓	0.05	5.07
↓	1.00	↓	↓	0.19	5.97
↓	↓	↓	↓	0.15	4.94
↓	↓	↓	↓	0.10	3.89
↓	↓	↓	↓	0.06	4.15
0.5	0.8	0.25	0.25	0.19	4.18